# EXPERIMENTAL INVESTIGATION OF FRP-REINFORCED CONCRETE COLUMNS UNDER CONCENTRIC AND ECCENTRIC LOADING

by
Nouran Zinelabdin Ahmed Elmesalami

A Thesis Presented to the Faculty of the
American University of Sharjah
College of Engineering
In Partial Fulfillment
of the Requirements
for the Degree of

Master of Science in
Civil Engineering

Sharjah, United Arab Emirates
June, 2019

## Approval Signatures

We, the undersigned, approve the Master's Thesis of Nouran Zinelabdin Ahmed Elmesalami

Thesis Title: Experimental Investigation of FRP-Reinforced Concrete Columns Under Concentric and Eccentric Loading

| **Signature** | **Date of Signature** (dd/mm/yyyy) |
|---|---|
| _____ | _____ |
| Dr. Farid Abed<br>Professor, Department of Civil Engineering<br>Thesis Advisor | |
| _____ | _____ |
| Dr. Ahmed Elrefai<br>Associate Professor, Laval University<br>Department of Civil and Water Engineering<br>Thesis Co-Advisor | |
| _____ | _____ |
| Dr. Sherif Yehia<br>Professor, Department of Civil Engineering<br>Thesis Committee Member | |
| _____ | _____ |
| Dr. Wael Abuzaid<br>Assistant Professor, Department of Mechanical Engineering<br>Thesis Committee Member | |
| _____ | _____ |
| Dr. Irtishad Ahmed<br>Head/ Program Director, Department of Civil Engineering | |
| _____ | _____ |
| Dr. Lotfi Romdhane<br>Associate Dean for Graduate Affairs and Research<br>College of Engineering | |
| _____ | _____ |
| Dr. Naif Darwish<br>Acting Dean, College of Engineering | |
| _____ | _____ |
| Dr. Mohamed El-Tarhuni<br>Vice Provost for Graduate Studies | |

## Acknowledgment

First and foremost, I thank Almighty Allah, the most merciful, the most gracious, for His uncountable blessings, and for always granting me strength and patience to make it through hard times.

Second, I express my deep gratitude and thanks to my advisors, Dr. Farid Abed and Dr. Ahmed Elrefai, for their support and guidance throughout, and for always trusting in me. I greatly appreciate their assistance, worthy discussions and suggestions. I would like to thank Dr. Farid Abed, not only for his assistance during my masters studies, but also for all his help and support for the past five years that I have worked with, and known him. I would like to return the favor in this achievement to both of my advisors, as it is no exaggeration that this work would not be as complete without them.

I would also like to thank my thesis committee, Dr. Sherif Yehia and Dr. Wael Abuzaid, for accepting to be committee members for my thesis, and for their insightful comments and fairness. I am also grateful to the civil engineering lab instructors at AUS, Mr. Arshi Faridi and Mr. Waleed Nawaz, and to the civil engineering lab technician, Mr. Mohamed Ansari, as well as to my colleague, Yazan AlHoubi, for their technical assistance in conducting the experimental work. I am also grateful to the civil engineering department at the American University of Sharjah for their support through the Graduate Teaching Assistantship, which was a great asset in completing my degree.

I would also like to thank all my friends and colleagues at AUS who were a true inspiration and motivation, and who stood by my side in the dark times.

I am also greatly thankful to Emirates Stone Company in Sharjah, for their generous donation of the concrete and steel materials, and for their help in preparing and casting the specimens. Many thanks as well to Galen L.L.C. in Russia, for their contribution of the FRP bars and ties.

Finally, and most importantly, I express my profound gratitude to my parents, my siblings and the rest of my family, for all what they have done for me during this time. Their unconditional support and encouragements throughout those two and a half years will never be forgotten my whole life. Their prayers, patience, consideration and sacrifices throughout my graduate studies, meant so much to me. I am forever indebted to them.

**Dedication**

*To my beloved parents and family…*

## Abstract

The problem of corrosion of steel in reinforced concrete (RC) structures has urged the need for alternative reinforcement materials. One possible alternative is fiber-reinforced polymer (FRP) bars, which are non-corrosive, non-magnetic, and have higher tensile strengths and higher strength-to-weight ratios than steel bars. Nevertheless, owing to the low compressive strength of FRP bars, the currently available FRP RC design codes, such as ACI440.1R-15 and CSA S806-12, neglect the contribution of FRP bars to the columns' ultimate capacities. In this study, the behavior of concrete columns reinforced with a relatively new type of FRP bars, basalt fiber-reinforced polymer (BFRP) bars, as well as glass fiber-reinforced polymer (GFRP) bars, is investigated. The study starts with a critical literature review on FRP-reinforced concrete columns, followed by analysis of experimental tests conducted on a total of 22 reinforced concrete square columns. The overall response of FRP RC columns is investigated considering several key parameters such as longitudinal reinforcement type (steel, GFRP and BFRP), BFRP longitudinal reinforcement ratio, transverse reinforcement type (steel and BFRP ties), BFRP transverse reinforcement spacing, and loading eccentricity (concentric and eccentric). The results showed that FRP RC columns demonstrated overall compression behavior similar to steel RC columns. Even though FRP RC columns had lower ultimate capacities than steel RC columns, the difference in the ultimate capacities decreased as load eccentricity increased. Moreover, FRP RC columns showed higher ductility than steel RC columns, at all load eccentricities. However, the contribution of FRP bars to the ultimate capacities of the columns was around 11% as compared to 31% for steel bars. Despite this, neglecting the strength contributions of FRP bars, as recommended by current FRP RC design codes, results in conservative predictions of the columns' ultimate capacities. BFRP ties are found to be efficient in confining the concrete core and in increasing the columns' deformation capacities. Reducing BFRP ties spacing would have more pronounced effect on confinement efficiency and ductility than on strength capacity of FRP RC columns.



**Keywords:** ***BFRP; GFRP; RC columns; BFRP ties; eccentricity; interaction diagrams; ductility.***

## Table of Contents

## List of Figures

## List of Tables

# Chapter 1. Introduction

In this chapter, the problem investigated is explained followed by a brief outline of the historical development of fiber-reinforced polymers (FRP). Then, the advantages of using FRP reinforcements in concrete structures are presented along with examples of some of their current applications. After that, the objectives of the research and its contribution to current research on the topic are explained.

## 1.1. Overview

The main motive behind the use of fiber-reinforced polymers (FRP) in concrete structures is the problem of corrosion of steel reinforcements. In steel reinforced concrete structures, the steel reinforcements are initially protected from corrosion by the alkaline environment of the concrete [1, 2]. However, in structures subjected to aggressive environments, such as marine structures and bridges which are exposed to deicing salts, marine salts, and combinations of temperature, moisture and chloride, the concrete alkalinity is reduced causing corrosion of steel reinforcements [1-3]. The corrosion of steel reinforcements in such structures increases the need for rehabilitation leading to increased maintenance costs [2, 3]. For example, in the United States, the annual cost of repairing and replacing bridge substructures, such as piers, is $2 billion, and is $1 billion dollars for marine piling systems, with corrosion of steel reinforcement contributing the most to the cost [4]. Also, in the European Union, the annual cost of maintaining, repairing and strengthening around 84,000 reinforced and pre-stressed concrete bridges is £215 million [5]. Several solutions were proposed and implemented for this issue such as using galvanized coatings, electro-static-spray fusion-bonded (powder resin) coatings, epoxy coatings, polymer-impregnated concrete and alloyed steel bars [1, 2]. Epoxy-coated steel reinforcements were found to be the best of these solutions [2]. Nevertheless, after corrosion was detected in structures reinforced with epoxy-coated steel, alternative solutions were needed [2]. Here, FRP reinforcements began to be considered as alternative reinforcements to steel in structures exposed to harsh environments.

The use of composites expanded after World War II, in the 1940s, but it was not until the 1960s when the use of FRP bars as concrete reinforcements was seriously considered [1, 2]. The effects of chloride-ion-induced corrosion on the deterioration of

bridges in the United States increased significantly in the 1970s [6], and therefore FRP bars first became commercially available in the late 1970s [2]. As the use of FRP materials expanded, their advantages became better known and additional uses of FRP materials developed. In the 1980s, nonmetallic reinforcements, which are non-conductive and non-magnetic, were needed for advanced technology such as in facilities for Magnetic Resonance Imaging (MRI) medical equipment. Other uses of FRP materials that arose included seawall construction, electronics laboratories, airport runways and substation reactor bases [7].

Other than their non-corrosive nature, there are several advantages of FRP reinforcements over steel reinforcements. FRP bars have higher tensile strength than steel, and are lighter in weight at one-fourth to one-fifth the weight of steel bars [2, 8, 9]. They are transparent to magnetic fields, and are thermally and electrically non-conductive [2, 9]. Since FRP bars are non-corrosive, smaller concrete covers can be used, no admixtures would be required for corrosion reduction and structures reinforced with FRP bars would have a greater service life than their steel counterparts in corrosive environments [2]. In addition, FRP bars have a lower carbon footprint than steel bars [10], and have high fatigue endurance [2]. Although FRP bars are not as easy to recycle as steel bars, reinforcing concrete structures with FRP bars can result in lower life cycle costs as compared to using steel reinforcement, owing to the non-corrosive properties of FRP bars [10].

FRP reinforcements have been used in several concrete structures worldwide. In Europe, the first use of FRP reinforcement was in a prestressed highway bridge, in Germany, in 1986 [11]. Since then, there has been an increase in the research and use of FRP reinforcement in Europe [12]. In the mid-1990s, Japan had more than 100 FRP reinforced concrete projects, making it the country with the most FRP reinforcement applications [2]. In the 2000s, China became the country with the largest FRP reinforcement applications ranging from bridge decks to underground works [13]. In Canada, more than 200 bridge structures have been constructed with Glass fiber-reinforced polymer (GFRP) bars as reinforcements for the bridges deck slabs and girders [14]. For instance, the Headingly Bridge in Manitoba, Canada, was constructed with Carbon fiber-reinforced polymer (CFRP) tendons for prestressing the girders, CFRP stirrups for two main girders, CFRP reinforcements for the deck slab and GFRP

reinforcements for the bridge curbs [15]. Another example in the United States, is the Emma Park Bridge in Utah which was constructed of precast concrete deck panels reinforced with GFRP bars [2]. Other existing structures constructed with FRP reinforcements include parking garages, water tanks, highway concrete pavements and MRI hospital room additions [2]. All of those currently existing structures have FRP reinforcements in their slabs or beams/girders elements. FRP reinforcements are not yet used in reinforced concrete (RC) columns or compression members. Additionally, most of the currently available research is on the use of FRP reinforcements in beams or slabs. Several studies have investigated the shear and flexural behavior of FRP-reinforced concrete beams, under normal conditions as well as under harsh exposure conditions [7,16-22]. Despite this, research on the use of internal FRP reinforcement in columns is still limited.

## 1.2. Thesis Objectives

The potential of fiber-reinforced polymer bars as alternative reinforcement to conventional steel bars in concrete structures is acknowledged and is widely accepted. Even though, recently, a number of studies have investigated the use of FRP bars as compression reinforcement in concrete columns, more research is needed in order to provide full understanding of FRP-reinforced concrete columns' behavior. Therefore, the main objective of this research is to investigate the potential of replacing the conventional steel reinforcements with FRP reinforcements, including basalt fiber-reinforced polymer (BFRP) and glass fiber-reinforced polymer (GFRP) bars, in concrete columns. The behavior of FRP-RC columns is studied in terms of their ultimate axial capacities under concentric and eccentric loading conditions, and their deformation capacities and ductility. The effects of varying test parameters on the overall behavior of the columns are also investigated. The main parameters investigated include longitudinal and transverse reinforcement types, BFRP longitudinal reinforcement ratios, BFRP transverse reinforcement spacing, and load eccentricity-to-width ratios.

## 1.3. Research Contribution

Currently, there is limited research on the use of FRP bars as compression reinforcement in RC columns, and several areas of this research are yet to be

investigated. The contributions of this study to current research in this field is as outlined below:

- Add to the existing knowledge on the potential of replacing conventional steel reinforcement with FRP reinforcement, and on the overall behavior of FRP-RC columns.
- Provide detailed analysis and investigation on the use of a relatively new type of FRP reinforcement, BFRP bars, in RC columns.
- Provide insight, for the first time, on the effects of confining BFRP-RC columns with BFRP ties.

### 1.4. Thesis Organization

The rest of the thesis is organized as follows: Chapter 2 presents background information on the mechanical and physical properties of FRP bars. This is followed by a state-of-the-art review on the use of FRP reinforcement as alternative to steel reinforcement in concrete columns. Chapter 3 describes the experimental program of the thesis, including details of the specimens tested and descriptions of the test set-ups. The results of the experimental tests are explained in Chapter 4, and detailed discussions of the results are provided in Chapter 5. Finally, Chapter 6 concludes the thesis and provides recommendations for future work.

# Chapter 2. Background and Literature Review

In this chapter, information about the mechanical and physical properties of FRP bars is discussed, with a focus on basalt FRP bars. An extensive review of the existing research on FRP-reinforced concrete columns is then presented, and gaps in knowledge of FRP-RC columns are identified.

## 2.1. Physical and Mechanical Properties of FRP bars

FRP reinforcements exhibit different mechanical behavior from steel reinforcements. Therefore, changes in the conventional design philosophies of reinforced concrete structures are needed where FRP reinforcements are used. FRP bars consist of high strength fibers such as glass, carbon, aramid or basalt, embedded in a polymer resin such as epoxy or vinylester [1, 2, 9, 23]. Unlike steel bars, FRP bars are anisotropic in nature and are elastic until failure with no yielding point [2, 9]. Moreover, FRP bars have lower modulus of elasticity than steel (around 20% to 25% that of steel) [1, 2, 9], and their ultimate tensile strength decreases as the bar diameter increases [1]. Also, FRP bars have a lower creep-rupture threshold than steel, and have different coefficient of thermal expansion in the longitudinal and radial directions [2]. Additionally, the mechanical properties of FRP bars are not consistent, and vary from one product to another [1, 2]. FRP bars produced by different manufacturers can have different mechanical properties due to differences in fiber volume fraction, shape of the cross-sections, properties of the resin and fiber orientation of the bars [1, 2]. It is therefore considered difficult to provide universal mechanical property values for FRP reinforcing bars [1]. There are currently some design guidelines and codes available for FRP reinforced concrete structures, which are developed by some countries and regions such as the United States [2, 24, 25], Canada [26, 27], Europe [28, 29] and Japan [30].

The most recent FRP composites are Basalt fiber-reinforced polymers (BFRPs) which emerged within the last decade [23]. Basalt FRPs are more cost-effective than Carbon fiber-reinforced polymers (CFRP), and have greater strength and modulus of elasticity, equivalent cost and higher chemical stability than E-glass FRPs [23]. Furthermore, BFRPs are five times stronger and have about one-third the density of low-carbon steel bars [23]. In addition, the manufacturing process of basalt fibers is more environmentally-friendly and is less expensive than that of carbon and glass fibers

[31]. Also, basalt fibers have higher energy absorption capacities than glass and carbon fibers and, unlike glass and carbon fibers, do not require extra additives to enhance their mechanical properties [31]. Moreover, the adhesion and bond strength of BFRP bars to concrete were found to be higher than for GFRP bars under different harsh exposure conditions [32, 33]. The currently available design codes for FRP reinforced concrete structures provide reference to the physical and mechanical properties of GFRP, CFRP and Aramid FRP (AFRP) bars, but not to BFRP bars. Research work is still ongoing in order to introduce BFRP bars into the current FRP design codes [23].

### 2.2. Literature Review

Currently, available design codes and guidelines for FRP-reinforced concrete structures, such as ACI440.1R-15 [2], CSA-S6-14 [34], and CSA-S806-12 [27] recommend nil contribution of FRP bars when used as reinforcement for compression members (such as columns) or as compression reinforcement in flexural members. Although standard test methods that characterize the tensile properties of FRP bars have been well established, no standard methodology is currently available to determine their compressive response [35]. Nevertheless, a number of studies devised compression test methods for FRP bars and, except a few studies, there is a general consensus that the compressive strengths and moduli of FRP bars are lower than their tensile values, as given in Table 2.1 [9, 36-43]. The low compressive modulus of FRP bars is attributed to the micro-buckling of internal fibers under compressive loading resulting in a premature failure of the bar in an “end-brooming” phenomenon [2]. Despite these findings, research on the use of FRP bars in compression is constantly advancing.

This chapter presents a comprehensive literature review on the use of FRP bars as compression reinforcement in RC columns. The results of more than 300 compression tests taken from 43 experimental investigations that were published in the scientific literature have been collected. A major part of these studies is presented in Table 2.2. Analytically, the design equations that many researchers have proposed to predict the compressive capacities of the tested columns were also collected and listed in Table 2.3. The equations were classified based on the method adopted in estimating the contribution of FRP bars to the capacity of the tested columns as will be detailed later in this paper. The main variables considered in the collected tests are as follows:

- Slenderness: This included short (non-slender) and slender columns, with the threshold for the slenderness ratio considered as 22 according to ACI318-14 [44] and CSA-S806-12 [27]. It was found that 90% of the collected tests were conducted on short FRP-reinforced concrete (FRP-RC) columns compared to 10% conducted on slender columns.

- Loading regime: 44% of the tested FRP-RC columns were concentrically-loaded compared to 40% and 16% tested under eccentric and seismic loadings, respectively.

- Columns' cross-sections: Cross-sections of the tested columns are given in Table 2.2. It was observed that 52% of the collected tests were carried out on circular FRP-RC columns measuring between 205 and 305 mm in diameter, followed by 39% square columns measuring between 120 and 610 mm, and 9% rectangular columns measuring between 160 and 260 mm.

- Concrete type: This includes normal strength concrete (NSC) of compressive strength ranging between 29 and 43 MPa, high-strength concrete (HSC) including fiber-reinforced high-strength concrete of compressive strength ranging between 55 and 93 MPa, and normal strength inorganic polymer concrete (IPC). It was observed that 72% of the tested FRP-RC columns were cast using NSC followed by 22% cast with HSC and 6% cast with IPC.

- Reinforcement: Three types of FRP materials were used in the collected data; namely, glass (GFRP), carbon (CFRP), and basalt (BFRP) bars, with reinforcement ratios that varied between 0.83 and 5.3%. Transverse reinforcement also varied in type, shape, diameter, and spacing as detailed in Table 2.2.

Table 2.2 also lists the specimens' dimensions, reinforcements, concrete type, and the loading conditions as reported in previous studies. The data collected in Table 2.2 are categorized into three main groups; namely, concentrically-loaded short columns, eccentrically-loaded short columns, and slender columns. Details about each group are given in the following sections.

**2.2.1. Behavior of short FRP-RC columns.** As previously stated, short columns consisted 90% of the collected data. Short columns are defined as columns having a slenderness ratio less than 22 according to ACI318-14 [44] and CSA-S806-12

[27]. Both concentric and eccentric loading tests were conducted on short columns as can be found in the literature and detailed below.

Table 2.1: Summary of the compressive properties of FRP bars as reported in previous studies

| Study | FRP Type | $\phi$ (mm) | $l_u$ (mm) | $f_{uT}$ (MPa) | $E_{ft}$ (GPa) | $f_{uc}/f_{uT}$ | $E_{fc}/E_{ft}$ |
|---|---|---|---|---|---|---|---|
| Wu [36] | Glass | 22 | ≥ 55 | 554 | 50.7 | 0.74 | 0.75 |
| | | 25 | ≥ 62.5 | - | 45.6 | - | 0.84 |
| Bedard [9] | Glass | - | - | 700 | 44.8 | 0.86 | 0.77 |
| Challal and Benmokrane [37] | Glass | 15.9, 19.1, and 25.4 | 44-70 | 690 | 42 | 0.77 | 1.02 |
| Kobayashi and Fujisaki [38]* | Carbon | 6, 8, 10 and 13 | - | - | - | 0.3-0.5 | - |
| | Aramid | 6, 8 and 10 | - | - | - | 0.1 | - |
| | Glass | 6, 8 and 10 | - | - | - | 0.3-0.4 | - |
| Deitz et al. [39] | Glass | 15 | 50 to 380 | 610 | 40 | 0.5 | 1.0 |
| Tavassoli et al. [40] | Glass | 25 | 50 and 160 | 1087 | 65.8 | 0.56 | 0.85 |
| | | 28 | 50, 160 and 275 | 1338 | 74.3 | 0.62 | 0.97 |
| Maranan et al. [41] | Glass | 15.9 | 50 | 1184 | 62.6 | 0.517 | - |
| Khorramian and Sadeghian [45] | Glass | 16 | 32 | 629 | 38.7 | 1.24 | 1.06 |
| Sun et al. [42] | Glass | 10 | 6.25 | 1103 | 92.4 | 0.62 | 0.65 |
| Xue et al. [43] | Glass | 15.9 | - | 654 | 39 | 0.36 | 0.92 |
| | | 19.1 | - | 729 | 44 | 0.38 | 0.91 |

*FRP reinforcement were embedded in concrete prisms
$\phi$ = diameter of FRP bar; $l_u$ = unbraced length of FRP bar tested; $f_{uT}$ = ultimate tensile strength of FRP bar; $E_{ft}$ = tensile modulus of elasticity of FRP bar; $f_{uc}/f_{uT}$ = ratio of compressive strength to tensile strength of FRP bar; $E_{fc}/E_{ft}$ = ratio of compressive elastic modulus to tensile elastic modulus of FRP bar.

***2.2.1.1. Concentrically-loaded short FRP-RC columns.*** Most of the studies conducted on concentrically-loaded short FRP-RC columns aimed at assessing the contribution of the longitudinal FRP bars to develop the load-carrying capacities of the tested columns. The ability of FRP bars to contribute to the columns' strength depends on the material of the FRP bars used [50]. GFRP bars are known by their low strength and modulus of elasticity compared to CFRP bars and thus contribute relatively less to columns' capacities. Previous studies reported that the contribution of GFRP bars to columns' capacities ranged between 3 and 14% of the total capacity of the tested

columns [41, 45-47, 49, 51, 52, 54, 56, 59, 60], compared to 6 and 19% when CFRP bars were used [50-52], and between 12 and 16% when steel bars were used [46, 47, 49-52]. Quantifying the contribution-to-capacity of FRP bars relative to that of steel bars was the focus of several studies. In this regard, a fair comparison between FRP and steel bars necessitates that both types of bars have equal axial stiffness, $\rho E$, where $\rho$ is the reinforcement ratio and E is the modulus of the bar's material. However, most tests were conducted on columns reinforced with either FRP or steel bars having equal reinforcement ratios rather than equal axial stiffness. In an attempt to rationally compare between the contribution of both types of bars to the columns' capacities, the axial stiffness of the longitudinal reinforcement of the tested columns, from the studies of De Luca et al. [46], Tobbi et al.[52], Afifi et al. [49], Afifi et al. [50], Hadhood et al. [54], Hadi et al. [56], Hadi et al. [59], and Khorramian and Sadeghian [45], was determined and normalized with respect to the concrete strength $0.85f'_c$ of the columns. Figure 2.1 shows the relationship between the normalized axial stiffness of the bars, $\rho E/0.85f'_c$, and the bars' contribution to the columns' capacities.

It can be depicted from Figure 2.1 that only a few tests were reported with equal normalized stiffness for FRP and steel bars. For $\rho E/0.85f'_c$ ranging between 65 and 68, the average contribution-to-capacity of GFRP bars was lower than that of steel bars whereas the contribution of CFRP bars was close to or even larger than that of steel bars. This finding was confirmed by plotting the best-fit lines for steel-RC, GFRP-RC and CFRP-RC columns, resembling the ratio of average bars' contribution to the normalized axial stiffness of the bars. It can be seen that the slope of the best-fit line for CFRP-RC columns is slightly higher (by about 11%) than that of steel-RC columns. On the other hand, the best-fit line of GFRP-RC columns shows a considerably flatter slope than those of CFRP-RC and steel-RC columns by 56 and 51%, respectively, indicating that the contribution of GFRP bars to the load-carrying capacities of RC columns is less than that of steel or CFRP bars, which can be attributed to the low compressive strength and modulus of the former bars.

In an attempt to compare between the capacities of steel-RC and FRP-RC columns, the axial capacities of several columns, $P_{max}$, were normalized against the concrete capacity in compression, $0.85f'_cA_g$ as shown in Figure 2.2.

Table 2.2: Summary of the compressive properties of FRP bars as reported in previous studies

| Reference | No. of specimens | $f'_c$ (MPa) | Dimensions-Cross-Section Shape *(mm)* | Longitudinal Reinforcement | | Transverse Reinforcement | | | | Loading eccentricity (*e/D* %) | FRP Contribution (%) |
|---|---|---|---|---|---|---|---|---|---|---|---|
| | | | | Type ($E_{fl}$) | Ratio *(%)* | Type | Shape | $\phi$ *(mm)* | *s (mm)* | | |
| **Previous studies conducted on short concentrically-loaded FRP-RC columns** | | | | | | | | | | | |
| De Luca et al. [46] | 5 | 34.5 | 610x3000 - S | G (44.2, 44.4) [a] | 1 | G | Ties | 12.7 | 305, 76 | 0 | < 5 |
| Tobbi et al. [47] | 8 | 32.6 | 350x1400 - S | G (48.2, 47.6) [a] | 1.9 | G | Ties | 12.7 | 80, 120 | 0 | 10 |
| Pantelides et al. [48] | 10 | 36 | 54x711 – Ci | G (43.3) | 1.6 | G | Spirals | 10 | 76 | 0 | - |
| Afifi et al. [49] | 9 | 42.9 | 300x1500 – Ci | G (55.4) | 1.1, 2.2, 3.2 | G | Spirals | 6.4, 9.5, 12.7 | 35, 40, 80, 120, 145 | 0 | 5-10 |
| Afifi et al. [50] | 9 | 42.9 | 300x1500 – Ci | C (140) | 1.0, 1.7, 2.4 | C | Spirals | 6.4, 9.5, 12.7 | 35, 40, 80, 120, 145 | 0 | 13 |
| Mohamed et al. [51] | 6 | 42.9 | 300x1500 – Ci | G (55.4) | 2.25 | G | Spirals -Hoops | 6.4, 9.5, 12.7 | 80 | 0 | 5-10 |
| Mohamed et al. [51] | 6 | 42.9 | 300x1500 – Ci | C (140) | 1.79 | C | Spirals -Hoops | 6.4, 9.5, 12.8 | 80 | 0 | 11-17 |
| Tobbi et al. [52] | 7 | 30 | 350x1400 – S | G (48.2, 47.6) [a] | 0.83, 1.06, 1.85 1.95 | G | Ties | 12.7 | 80, 120 | 0 | - |
| Tobbi et al. [52] | 1 | 30 | 350x1400 - S | C (137) | 1.65 | C | Ties | 9.5, 12.7 | 60, 67, 80, 120 | 0 | - |
| Afifi et al. [53] | 12 | 42.9 | 300x1500 – Ci | C (140) | 1.1, 2.2, 3.2 | C | Spirals -Hoops | 6.4, 9.5, 12.7 | 35, 40, 80, 120, 145 | 0 | 6-19 |
| Maranan et al. [41] | 8 | IPC 38 | 250x1000 – Ci | G (62.6) | 2.43 | G | Spirals -Hoops | 9.5 | 50, 100, 200 | 0 | 7.6 |
| Hadhood et al. [54] | 2 | 70.2 | 305x1500 – Ci | G (54.9) | 2.18, 3.27 | G | Spirals | 9.5 | 80 | 0 | 5 |
| Hales et al. [55] | 3 | 90 | 305x760 – Ci | G (43) | 1.65 | G | Spirals | 10 | 76 | 0 | - |
| Hadi et al. [56] | 2 | 37 | 205x800 – Ci | G (50) | 2.3 | G | Helices | 9.5 | 30, 60 | 0 | 11.4-13.4 |
| Hadi and Youssef [57] | 1 | 32 | 210x800 – S | G (67.9) | 1.15 | G | Ties | 9.5 | 50 | 0 | - |
| Hadhood et al. [58] | 1 | 35 | 305x1500 – Ci | C (141) | 2.17 | C | Spirals | 9.5 | 80 | 0 | - |
| Hadi et al. [59] | 2 | 85 | 210x800 – Ci | G (52) | 2.19 | G | Helices | 9.5 | 30, 60 | 0 | 6.5 |
| Hadhood et al. [60] | 4 | 30.5, 42.9 | 305x1500 – Ci | G (54.9) | 2.2 | G | Hoops | 9.5 | 80 | 0 | 5-7 |
| Elchalakani and Ma [35] | 3 | 32 | 160x260x1200 - R | G (46.3) | 1.83 | G | Ties | 6.35 | 75, 150, 250 | 0 | 3.2 |
| Hadhood et al. [61] | 1 | 70 | 305x1500 - Ci | C (141) | 2.2 | C | Spirals | 9.5 | 80 | 0 | - |
| Hasan et al. [62] | 3 | 85, and F-HSC 93 | 210x800 - Ci | G (67.8) | 2.2 | G | Helices | 9.5 | 30, 60 | 0 | - |

| | | | | | | | | | | | |
|---|---|---|---|---|---|---|---|---|---|---|---|
| Khorramian and Sadeghian [45] | 2 | 37 | 150x500 - S | G (38.7) | 5.3 | -* | - | - | - | 0 | 3-8 |
| Zhang and Deng [63] | 10 | F-NSC 50 | 350x1200 - S | G (45) | 1.39, 2.09, 2.64 | G | Ties | 8, 10, 12 | 38, 60, 90, 130 | 0 | 2-5.5 |
| Elchalakani et al. [64] | 3 | 26 | 160x260x1200 - R | G (50) | 2.22 | G | Ties | 8 | 75, 150, 250 | 0 | 10.8 |
| Tabatabaei et al. [65] | 11 | 40.5 | 300x1600 - Ci | G (51.2) | 1.6 | G | Spirals | 9.5 | 80 | 0 | 2.6-5.3 |
| **Previous studies conducted on short eccentrically-loaded FRP-RC columns** | | | | | | | | | | | |
| Fan and Zhang [66] | 8 | IPC 34.9 | 120x900 - S | B (48) | 1.4 | St | Ties | 6 | 100 | 16.67, 66.67 | NA |
| Hadhood et al. [54] | 8 | 70.2 | 305x1500 - Ci | G (54.9) | 2.18, 3.27 | G | Spirals | 9.5 | 80 | 8.2, 16.4, 32.8, 65.6 | NA |
| Hadhood et al. [58] | 4 | 35 | 305x1500 - Ci | C (141) | 2.17 | C | Spirals | 9.5 | 80 | 8.2, 16.4, 32.8, 65.6 | NA |
| Hadi and Youssef [57] | 3 | 32 | 210x800 - S | G (67.9) | 1.15 | G | Ties | 9.5 | 50 | 11.9, 23.8 | NA |
| Hadi et al. [56] | 6 | 37 | 205x800 - Ci | G (50) | 2.3 | G | Helices | 9.5 | 30, 60 | 2.2, 24.4 | NA |
| Sun et al. [42] | 9 | 33.51 | 180x250x1000 - R | C (92.4) | 1.05 | St | Ties | 4 | 125 | 30, 50, 70 | NA |
| Hadi et al. [59] | 6 | 85 | 205x800 - Ci | G (52) | 2.19 | G | Helices | 9.5 | 30, 60 | 11.9, 23.8 | NA |
| Hadhood et al. [60] | 4 | 35, 42.9 | 305x1500 - Ci | G (54.9) | 2.2 | G | Hoops | 9.5 | 80 | 8.2, 16.4, 32.8, 65.6 | NA |
| Elchalakani and Ma [35] | 6 | 32 | 160x260x1200 - R | G (46.3) | 1.83 | G | Ties | 6.35 | 75, 150, 250 | 9.62, 17.3 | NA |
| Hadhood et al. [61] | 4 | 70 | 305x1500 - Ci | C (141) | 2.2 | C | Spirals | 9.5 | 80 | 8.2, 16.4, 32.8, 65.6 | NA |
| Hasan et al. [62] | 9 | 85, and F-HSC 93 | 210x800 - Ci | G (67.8) | 2.2 | G | Helices | 9.5 | 30, 60 | 11.9, 23.8 | NA |
| Khorramian and Sadeghian [45] | 7 | 37 | 150x500 - S | G (38.7) | 5.3 | -* | - | - | - | 10, 20, 30 | NA |
| Guérin et al. [67] | 12 | 40 | 405x2000 - S | G (51.3, 54.4) [a] | 1.0, 1.4, 2.5 | G | Ties | 10 | 152, 203 | 9.88, 19.75, 39.5, 79 | NA |
| Guérin et al. [68] | 8 | 42.3 | 405x2000 - S | G (51.3, 48.2) [a] | 1.0 | G | Ties | 10 | 152 | 10, 20, 40, 80 | 3-13 |
| Elchalakani et al. [64] | 6 | 26 | 160x260x1200 - R | G (50) | 2.22 | G | Ties | 8 | 75, 150, 250 | 9.62, 19.23, 28.85 | NA |
| **Previous studies conducted on slender FRP-RC columns** | | | | | | | | | | | |
| Maranan et al. [41] | 2 | IPC 38 | 250x2000 - Ci | G (62.6) | 2.43 | G | Spirals -Hoops | | 50, 100, 200 | 0 | 9.2 |
| Hales et al. [55] | 6 | 90 | 305x3730 - Ci | G (43) | 1.65 | G | Spirals | 10 | 76 | 0. 8.2, and 33.4 | - |
| Xue et al. [43] | 15 | 29.1, 39, 40.3, and 55.2 | 300x300 - S | G (36, 40) [a] | 0.9, 1.34, 2.55 | St | Ties | 8 | 150 | 0, 20, 50, and 100 | - |

*No ties were used in this study

[a]Values of $E_{fl}$ refer to two different bar types or two different bar sizes

$f'_c$ = compressive strength of concrete; $E_{fl}$ = tensile elastic modulus of FRP bars, reported in GPa; $\phi$ = diameter of FRP bar; $s$ = transverse reinforcement spacing; IPC = inorganic polymer concrete; F-HSC = fiber high-strength concrete; F-NSC = fiber normal-strength concrete; S = Square; Ci = Circular; R = Rectangular; G = GFRP; C = CFRP; B = BFRP; St = steel; $e/D$ = eccentricity-to-diameter ratio

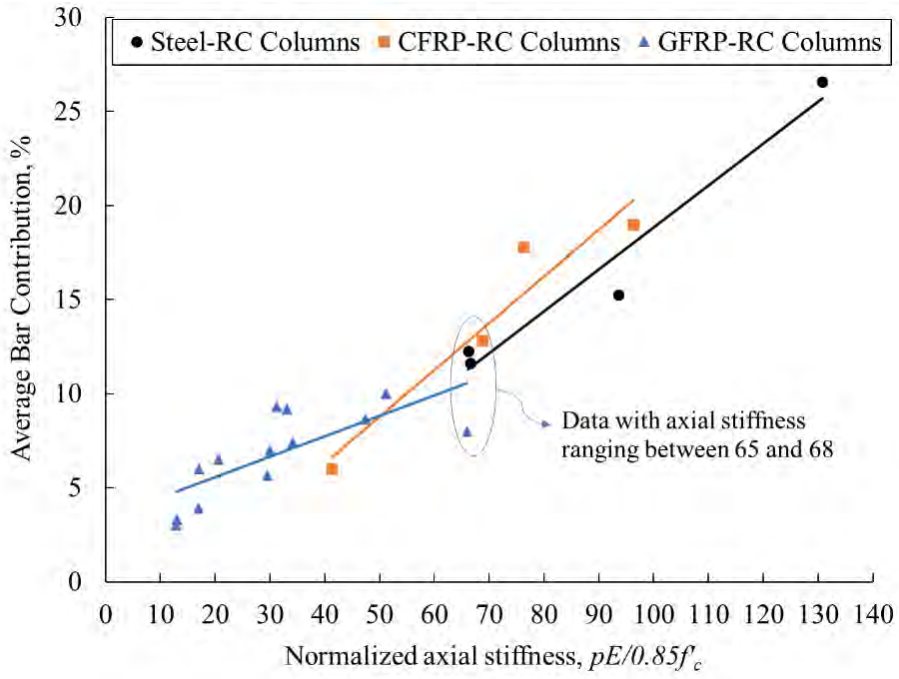


Figure 2.1: Normalized axial stiffness versus the contribution-to-capacity of FRP bars

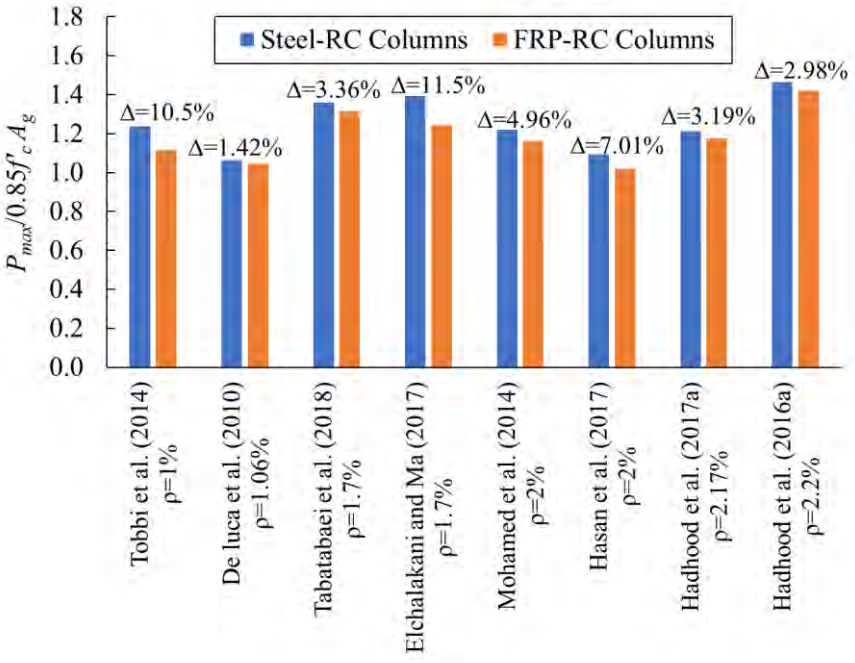


Figure 2.2: Axial capacities of concentrically-loaded FRP-RC columns normalized to $0.85f'_cA_g$

The data collected from each study refer to the average capacities of the tested columns having similar longitudinal reinforcement ratios but not necessarily similar transverse reinforcement ratios. Figure 2.2 also shows the difference between the normalized

capacities of steel-RC and FRP-RC columns, $\Delta$, for different reinforcement ratios, $\rho$. It can be observed that steel-RC columns attained slightly higher capacities than their FRP-RC counterparts, having similar reinforcement ratios, with percentage differences ranging between 1.42% (for $\rho$ = 1.06%) and 11.5% (for $\rho$ = 1.7%), which can also be attributed to the higher modulus of steel bars as compared to that of FRP bars. This small variance in capacities between the steel-RC and FRP-RC columns indicates the potential of FRP bars to contribute to the capacity of RC columns as equivalently to steel bars.

***2.2.1.2. Eccentrically-loaded short FRP-RC columns.*** The condition of pure concentric compressive load is atypical in RC columns since bending moments usually exist. Bending moments significantly reduce the ultimate capacities of the columns due to the non-uniform stress distribution obtained. Moreover, eccentric loading exposes part of the concrete section to compression resulting in compressive stresses on one side of the column and tensile stresses on the opposite side.

Most of the collected studies reported that eccentrically-loaded FRP-RC columns failed abruptly in compression either by concrete crushing or FRP rupture in compression with no evidence of failure of FRP bars in tension [35, 45, 56-59, 61, 62, 67]. At high eccentricities, a less brittle flexural-compression failure was observed when the rupture of FRP bars in compression occurred followed by the rupture of bars in tension [42, 54, 58, 61, 67, 68] Hadhood et al. [60] suggested that failure of eccentrically-loaded GFRP-RC columns would not be tension-controlled for reinforcement ratios greater than 1%. In comparison, steel-RC columns usually fail in a less explosive mode due to buckling of bars in compression [57, 59, 61, 62].

A number of studies suggested that the contribution-to-capacity of FRP bars in eccentrically-loaded columns should be ignored [35, 57, 69], which was backed up by the fact that columns might fail due to buckling prior to the rupture of the bars. However, other studies showed that such contribution is significant and should not be ignored [42, 56, 58, 67]. Hadhood et al. [60] reported that ignoring the contribution of GFRP bars in compression underestimated the columns' capacities by 27% on average. In a more recent study, Guérin et al. [68] reported that GFRP bars in short square columns contributed 3, 5, and 13% of the load-carrying capacities at eccentricity-to-width ratios, *e/D*, of 10 to 20, 40, and 80%, respectively, while neglecting the bars in

tension. Hadhood et al. [58] recommended that the maximum compression strength of CFRP bars in eccentric columns be limited to 40% of the bars' tensile strength.

Moreover, an obvious behavior of eccentrically-loaded RC short columns is the decrease of their axial capacities as the *e/D* ratio increases. This behavior was reported to be more pronounced in FRP-RC columns as compared to steel-RC columns at low to moderate *e/D* ratios ranging between 12 and 24% [56, 57, 59, 62]. At large eccentricities, comparable load-carrying capacities were reported for both FRP-RC and steel-RC columns having the same reinforcement ratios [58, 61]. This can be attributed to the high strains developed in FRP bars at ultimate resulting in high contribution-to-capacity of FRP bars in tension.

Figure 2.3 shows the difference between the normalized capacities of steel-RC and FRP-RC columns, Δ, for various longitudinal reinforcement ratios, $\rho$, as obtained from the collected literature. It can be noticed that Δ ranged between 2.1 and 12.4%, indicating comparable capacities of both types of columns. The only exception occurred in the study conducted by Hadi and Youssef [57] in which Δ ranged between 17.6 and 18.9%.

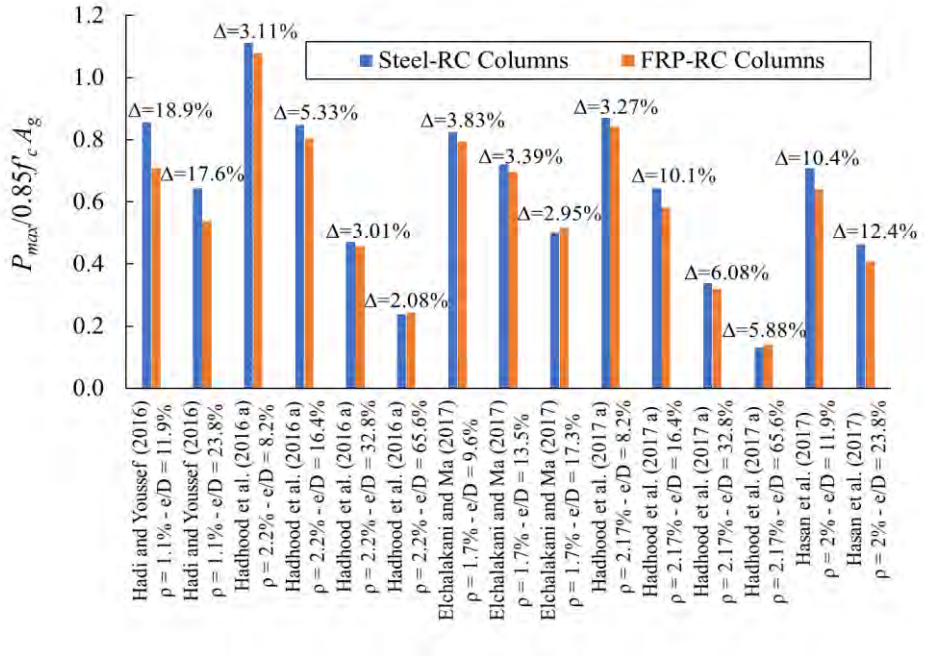


Figure 2.3: Axial capacities of eccentrically-loaded FRP-RC columns normalized to $0.85f'_cA_g$

***2.2.1.3. Ductility of FRP-RC short columns.*** Many parameters such as the ratio and distribution of the longitudinal reinforcement, the amount and spacing of transverse reinforcement, and the loading conditions affect the ductility of FRP-RC columns. Afifi et al. [49] reported that increasing the reinforcement ratio resulted in an increase in ductility of concentrically-loaded GFRP-RC columns. Similar conclusions were obtained by Afifi et al. [50] after testing axially-loaded CFRP-RC columns. Spirals with closer spacing provide more confinement to concrete core and prevent buckling of the longitudinal bars and hence increase the energy dissipation post the peak loads [35, 49, 50, 59, 70].

Researchers adopted different approaches to determine the ductility of FRP-RC columns resulting in discrepancies in ductility results. Pessiki and Pieroni [71] defined columns' ductility as the ratio of displacement corresponding to 85% of the ultimate load, $\Delta_{85}$, to that corresponding to the limit of the elastic behavior, $\Delta_1$. Following this approach, Pantelides et al. [48] reported that concentrically-loaded GFRP-RC columns exhibited equal or greater ductility than their steel-RC counterparts. Afifi et al. [49] determined the ductility indices of circular concrete columns reinforced with GFRP bars and spirals between 1.19 and 4.75, depending on the longitudinal reinforcement ratio provided and on the degree of confinement of the concrete core.

Alternatively, ductility of FRP-RC columns was determined as the ratio of the area under the axial load-displacement curve up to the ultimate displacement to the area under the curve up to the displacement corresponding to the limit of the elastic behavior. Following such approach, it was found that GFRP-HSC columns ($f'_c$ = 85 MPa) had 30% lower ductility than their steel-HSC counterparts when tested under concentric loading. However, under eccentric loading, GFRP-HSC columns had higher ductility than steel-HSC columns and their ductility increased as the load eccentricity increased [59]. It was also reported that, using both approaches, concentrically-loaded GFRP-RC columns showed lower ductility than that of steel-RC columns but experienced similar ductility under eccentric loading [57].

**2.2.2. Behavior of slender FRP-RC columns.** Slender columns encounter secondary moments that reduce their axial load-carrying capacities in comparison to those of short columns. The use of FRP bars as longitudinal reinforcement in slender columns adds another dimension of complexity due to the brittle nature of FRP bars

and their low compressive strength. The conducted review reveals substantial lack of information on the behavior of FRP-RC slender columns, which was attributed to the challenging experimental testing and the lack of comprehensive conclusions on the behavior of non-slender (short) columns.

The reported test results indicate that concentrically-loaded slender columns reinforced with GFRP bars exhibit similar capacities to their steel-reinforced counterparts [43, 55]. Failure of GFRP-RC columns generally occurs due to concrete crushing followed by the crushing of GFRP bars in compression whereas steel-RC columns fail due to buckling of their steel reinforcement. At large eccentricities, the performance of both types of columns is always governed by the stability of the columns rather than their capacities. Columns at large eccentricities fail due to buckling regardless of the type of their longitudinal reinforcement [55].

Concrete strength, rather than the longitudinal reinforcement ratio, has a significant effect on the load-carrying capacities of the FRP-RC slender columns since failure is usually governed by crushing of concrete. Xue et al. [43] reported that increasing the concrete strength of square GFRP-RC columns by 38 and 90% increased the columns' capacities by 60 and 114%, respectively. However, increasing the GFRP reinforcement ratio by 49 and 183% increased the capacities of the slender columns by only 4.3% and 16.6%, respectively [43]. In their parametric study on 11,0000 columns, Mirmiran et al. [72] concluded that the variations in strengths of FRP bars didn't affect the slenderness limits of RC columns.

The reported results also show the significance of confining the longitudinal bars with closely-spaced spirals or ties to prevent buckling of the longitudinal reinforcement. Hales et al. [55] concluded that GFRP spirals had a great potential to provide such confinement. Nonetheless, to the authors' knowledge, none of the previous studies have quantified the effect of confinement on the axial performance of slender FRP-RC columns.

**2.2.3. Effect of type of concrete on the behavior of FRP-RC columns.** While most of previous studies reported on FRP-RC columns cast with NSC ($f'_c$ between 29 and 43 MPa), a few studies reported on the advantages of using other concrete types such as high strength concrete (HSC), fiber-reinforced concrete (FRC), and inorganic polymer concrete (IPC). As previously stated, failure of NSC-columns reinforced with

FRP bars is usually governed by concrete crushing rather than the rupture of the bars. Theoretically, the use of HSC and FRC mixes can lead to high strains in the bars at ultimate resulting in more efficient utilization of the high tensile strength of FRP bars; and hence a considerable increase in the load-carrying capacities of FRP-RC columns [54, 61].

***2.2.3.1. High-strength concrete (HSC).*** A few studies have investigated the behavior of FRP-RC columns cast with HSC [54, 55, 59, 61, 62]. The results showed that the failure modes of FRP-RC columns cast in NSC and HSC were governed by concrete crushing, in particular when no or low eccentricities exist. Unexpectedly, Hadhood et al. [61] and Hadi et al. [59] reported that strains recorded at ultimate in the longitudinal FRP bars in NSC columns were close to or even higher than those recorded in HSC columns, indicating the insignificant effect of HSC in increasing the capacities of FRP-RC columns.

In comparison to steel-HSC columns, FRP-HSC columns showed equal or slightly lower load-carrying capacities under low to moderate load eccentricities [59, 61, 62]. However, at large eccentric loading ($e/D$ = 65.6%), FRP-HSC columns showed higher capacities than steel-HSC columns, reflecting the ability of FRP bars to develop higher strains at high levels of eccentric loading [61]. The shortage in data on the use of HSC in FRP-RC columns suggests that more tests are definitely needed to confirm the available conclusions.

***2.2.3.2. Fiber-reinforced concrete.*** It has been established that steel fibers control concrete cracking due to the bridging effect that they offer at crack locations and thus increase the concrete's ductility. It was reported that the addition of steel or polyvinyl alcohol (PVA) fibers in concrete columns reinforced with GFRP bars resulted in significant enhancement in their peak loads, confinement efficiency, and ductility [62, 63]. Hasan et al. [62] reported that GFRP-reinforced columns cast with steel-fiber high strength concrete (SFHSC) had similar ductility as steel-reinforced columns cast with HSC. The former columns also showed higher capacities than the steel-reinforced ones. More tests are definitely needed to support those findings.

***2.2.3.3. Inorganic polymer concrete (IPC).*** In order to reduce the carbon footprint associated with concrete and to enhance the sustainability of concrete infrastructure, the use of IPC mixes has attracted the attention of many researchers. In

addition to the low cost and wide availability of the materials used in IPC mixes, IPC is characterized by its low drying shrinkage and creep and its good resistance to fire, freeze-thaw cycles, and acid attack [66]. IPC mixes also exhibit high ductility indicated by its tensile strain hardening behavior and high flexural deformation capacity [41, 73-75]. Therefore, FRP-reinforced columns cast with IPC could have better deformation capacity than those cast in ordinary Portland cement concrete (OPC).

A few results have been reported on the load-carrying capacities of FRP-reinforced columns cast with IPC compared to those cast in OPC. Fan and Zhang [66] reported that eccentrically-loaded BFRP-IPC columns showed ultimate capacities about 70% of the capacities of the control ones (steel-reinforced columns cast in OPC). Elchalakani and Ma [35] and Elchalakani et al. [64] reported negligible effect of using geopolymer concrete (GPC) in FRP-RC columns and reported only 3.2% higher capacities than those cast with OPC. The discrepancy in the reported capacities could be attributed to the variation in the mechanical properties of IPC used in each test, which vary widely depending on the mix constituents and their relative proportions [76].

It was evident from the conducted literature that IPC mixes could better utilize the high strength of FRP bars than OPC. However, and due to the lack of studies on the topic, more tests are deemed necessary to gain further understanding of the behavior of FRP-reinforced columns cast with IPCs under different loading conditions.

**2.2.4. FRP-RC columns under seismic loading.** A few studies investigated the behavior of FRP-RC columns under lateral cyclic load simulating seismic excitations [40, 77-80]. FRP bars do not yield, which results in a linear elastic moment-curvature in FRP-RC columns with no post-peak decline. Unlike steel spirals, FRP spirals provide increased levels of confinement with increased deformation due to their higher strains at ultimate. Large deformations delay crushing of the concrete core at ultimate in columns reinforced with FRP transverse reinforcement. This conclusion was confirmed by Tavassoli et al. [40], Tavassoli and Sheikh [77], and Ali and El-Salakawy [78] who reported that GFRP spirals or stirrups prevented the expansion of the concrete core in all of FRP-RC columns up to failure. Steel transverse reinforcement were reported to be less effective than their GFRP counterparts in confining the concrete core after yielding, which was attributed to the significant loss of stiffness in steel bars at this stage [40, 77, 78].

RC columns reinforced with longitudinal and transverse GFRP bars showed high levels of deformability and achieved lateral drift ratios higher than the design values when subjected to lateral cyclic quasi-static loading [40]. Elshamandy et al. [80] reported that GFRP-RC columns achieved drifts between 50 and 180% more than the estimated drifts according to most building codes. These findings confirmed those of Ali and El-Salakawy [78] who reported that the drift capacities of GFRP-RC columns ranged between 8.5 to 12.5% exceeding the 2.5 and 4% minimum drift capacities imposed by the National Building Code of Canada, NBCC [81] and the CSA-S806-12 [27], respectively. Increasing the longitudinal reinforcement ratio increased the lateral capacity but resulted in low deformability at failure. In this regard, Ali and El-Salakawy [78] reported that GFRP-RC columns showed about 50% lower energy absorption during reversed cyclic loading than that of steel-RC ones.

The splice length of the longitudinal bars has a significant effect on the drift ratios that could be attained by FRP-RC columns. Naqvi et al. [79] reported that GFRP-RC columns with splice length of 40 times the bar diameter performed well at low drift ratios but showed significant strength degradation at high drift ratios when subjected to simultaneous axial and quasi-static cyclic reversed loads. Increasing the splice length to 60 times the bar diameter resulted in drift ratios at failure of 5 and 3.13 times those recommended by NBCC [81] and CSA-S806-12 [27], respectively.

**2.2.5. Hybrid (steel-FRP) reinforced columns.** The concept of supplementing FRP bars with steel bars in a hybrid system to reinforce concrete structures has attracted many researchers as a practical solution to overcome the ductility and serviceability problems of purely FRP-RC members. In hybrid systems, the addition of steel reinforcing bars ensures the ductility of the concrete member and enhances its serviceability while FRP bars maintain its load-carrying capacity [82]. Near-surface-mounted (NSM) technique is one form of the hybrid construction in which FRP bars are placed near the tensile surface of concrete to strengthen steel-RC members. Research studies conducted on NSM hybrid reinforcement showed its effectiveness in restoring the strength and serviceability of the concrete columns [83]. However, the use of hybrid systems in reinforcing RC columns is relatively new and has rarely been investigated by researchers. Hales et al. [55] reported that slender RC columns reinforced longitudinally with hybrid GFRP and steel bars achieved higher load-carrying capacities than those reinforced with steel or GFRP reinforcement only.

Ibrahim et al. [84] showed that hybrid-RC columns reinforced with 2% steel and 0.8% BFRP longitudinal bars and confined with BFRP jackets achieved comparable lateral strength to columns reinforced longitudinally with 4% steel. This shows that hybrid steel-FRP reinforcements can be a viable method of reinforcing RC columns subject to seismic loads.

**2.2.6. FRP transverse reinforcement.** A number of research studies have investigated the behavior of RC columns having FRP as transverse reinforcement [40, 41, 48, 51, 77]. Different aspects of transverse reinforcements were investigated including their shape, spacing, configuration, and volumetric ratio. As previously stated, FRP transverse reinforcement provides increased levels of confinement to the concrete core with increased deformation capacities due to their high strains at ultimate [35, 46, 50, 52, 53, 58, 60, 78, 85].

***2.2.6.1. Effect of spacing and volumetric ratio.*** FRP transverse reinforcements showed more pronounced effects on ductility and confinement efficiency than on capacities of FRP-RC columns [49, 50]. Improvements of 3 to 6% in strength versus 57 to 208% in ductility and 21 to 43% in confinement efficiency were observed as the spiral spacing was reduced from 120 to 40 mm, respectively [49, 50]. Similar findings were reported by Hadi et al. [56] who demonstrated that reducing spacing of GFRP helices from 60 to 30 mm resulted in an increase in peak loads and ductility by 7 and 29%, respectively. Elchalakani and Ma [35] reported that rectangular RC columns reinforced with longitudinal and transverse GFRP bars were found to be more ductile than their steel-RC counterparts. The provisions of CSA-S806-12 [27] and ACI440.1R-15 [2] for FRP reinforcement mandate the spacing of transverse FRP reinforcement to be equal to the least column dimension, 16 times the diameter of the longitudinal bars, or 48 times the diameter of the ties, and with a maximum of 75 mm for spirals. These requirements are similar to those mandated by ACI 318-14 [44] and CSA-A23.3-14 [86] for steel transverse reinforcement. Nevertheless, several studies concluded that larger volumetric ratios and/or smaller spacing are required for FRP reinforcement to perform comparably to their steel counterparts [46-50, 56, 59, 67, 68, 70, 87]. These requirements were justified by the lower modulus of elasticity of FRP reinforcement as compared to steel [55].

Guérin et al. [67, 68] reported that using a maximum GFRP tie spacing of half

the limit mandated in ACI318-14 [44] was adequate to prevent buckling of the longitudinal reinforcement and to confine the concrete core in post-peak stages. De Luca [46] reported that FRP transverse reinforcement shouldn't be designed according to the same requirements of steel transverse reinforcement, as this would result in undesirable brittle failure of FRP-reinforced columns. Based on a thorough theoretical analysis, Zadeh and Nanni [87] suggested limits on the maximum spacing of FRP ties of at least the smallest column dimension, 12 times the diameter of the longitudinal bars, or 24 times the diameter of the ties used.

On the other hand, some studies reported that the design provisions of CSA S806-12 [27] for FRP transverse reinforcement ensured adequate confinement of the concrete core of FRP-reinforced columns up to the estimated axial capacities [51, 53, 54, 59]. A minimum volumetric ratio of 1.5% of FRP transverse reinforcement was recommended to ensure ductile and less explosive mode of failure at ultimate [49-51], contradictory to the minimum ratio specified in CSA S-806-12 [27], which can reach values less than 1.5%. In general, FRP spirals of small size placed at close spacing are always recommended over spirals with large size and large spacing to ensure ductility and confinement efficiency of the concrete core.

***2.2.6.2. Effect of shape.*** Previous studies showed that GFRP or CFRP spirals provided more confinement and improved columns ductility and, in some cases, higher strengths over GFRP or CFRP hoops [41, 51, 53]. This is attributed to the continuous nature of spirals that provide uniform lateral confining pressure to the concrete core [41, 51]. The effects of different tie configurations on the strength and toughness of the confined concrete were investigated by Tobbi et al. [47]. Of the four different tie configurations shown in Figure 2.4, configuration 4 was found to be the most effective in improving the strength and toughness of the confined concrete [47, 52, 85].

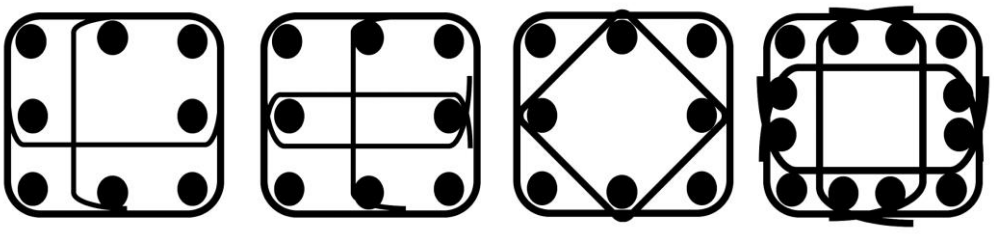

Figure 2.4: Different configurations of GFRP ties tested by Tobbi et al. [47]

**2.2.7. Design equations for FRP-RC columns.** Table 2.3 lists the design equations proposed in previous studies to determine the axial capacities of FRP-RC columns. Ratios of the predicted-to-experimental capacities, $P_{pred}/P_{exp}$, using the proposed equations are also listed in Table 2.3 and shown in Figure 2.5. As stated previously, while some researchers suggested neglecting the contribution of the longitudinal FRP bars to the columns' capacities, other researchers adopted various philosophies to determine such contribution. Figure 2.5 shows the variation in FRP contribution to the columns' capacities as determined in previous studies. It can be observed that the majority of these studies (58% of the collected data) have reported that FRP contribution ranges between 5 and 12% whereas 21% of the collected data reported a contribution of more than 12%, exceeding the commonly-reported contribution for steel bars. The following sections summarize the different approaches that previous researchers have adopted to determine the contribution of FRP bars to the ultimate capacities of FRP-RC columns.

***2.2.7.1. Approach 1: Neglecting the contribution of FRP bars in compression.*** Currently, the design guidelines ACI-440.1R-15 [2] prohibit the use of FRP bars as reinforcement in compression members. According to CSA-S806 [27], the nominal unconfined axial load capacity of columns with FRP longitudinal reinforcement is calculated as per Equation 2.1 (Table 2.3), in which the contribution of FRP bars to the columns' capacities is nil. As shown in Figure 2.5a, neglecting the contribution of FRP bars to the capacities of FRP-RC columns underestimated the columns capacities by 23% on average.

***2.2.7.2. Approach 2: Contribution of FRP bars based on reduced tensile strength.*** The concept of using a reduction factor to account for the low compressive strengths of FRP bars has been adopted by several researchers. The proposed equations consider the contribution of concrete in addition to a reduced contribution from the FRP bars as shown in Equation 2.2 and Equation 2.3 in Table 2.3. The reduction factor, $\alpha_f$, represents the ratio of compressive strength to the tensile strength of FRP bars. Tobbi et al. [47] considered $\alpha_f = 0.35$ as suggested by Wu [36] and Kobayashi and Fujisaki [38]. The proposed equation (Equation 2.2 in Table 2.3) yielded a ratio $P_{pred}/P_{exp}$ between 0.92 and 1.02 for GFRP-RC columns as reported in Tobbi et al. [47] and Afifi et al. [49]. For CFRP bars, Afifi et al. [50] proposed that $\alpha_f$, be taken as 0.25 as estimated from the test results (Equation 2.3 in Table 2.3).

Table 2.3: Summary of the design equations available in the literature for FRP-RC columns

| Reference | Proposed Equation | Equation | FRP | $P_{pred}/P_{exp}$ |
|---|---|---|---|---|
| Approach 1: No contribution-to-capacity for FRP bars | | | | |
| CSA-S806 [27] | $P_{pred} = \alpha_1 f_c'(A_g - A_f)$ $(\alpha_1 = 0.85)$ | 2.1 | All* | 1.0 |
| Approach 2: Contribution-to-capacity of FRP bars based on reduced compressive strengths | | | | |
| Tobbi et al. [47] | $P_{pred} = \alpha_1 f_c'(A_g - A_f) + \alpha_f f_{fu} A_f$ $(\alpha_1 = 0.85;\ \alpha_f = 0.35)$ | 2.2 | G | 1.0 |
| Afifi et al. [49] | $P_{pred} = \alpha_1 f_c'(A_g - A_f) + \alpha_f f_{fu} A_f$ $(\alpha_1 = 0.85;\ \alpha_f = 0.35)$ | 2.2 | G | 0.92 to 1.02 |
| Afifi et al. [50] | $P_{pred} = \alpha_1 f_c'(A_g - A_f) + \alpha_f f_{fu} A_f$ $(\alpha_1 = 0.85;\ \alpha_f = 0.25)$ | 2.3 | C | 0.91 to 0.99 |
| Approach 3: Contribution-to-capacity of FRP bars based on concrete strains at ultimate | | | | |
| Pantelides et al. [48] | $P_{pred} = \alpha_1 f_{cc}' A_c + 0.003 E_{ft} A_f$ $(\alpha_1 = 0.85)$ $(f_{cc}' = f_c' + 3.3\varphi_f k_a f_{lf})$ $\left(f_{lf} = \frac{2E_T A_{spFRP} \varepsilon_{fe}}{s d_c}\right)$ $(\varepsilon_{fe} = k_e \varepsilon_{fu})$ $(\varphi_f = 0.95,\ k_a = 1.0,\ k_e = 0.55)$ | 2.4 | G | 0.87 |
| Mohamed et al. [51] | $P_{pred} = \alpha_1 f_c'(A_g - A_f) + 0.002\ E_{ft} A_f$ $(\alpha_1 = 0.85)$ | 2.5 | G<br>C | 0.89 to 0.95<br>0.91 to 1.0 |
| Tobbi et al. [52] | $P_{pred} = \alpha_1 f_c'(A_g - A_f) + \varepsilon_{co} E_{ft} A_f$ $(\alpha_1 = 0.85)$ | 2.6 | All* | 0.89 to 1.0 |
| Hadi et al. [56] | $P_{pred1} = \alpha_1 f_c'(A_g - A_f) + 0.003 E_{ft} A_f$<br>$P_{pred2} = \alpha_1 f_{cc}'(A_c - A_f) + \varepsilon_{cc} E_{ft} A_f$<br>$(\alpha_1 = 0.85)$ | 2.7<br>2.8 | G | 0.9 to 0.92 |
| Maranan et al. [41] | $P_{pred} = \alpha_1 f_c'(A_g - A_f) + 0.002 E_{ft} A_f$ $(\alpha_1 = 0.9)$ | 2.9 | G | 0.9 to 1.47 |
| Hadhood et al. [58] | $P_{pred} = \alpha_1 f_c'(A_g - A_f) + 0.0035 E_{ft} A_f$ $(\alpha_1 = 0.85 - 0.0015 f_c' \geq 0.67)$ | 2.10 | C | 0.82 |
| Hadhood et al [61] | $P_{pred} = \alpha_1 f_c'(A_g - A_f) + 0.0035 E_{ft} A_f$ $(\alpha_1 = 0.85 - 0.0015 f_c' \geq 0.67)$ | 2.10 | C | 0.94 |
| Youssef and Hadi [69] | $P_{pred} = \alpha_1 f_c'(A_g - A_f) + \varepsilon_{co} E_{ft} A_f$ $(\alpha_1 = 0.85)$ | 2.11 | G | 0.974 |
| Hadhood et al. [60] | $P_{pred} = \alpha_1 f_c'(A_g - A_f) + 0.003 E_{ft} A_f$<br>$P_{pred} = \alpha_1 f_c'(A_g - A_f) + 0.0024 E_{ft} A_f$<br>$P_{pred} = \alpha_1 f_c' A_g$<br>$P_{pred} = \alpha_1 f_c'(A_g - A_f)$ $(\alpha_1 = 0.85)$ | 2.12a<br>2.12b<br>2.12c<br>2.12d | G<br>G<br>G<br>G | 0.83<br>0.81<br>0.74<br>0.73 |
| Xue et al. [43] | $P_{pred} = \alpha_1 f_c' A_g + 0.002 E_{ft} A_f$ $(\alpha_1 = 0.85)$ | 2.13 | G | 1.10 |

*All = all types of FRP bars

$A_c$= area of confined concrete core measured to the outside diameter of spiral; $A_f$= area of FRP longitudinal reinforcement; $A_g$= gross area of column section; $E_{ft}$= tensile modulus of elasticity of FRP bars; $f_c'$= compressive strength of concrete; $f_{cc}'$= compressive strength of confined concrete; $f_{fu}$= FRP tensile strength; $P_{pred1}$= nominal capacity corresponding to first peak load; $P_{pred2}$= nominal capacity corresponding to second peak load; $\alpha_1$= reduction factor; $\varepsilon_{cc}$= strain in confined concrete core; $\varepsilon_{co}$= concrete strain at peak stress; $\varepsilon_{fu}$= ultimate strain in FRP; $A_{spFRP}$ = area of FRP spiral; $d_c$= spiral outside diameter; $s$ = spiral pitch.

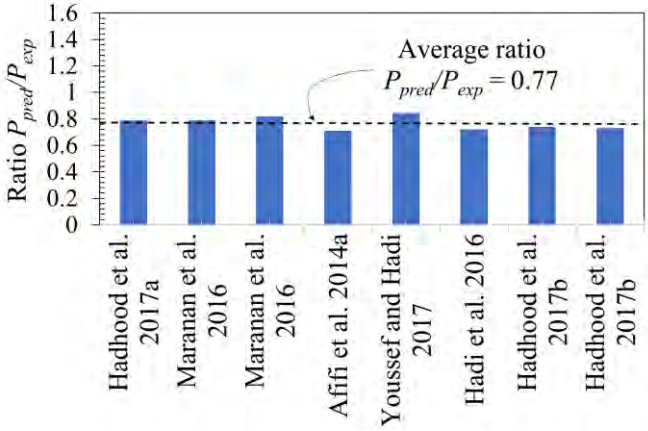


(a) Approach 1: Neglecting the contribution of FRP bars in compression

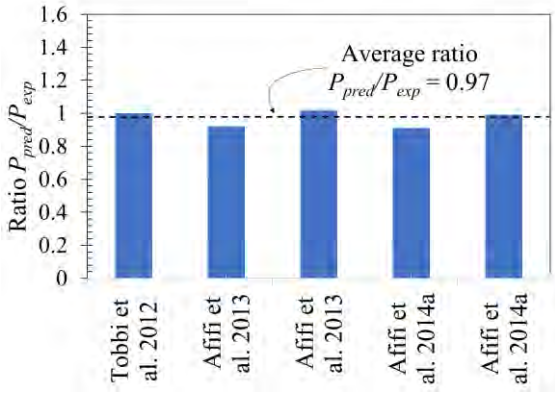


(b) Approach 2: Contribution of FRP bars based on a percentage reduction of their tensile strength

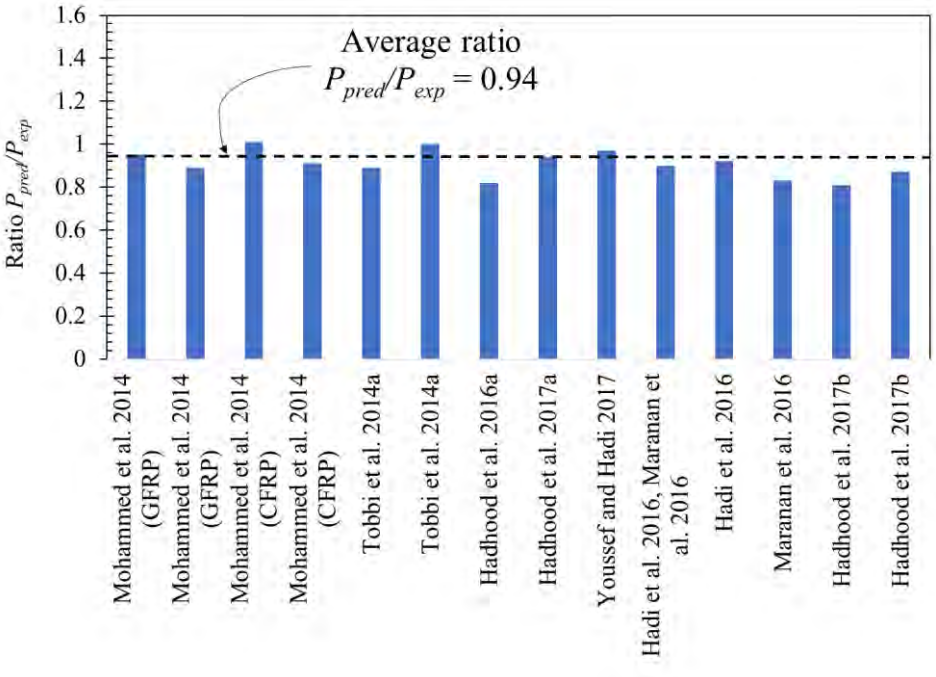


(c) Approach 3: Contribution of FRP bars based on their strength at certain level of concrete strain

Figure 2.5: Ratio of predicted-to-experimental capacities, $P_{pred}/P_{exp}$, of FRP-RC columns using different approaches

Using Equation 2.3, the ratio $P_{pred}/P_{exp}$ for CFRP-RC columns ranged between 0.91 to 0.99 with an average ratio of 0.97 as shown in Figure 2.5b. More research, however, is needed to generalize the value of $\alpha_f$ for different types of FRP bars. For this reason, other researchers suggested design equations that are based on strain compatibility between FRP bars and concrete as explained in the following section.

***2.2.7.3. Approach 3: Contribution of FRP bars based on concrete compressive strain.*** Design equations developed using this approach account for the strains developed in FRP bars, $\varepsilon_f$, to determine their contribution-to-capacity of FRP-RC columns (Equation 2.4 to Equation 2.13 in Table 2.3). Based on the strain compatibility between concrete and FRP bars, $\varepsilon_f$ was taken equal to the strain developed in concrete, $\varepsilon_c$, at ultimate, which ranged between 0.2 and 0.35%. Using this approach leads to an average ratio $P_{pred}/P_{exp}$ = 0.94 as shown in Figure 2.5c, which indicates a slight underestimation of capacities of FRP-RC columns by approximately 8%.

Pantelides et al. [48] recommended the use of Equation 2.4 (Table 2.3) that considered only the confined concrete core strength, $f'_{cc}$, while predicting the capacities of FRP-RC columns to reflect the spalling of concrete cover observed at failure. Confinement expressions initially developed for columns wrapped with external FRP jackets [88] were modified for the case of FRP spirals. Mohamed et al. [51] recommend that $\varepsilon_f$ be taken as 0.002, which is the strain limit developed in FRP bars at the onset of micro-cracking in the plastic stage of concrete (Equation 2.5 in Table 2.3). In their equation, Tobbi et al. [52] used $\varepsilon_f$ equal to the concrete strain at its peak stress, $\varepsilon_{co}$ (Equation 2.6 in Table 2.3).

Hadi et al. [56] proposed Equation 2.7 and Equation 2.8 in Table 2.3 corresponding to the peak loads that the GFRP-RC columns exhibited prior to failure. The first peak represents the maximum axial load carried by the gross concrete section while the second peak represents the maximum axial load carried by the confined concrete core only, after the concrete cover has spalled off. The authors suggested that $\varepsilon_f$ be taken equal to the concrete strain at ultimate ($\varepsilon_f$ = 0.003) for the first peak load and to the confined concrete core strain, $\varepsilon_{cc}$, for the second peak load.

Maranan et al. [41] proposed a strain limit of $\varepsilon_f$ = 0.002 for FRP-RC columns cast with geo-polymer concrete, which is the strain at which the plastic deformation of geo-polymer concrete initiates (Equation 2.9 in Table 2.3). The authors proposed a

higher concrete strength reduction factor $\alpha_1$ of 0.9 instead of 0.85 owing to the higher modulus and deformation of geo-polymer concrete compared to those of normal concrete. On the other hand, Hadhood et al. [58, 61] proposed the reduction factor $\alpha_1$ to be calculated according to CSA S806-12 [27] as $0.85 - 0.0015f'_c \geq 0.67$ (Equation 2.10 in Table 2.3). They also proposed that the strain level in FRP bars be equal to the concrete strain at failure (0.0035 according to CSA S806-12 [27]). Youssef and Hadi [69] also proposed the use of $\varepsilon_f = 0.003$ whereas $\alpha_1$ was taken as 0.85 (Equation 2.11 in Table 2.3).

In a comparative study, Hadhood et al. [60] proposed four design equations for FRP-RC columns considering different contributions of GFRP bars to the ultimate columns' capacities (Equation 2.12 in Table 2.3). In the first equation (Equation 2.12a), full contribution of the GFRP bars in compression was assumed by taking the compression modulus of GFRP bars, $E_{fc}$, equal to its tensile modulus, $E_{ft}$. In Equation 2.12b, $E_{fc}$ was taken as 80% of $E_{ft}$, according to the findings of Wu [36] while in Equation 2.12c and Equation 2.12d, the contribution of GFRP bars in compression was ignored while disregarding the concrete displaced by the bars in the former equation and considering it in the latter one. The results showed that the predicted capacities using Equation 2.12a and Equation 2.12b correlated well with the experimental results ($P_{pred}/P_{exp}$ ratio = 0.83 and 0.81, respectively). Using Equation 2.12c and Equation 2.12d provided conservative values with $P_{pred}/P_{exp}$ ratio = 0.74 and 0.73, respectively. In a more recent study, Xue et al. [43] proposed a design equation (Equation 2.13) for slender FRP-RC rectangular axially-loaded columns. The authors proposed that strain in FRP bars be limited to 0.002 with $\alpha_1$ taken as 0.85.

**2.2.8. Analysis of previous data.** The design equations proposed for FRP-RC columns, given in Table 2.3, are used to analytically determine the nominal axial compressive capacities of 91 concentrically-loaded short columns collected from previous studies. Values of the required parameters such as concrete compressive strength, $f'_c$, column cross-sectional area, $A_g$, longitudinal reinforcement area, $A_f$, modulus of elasticity of FRP bars, $E$, ultimate tensile strength of FRP bars, $f_{fu}$, and concrete strain, $\varepsilon_c$, were collected for all columns under study. The predicted axial capacities of all columns were then compared against the experimental capacities obtained in each study. The average ratio of predicted-to-experimental ratio, $P_{pred}/P_{exp}$, was calculated using each equation. Figure 2.6 shows the variation of the $P_{pred}/P_{exp}$ ratio

with the design equation used. It should be noted that Equation 2.4 and Equation 2.8 include the compressive strength of confined concrete, $f'_{cc}$, which in turn varies with the spiral stress at maximum load (in Equation 2.4) and on the second peak load (in Equation 2.8). Since such parameters can only be obtained experimentally, Equation 2.4 and Equation 2.8 could not be applied to other studies and are therefore excluded from Figure 2.6.

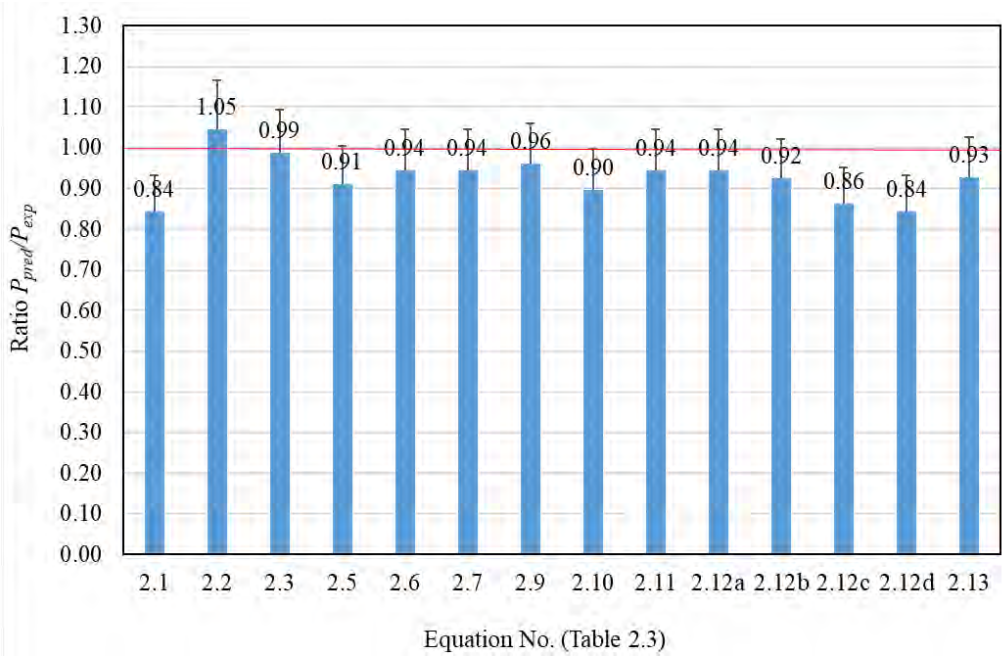


Figure 2.6: Variation of the predicted-to-experimental capacities ratio, $P_{pred}/P_{exp}$, with the design equations

Figure 2.6 shows that Equations 2.1, 2.12c, and 2.12d, which neglect the contribution of FRP bars to the load-carrying capacities of the columns, are quite conservative with average ratios of $P_{pred}/P_{exp}$ of 0.84, 0.86, and 0.84, respectively. It can also be seen that all equations yield average ratios of $P_{pred}/P_{exp}$ that are less than 1.0, with standard deviations varying between 0.088 and 0.105, except Equation 2.2 that yields an average $P_{pred}/P_{exp}$ ratio of 1.046. This finding confirms that assuming the contribution-to-capacity of FRP bars as 35% of their ultimate tensile strength, as suggested in Equation 2, overestimates the columns' capacities resulting in unconservative design. Moreover, the results of Figure 2.6 show that considering the contribution-to-capacity of FRP bars based on the ultimate concrete strain (of values

from 0.002 to 0.0035), as in Equations 2.5, 2.6, 2.7, 2.9, 2.10, 2.11, 2.12a, 2.12b, and 2.13, can yield accurate predictions of the ultimate capacities of FRP-RC columns with $P_{pred}/P_{exp}$ ratios of 0.89 to 0.96 and standard deviations of 0.094 to 0.102, respectively. Figure 2.6 shows that Equation 2.3 gives the most accurate prediction of the ultimate capacity of FRP-RC columns with an average $P_{pred}/P_{exp}$ ratio of almost 1.0 ($P_{pred}/P_{exp}$ = 0.99) and a standard deviation of 0.105. Recall that Equation 2.3 assumes the contribution-to-capacity of FRP bars as 25% of their ultimate tensile strength.

**2.2.9. Load-bending moment interaction diagrams for FRP RC columns.** Some studies developed axial load-bending moment (*P-M*) interaction diagrams for FRP RC columns from experimental results. They also developed *P-M* interaction diagrams theoretically and compared with the experimental *P-M* interaction diagrams. All of those studies suggested that *P-M* interaction diagrams can be satisfactorily developed for FRP RC columns based on simple sectional analysis procedures and assumptions consistent with those applicable to steel RC columns [54, 56, 58-62, 69, 89], which are as outlined below: Strain in the FRP bars and concrete are assumed to be directly proportional to the distance from the neutral axis i.e. plain sections remain plain after deformation.

a) A perfect bond is assumed between the FRP bars and concrete.

b) The equilibrium of forces and strain compatibility are satisfied.

c) The strength of concrete in tension is ignored.

d) The strength factors for concrete and FRP bars are set to unity.

e) A linear elastic stress-strain relationship till failure is used for the FRP bars in both tension and compression.

One difference observed in the *P-M* interaction diagrams between steel and FRP RC columns is that *P-M* interaction diagrams for FRP RC columns do not exhibit balance points and rather show points of sudden brittle failure [69, 90, 91]. This was attributed to the brittle nature of FRP bars as compared to steel bars, which are more ductile [90, 91]. However, this was contradicted in research by Hadhood et al. [54] in which it was found that load-bending moment interaction diagrams for GFRP RC columns have the characteristic inflection or balance points for steel RC columns.

**2.2.10. Concluding remarks from analysis of literature.** The results of more than 300 compression tests taken from 43 experimental studies have been collected.

The design equations proposed in the literature by different researchers were used to predict the load-carrying capacities of the tested columns in an attempt to provide an insight into their structural behavior. The following conclusions can be drawn from this literature analysis:

- The results of compressive strength on FRP bars showed that the compression strength and modulus of FRP bars ranged from 10 to 86% and 65 to 97% of their tensile strength and modulus, respectively, depending on the type of fibers of the bar.
- The analysis of previous data shows that the contribution of GFRP bars to the load-carrying capacities of RC columns is less than that of steel and CFRP bars whereas the contribution-to-capacity of CFRP bars is the same as or higher than that of steel bars. GFRP bars contribute by 3 to 14% to the total capacity of the columns compared to 6 and 19% for CFRP bars and 12 and 16% for steel reinforcing bars.
- Overall, FRP-reinforced columns exhibit lower load-carrying capacities than steel-reinforced columns when exposed to similar loading conditions depending on the reinforcement ratio provided. Columns reinforced with FRP bars exhibit 1.5 to 20% lower capacities than their counterpart steel-reinforced columns having equal longitudinal reinforcement ratios. However, they exhibit only 7 to 8% lower capacities than steel-reinforced columns with equal axial stiffness, which indicates the comparable behavior of both types of columns.
- At large load eccentricities, FRP-reinforced columns exhibit almost equal load-carrying capacities as their steel-reinforced counterparts having the same reinforcement ratios. This is attributed to the high strains developed in FRP bars at ultimate resulting in high contribution-to-capacity of FRP bars in tension.
- FRP-reinforced columns undergo similar failure modes as steel-reinforced columns. Eccentrically-loaded FRP-reinforced columns generally fail in compression due to concrete crushing at low to moderate eccentricities ($e/D = 8 – 60\%$) whereas columns loaded with high eccentricities ($e/D = 65 – 80\%$) are prone to fail in a flexural-tension mode.
- Similar to steel-reinforced columns, the ductility of FRP-reinforced columns is governed by the type of concrete used, the reinforcement ratio and type of the longitudinal reinforcement, and most importantly, by the volumetric ratio and type of transverse reinforcement. The ductility of FRP-reinforced columns is generally

lower than that of steel-reinforced columns under concentric loading but is higher at high load eccentricities.

- Concentrically-loaded slender columns reinforced with FRP bars exhibit similar or higher capacities to their steel-reinforced counterparts. At large eccentricities, the performance of both types of columns is governed by the stability of the columns rather than the type of their longitudinal reinforcement.
- FRP-reinforced columns achieve lateral drift ratios higher than the estimated drifts according to most building codes when subjected to lateral cyclic quasi-static loading. Increasing the longitudinal reinforcement ratio increases the lateral capacity of the columns but results in low deformability at failure.
- Large volumetric ratios and small spacing are required for FRP transverse reinforcements to achieve similar performance of steel transverse reinforcements in terms of ductility and confinement efficiency.
- Hybrid reinforcement is a promising alternative to all-FRP and all-steel reinforced columns. Hybrid-reinforced slender columns can achieve higher capacities and better overall performance than slender all-FRP and all-steel reinforced columns.
- Design equations implementing reduced compressive strengths of FRP bars (Approach 2) and strain compatibility between FRP bars and concrete (Approach 3) can predict accurately the load-carrying capacities of short columns reinforced with GFRP and CFRP bars with average $P_{pred}/P_{exp}$ ratio of 0.97 and 0.94, respectively. Neglecting the contribution-to-capacity of FRP bars (Approach 1) results in significant discrepancies between the predicted and experimental capacities.

# Chapter 3. Experimental Program

In this chapter, the methodology followed in this research is explained. The test matrix and the specimens design and fabrication procedure are described, followed by details on the materials properties. Finally, the instrumentation used in the tests as well as the test procedure are presented.

## 3.1. Experimental Scope

In this study, twenty-two reinforced concrete columns are tested under both concentric and eccentric loads. The columns are divided into two groups as given in Table 3.1. Group 1 consists of twelve columns described as follows: three columns reinforced with steel bars to serve as control specimens, three other columns reinforced with GFRP bars, and six columns reinforced with BFRP bars. Group 2 includes ten columns, all reinforced with BFRP bars. Columns of Group 1 are reinforced transversely with steel ties while those of Group 2 are reinforced with BFRP ties. Columns of each group are tested either under concentric or eccentric axial loads. The test parameters include the type and the ratio of the longitudinal and transverse reinforcements in addition to the eccentricity-to-depth ratio (*e/h*) of the applied load.

For Group 1, the first letter in the columns' label refers to the longitudinal reinforcement type (*S*=steel, *B*=basalt, *G*=glass). The first number refers to the longitudinal reinforcement diameter (16 or 20 mm) and the second number refers to the eccentricity value (0, 40 or 80 mm). For Group 2, the size of the longitudinal reinforcement is fixed in all columns (20 mm), and the first number in the column identification refers to the tie spacing (60, 120, or 180 mm) with the letter *T* referring to the ties.

## 3.2. Specimens Design and Fabrication

Details and dimensions of the column specimens are shown in Figure 3.1 and Figure 3.2, for columns tested under eccentric and concentric loading, respectively. The columns tested under eccentric loads are fabricated with corbels or haunches at the columns' ends as shown in Figure 3.1 to allow for the application of the eccentric load. All columns have square cross-sections of 180 x 180 mm, with concentrically-loaded columns measuring 1000 mm in height and the eccentrically-loaded columns measuring 1100 mm in height. The cross section of the columns is shown in Figure 3.3. A clear concrete cover of 27.5 mm is maintained in all columns.

Table 3.1: Test Matrix

| | Column ID | Longitudinal Reinforcement | | | Eccentricity (mm) | *e/h* (%) | Transverse Reinforcement | |
|---|---|---|---|---|---|---|---|---|
| | | Type | Bar Diameter (mm) | Reinforcement Ratio (%) | | | Type | Tie Spacing (mm) |
| **Group 1** | S-16-0 | Steel | 16 | 2.48 | 0 | 0 | Steel | 180 |
| | S-16-40 | Steel | 16 | 2.48 | 40 | 22.2 | Steel | 180 |
| | S-16-80 | Steel | 16 | 2.48 | 80 | 44.4 | Steel | 180 |
| | B-16-0 | BFRP | 16 | 2.48 | 0 | 0 | Steel | 180 |
| | B-16-40 | BFRP | 16 | 2.48 | 40 | 22.2 | Steel | 180 |
| | B-16-80 | BFRP | 16 | 2.48 | 80 | 44.4 | Steel | 180 |
| | B-20-0 | BFRP | 20 | 3.88 | 0 | 0 | Steel | 180 |
| | B-20-40 | BFRP | 20 | 3.88 | 40 | 22.2 | Steel | 180 |
| | B-20-80 | BFRP | 20 | 3.88 | 80 | 44.4 | Steel | 180 |
| | G-16-0 | GFRP | 16 | 2.48 | 0 | 0 | Steel | 180 |
| | G-16-40 | GFRP | 16 | 2.48 | 40 | 22.2 | Steel | 180 |
| | G-16-80 | GFRP | 16 | 2.48 | 80 | 44.4 | Steel | 180 |
| **Group 2** | B-T60-0 | BFRP | 20 | 3.88 | 0 | 0 | BFRP | 60 |
| | B-T60-40 | BFRP | 20 | 3.88 | 40 | 22.2 | BFRP | 60 |
| | B-T60-80 | BFRP | 20 | 3.88 | 80 | 44.4 | BFRP | 60 |
| | B-T120-0 | BFRP | 20 | 3.88 | 0 | 0 | BFRP | 120 |
| | B-T120-40 | BFRP | 20 | 3.88 | 40 | 22.2 | BFRP | 120 |
| | B-T120-80 | BFRP | 20 | 3.88 | 80 | 44.4 | BFRP | 120 |
| | B-T180-0 | BFRP | 20 | 3.88 | 0 | 0 | BFRP | 180 |
| | B-T180-40 | BFRP | 20 | 3.88 | 40 | 22.2 | BFRP | 180 |
| | B-T180-80 | BFRP | 20 | 3.88 | 80 | 44.4 | BFRP | 180 |
| | B-T60-80 (replicate) | BFRP | 20 | 3.88 | 80 | 44.4 | BFRP | 60 |

For specimens of Group 1, ties of diameter 10 mm and spacing 180 mm are used according to the recommendations of CSA S806-12 [27] and ACI 440.1R-15 [2]. Several researchers have concluded that smaller tie spacing is required for BFRP ties to attain similar performance to that of steel ties [35, 41, 46, 47, 49, 50, 53, 56, 92]. Therefore, tie spacing of 180 mm, 120 mm and 60 mm are used for columns of Group 2, to investigate the effects of reducing the tie spacing on the overall behavior of BFRP-RC columns. The ties spacing is reduced to 35 mm at the end of the columns and at the corbels to avoid premature failure at the columns ends.

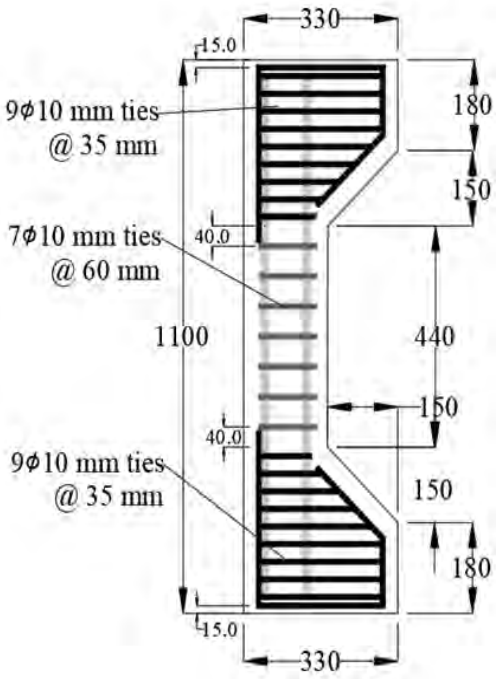


(a) Columns with tie spacing of 60 mm

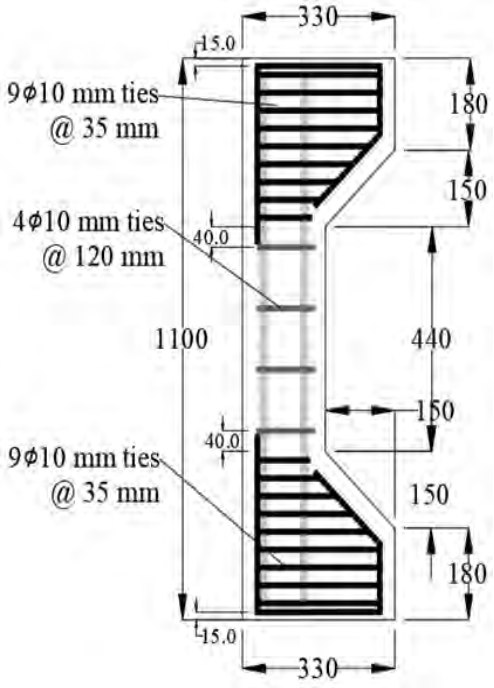


(b) Columns with tie spacing of 120 mm

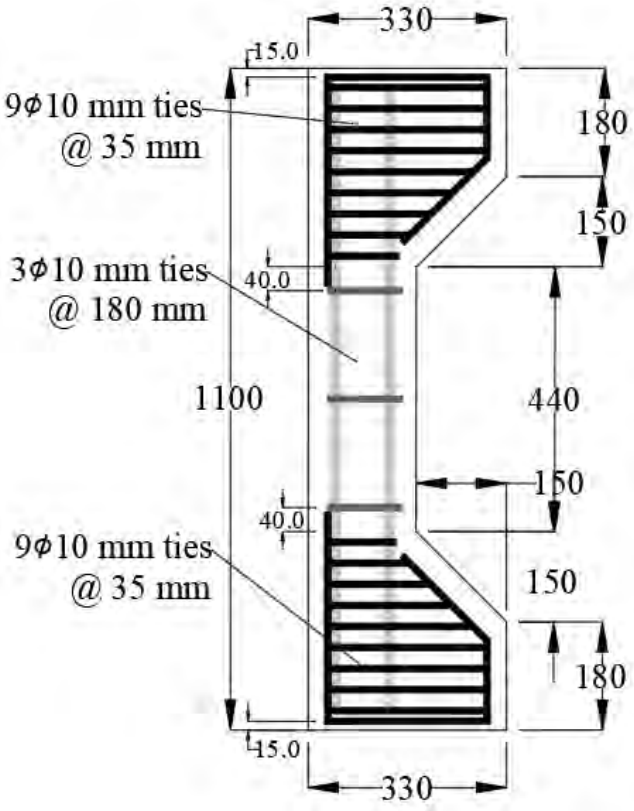


(c) Columns with tie spacing of 180 mm

Figure 3.1: Eccentric columns dimensional details (in mm)

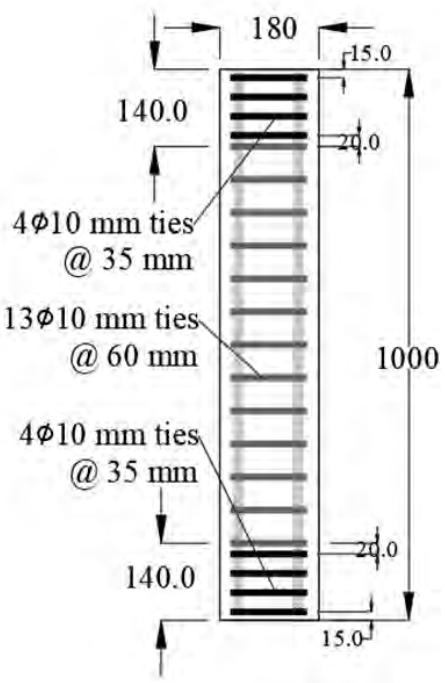


(a) Columns with tie spacing of 60 mm

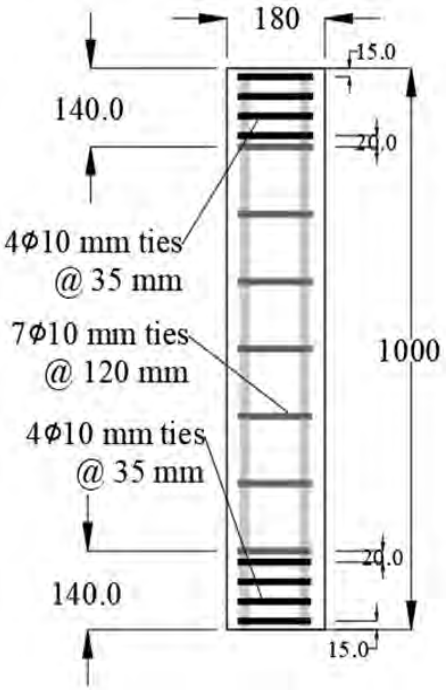


(b) Columns with tie spacing of 120 mm

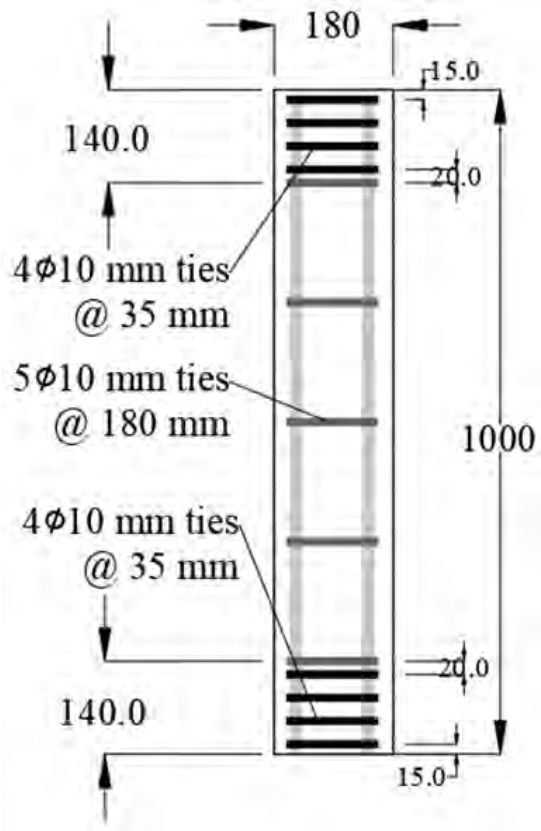


(a) Columns with tie spacing of 180 mm

Figure 3.2: Concentric columns dimensional details (in mm)

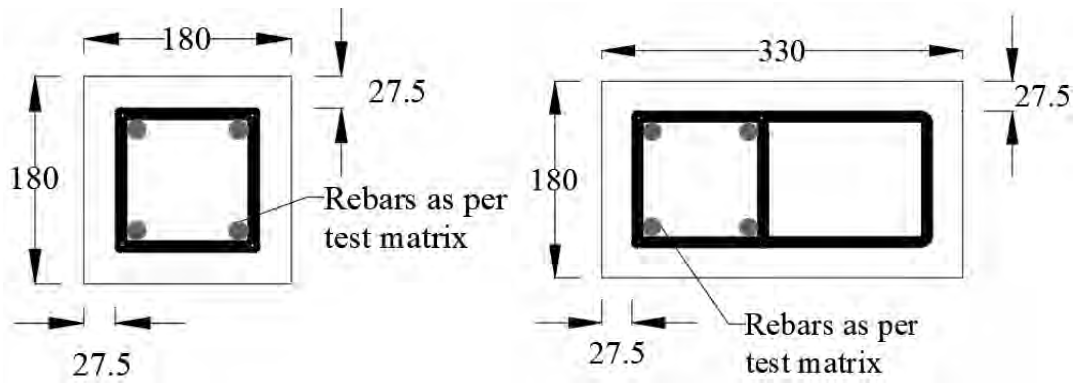


(a) Section at mid-height (b) Section at corbel

Figure 3.3: Columns Cross Section (in mm)

The selected columns' dimensions are dictated by the limitations of the available testing machine. The dimensions are selected to ensure the columns are large enough to meet the definition of columns as specified by design codes, are small enough to be maneuverable and to fit in the testing machine, while having ultimate capacities close to but not exceeding the maximum capacity of the testing machine of 2000 kN.

The Canadian Highway Bridge Design Code CAN/CSA S6-06 [93] defines a column as a compression member having a height-to-diameter ratio of 2.5 or more. According to ACI 318-11 [94], a column is a member primarily used to sustain axial compressive loads with a ratio of height to the least lateral dimension of at least 3. Moreover, ACI 318-14 [44] and CSA S806-12 [27] design codes, specify that columns having slenderness ratios, as calculated by Equation 3.1, of more than 22 shall be considered as slender columns. The columns tested in this study are designed with height-to-lateral dimension ratios of at least 4, to match the previous definitions, and with slenderness ratios of less than 22, to be considered as short columns.

$$\frac{L_e}{r} \leq 22 \qquad (3.1)$$

where, $L_e$ = effective column length,

and $r$ = radius of gyration of column's cross section.

All BFRP-RC columns are designed following the recommendations of CSA S806-12 [27]. Since there are currently no design guidelines for the design of FRP-RC columns, different approaches are used in the literature to determine the needed FRP

longitudinal reinforcement ratios. One of those approaches is the use of the equivalent strength method, which equates the force developed in the steel bars to that of the FRP bars using the relation ($f_y A_{st} = f_{fu} A_f$), where $f_y$ is the steel yield strength, $f_{fu}$ is the ultimate tensile strength of FRP, and $A_{st}$ and $A_f$ are the total longitudinal reinforcement areas of steel and FRP, respectively. This approach is adopted by a few researchers [51, 66]. Another approach is to use the same longitudinal reinforcement ratio for both steel and FRP bars for comparison purpose. In this study, both approaches are investigated. BFRP-RC columns having longitudinal reinforcement ratio of 2.48% are designed to have equal reinforcement ratio to steel-RC columns whereas BFRP-RC columns having longitudinal reinforcement ratios of 3.88% are designed to have four 20 mm diameter BFRP bars based on the equivalent strength of four 16 mm diameter steel bars ($f_y A_{st} = 0.35\ f_{fu} A_f$). A reduction factor of 0.35 is used to account for the lower compressive strength of BFRP bars compared to their tensile strength as suggested by some researchers [38, 42, 43] and as adopted in [47, 49].

### 3.3. Materials

All columns are cast with normal weight ready-mixed concrete. The average compressive strength of concrete is determined from the strength of three concrete cylinders of 150 mm x 300 mm tested according to ASTM C39 [95], and from the average compressive strength of three 150 x 150 x 150 mm concrete cubes, tested according to BS 1881-116:1983 [96]. Also, the tensile strength of concrete is determined by testing three concrete cylinders measuring 150 x 300 mm, in accordance with ASTM C496 [97].

The reinforcement cages are first prepared and then placed into wooden formwork to cast the columns. All columns are cast horizontally. Figure 3.4 shows some photos of the fabrication process. The columns are cured with wet burlap for 28 days, and the concrete cubes and cylinders are tested on the same day as the start of testing of the columns. All columns of Group 1 are cast in one day and from the same concrete batch, having an average cylinder compressive strength of 34.4 MPa. Columns of Group 2 are cast on another day from a concrete batch with an average cylinder compressive strength of 28.4 MPa. A summary of the concrete properties of both groups is shown in Table 3.2.

(a)

(b)

(c)

(d)

Figure 3.4: Fabrication process showing (a) a cage of an eccentrically-loaded column, (b) a cage of a concentrically-loaded column, (c) wooden formwork, and (d) a cage placed in the formwork

Table 3.2: Concrete properties for columns of Groups 1 and 2

| | Average cube compressive strength (MPa) | Average cylinder compressive strength (MPa) | Average split-tensile strength (MPa) | Average modulus of elasticity (GPa) |
|---|---|---|---|---|
| **Group 1** | 42.3 | 34.4 | 2.0 | 24.1 |
| **Group 2** | 31.7 | 28.4 | 2.3 | 22 |

The steel bars are tested in accordance with the provisions of ASTM A615 [98] to determine their tensile properties. A sample steel stress-strain curve is shown in Figure 3.5. The BFRP and GFRP bars used in this study are sand coated, and, in addition to the BFRP ties, are provided by Galen L.L.C., Russia. Samples of FRP bars and ties are shown in Figure 3.6.

The tensile properties of the BFRP and GFRP bars are determined according to ASTM D7205 [99]. The FRP bars are cut to have a minimum gage length of 40 times the bar diameter. Accordingly, BFRP and GFRP specimens of 16 mm diameter are cut at a gage length of 640 mm and a total grip length of 800 mm while BFRP bars of 20 mm diameter are cut at a gage length of 800 mm and a total grip length of 900 mm. Steel tubes with a thickness of 4.8 mm are fabricated to be used in gripping the FRP bars. A nano-grout material is used as an anchor filling material between the FRP bar and the steel tube. A 10 mm long strain gauges are mounted at mid-height of the FRP bars to measure the strain in the bars during testing. Figure 3.7 shows samples of the FRP bars prepared for the tensile tests. Representative stress-strain curves of the BFRP and GFRP longitudinal bars are shown in Figure 3.8. Properties of the steel, BFRP, and GFRP bars are shown in Table 3.3.

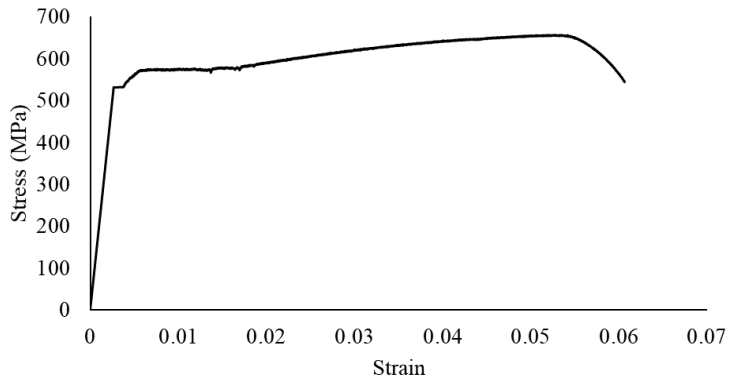


Figure 3.5: Steel bars stress-strain curve

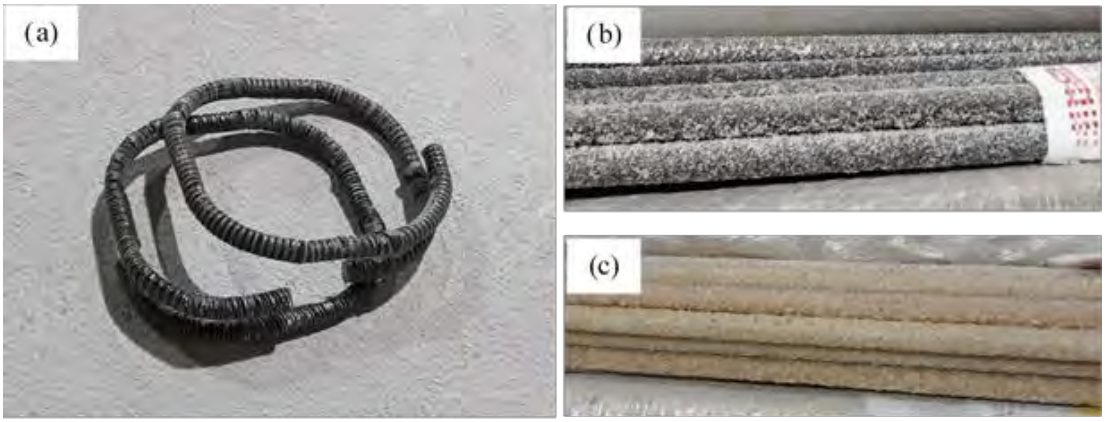


Figure 3.6: Samples of (a) BFRP ties, (b) BFRP bars, and (c) GFRP bars used in the study

(a)

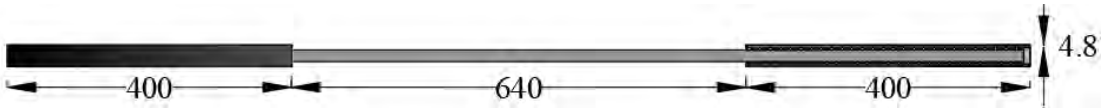


(b)

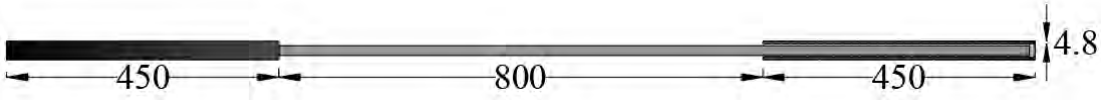


(c)

Figure 3.7: (a) BFRP bars prepared for tensile tests, schematic with dimensions (in mm) for (b) 16 mm diameter bars and (c) 20 mm diameter bars

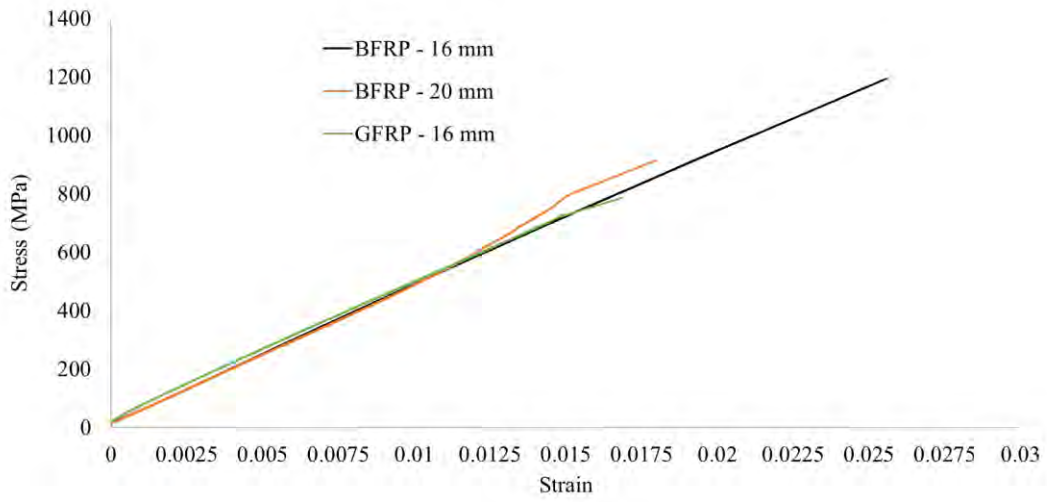


Figure 3.8: FRP bars stress-strain curves

Table 3.3: Properties of Steel and FRP Reinforcements

| Bar Type | Bar Diameter (mm) | Cross-sectional Area (mm²) | Yield Strength (MPa) | Ultimate Tensile Strength (MPa) | Modulus of Elasticity (GPa) | Ultimate Tensile Strain |
|---|---|---|---|---|---|---|
| BFRP | 16 | 201.1 | - | 1242±40 | 49.3±1.1 | 0.0252±0.0014 |
| BFRP | 20 | 314.2 | - | 913±8.8 | 45.9±5.5 | 0.0202±0.0026 |
| GFRP | 16 | 201.1 | - | 785±43 | 44.9±1.3 | 0.0175±0.0014 |
| Steel | 16 | 201.1 | 498±14.3 | 612±30.9 | 200 | 0.0575±0.0028 |
| BFRP Ties | 10 | 78.5 | - | na | na | na |
| Steel Ties | 10 | 78.5 | | 645±9.8 | 200 | 0.0847±0.0056 |

*na = not available

## 3.4. Instrumentation

The column specimens are instrumented using electrical strain gauges that are installed on their longitudinal reinforcement and on the concrete surface. Prior to casting the columns, strain gauges are installed on two of the longitudinal bars of each column at mid-height, one on the compression side and one on the tension side, to capture the axial strains in the bars during testing. After curing, three strain gauges are installed on the concrete surface: one in the vertical direction on the tension side, one in the vertical direction on the compression side, and one in the horizontal direction on the tension side. All strain gauges are mounted at mid-height of the specimens where maximum strains are expected. Before testing, one linear variable differential transducers (LVDT) is mounted vertically and another LVDT is mounted horizontally

to measure the vertical and lateral displacements, respectively, at mid-heights of the columns during loading. A schematic of the columns' instrumentation is shown in Figure 3.9. The strain gauges and LVDTs are connected to an automatic data acquisition system that records data at a rate of 10 readings per second.

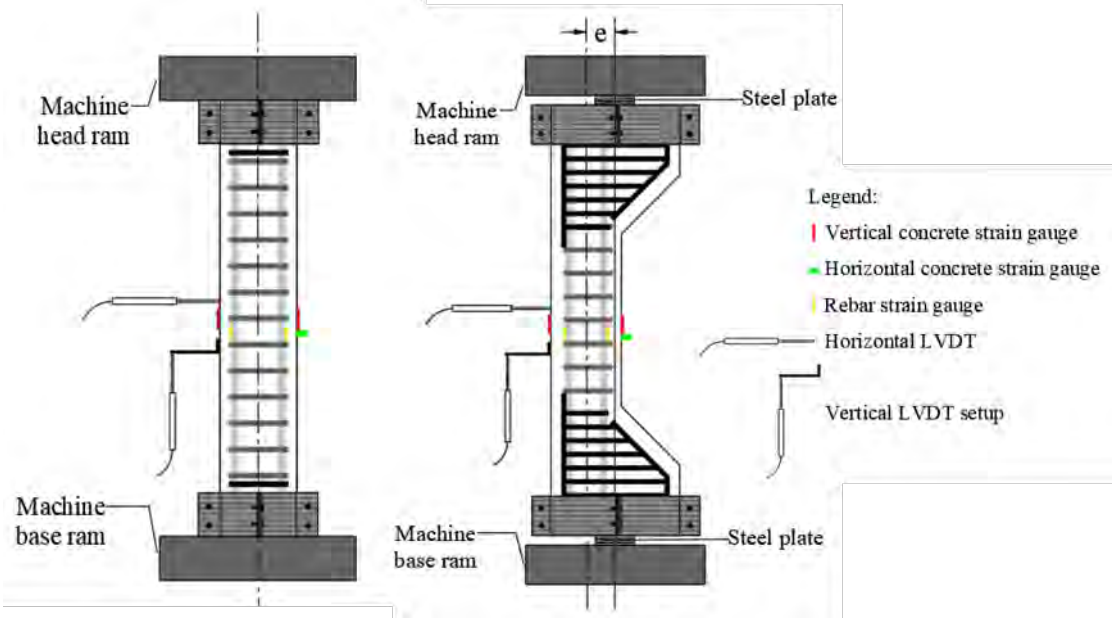


Figure 3.9: Schematic of column instrumentation and test setup

### 3.5. Testing Procedure

The columns are tested using a Universal Testing Machine (UTM) of a maximum capacity of 2000 kN available in the construction materials lab of the Civil Engineering Department at the American University of Sharjah. A displacement-controlled load is applied to all column specimens at a rate of 0.3 mm/min. The concentrically-loaded columns are mounted in such a way that their longitudinal axis coincides with the line of action of the applied force.

The test setup for the eccentric loading can be depicted in Figure 3.9. All columns are confined at both ends with 6 mm thick steel caps having inner dimensions equal to the columns' end dimensions and a total depth of 100 mm, to prevent premature failure at the columns' ends and thereby ensure failure within the column's length. Photos of the test setup for concentric and eccentric columns are shown in Figure 3.10.

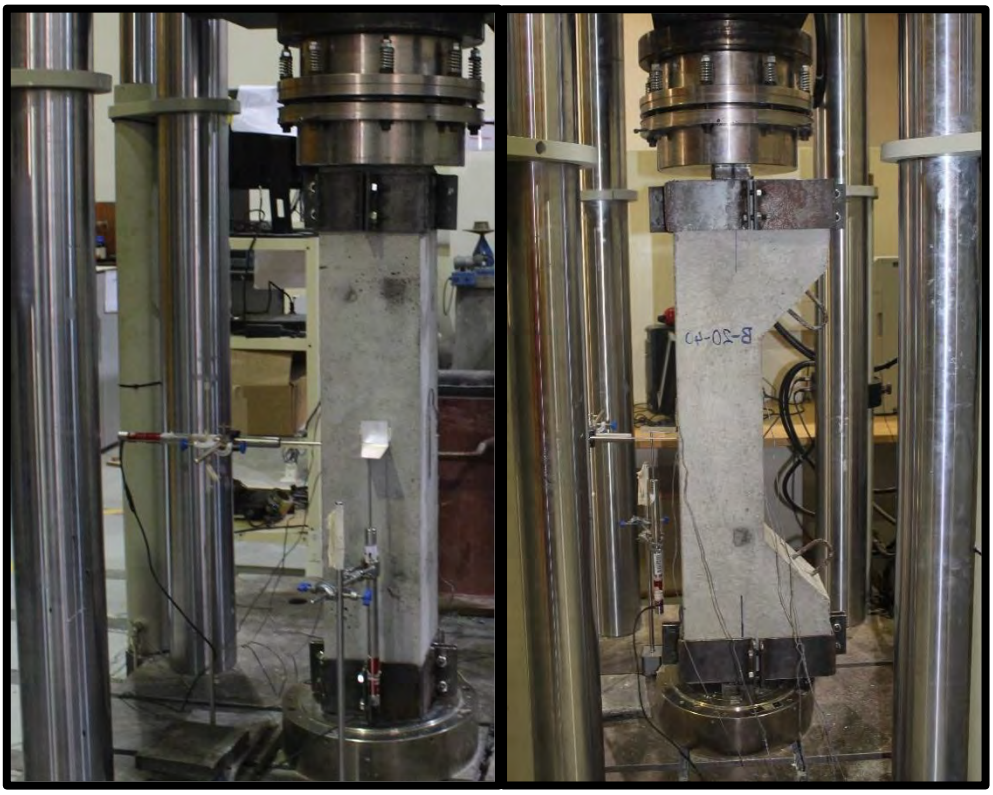

Figure 3.10: Photos of typical test setups for concentric columns (left) and eccentric columns (right)

# Chapter 4. Experimental Results

In this chapter, test results of all specimens are presented and discussed. The overall behavior and strength of the columns are discussed in terms of the failure modes, load-displacement, load-deflection and load-strain relationships.

## 4.1. Failure Modes

The failure modes of the tested columns were mainly affected by the level of eccentricity, and by the transverse reinforcement type and spacing. In general, failure modes were observed to be similar for columns subjected to the same loading condition, regardless of the longitudinal reinforcement type or ratio. However, under high eccentric loads, failure modes of columns were also affected by the type and ratio of longitudinal reinforcement. Photos of column specimens tested under concentric loads are shown in Figure 4.1, for Groups 1 and 2. Also, photos of column specimens tested under 40 mm and 80 mm eccentricities are shown in Figures 4.2 to 4.5, for columns of Groups 1 and 2.

**4.1.1. Concentrically-loaded columns.** Columns tested under pure axial loads, S-16-0, B-16-0, B-20-0, G-16-0, B-T60-0, B-T120-0 and B-T180-0, showed similar responses up to failure. No cracks were visible on the concrete cover up to about 83% of the peak loads. Limited vertical and horizontal hairline cracks started to appear at the columns' mid-heights at approximately 83% to 99% of the columns' peak loads. At this stage, several cracks appeared, and propagated from mid-height towards the columns' ends and around the columns. The cracks increased in numbers and widened as the load level increased up to peak. However, the concrete cover remained intact and attached to the concrete core, and did not spall off, even after peak loads were reached. At the end of the tests, inclined failure planes formed in the tested specimens (marked by red dashed lines on Figure 4.1). The diagonal failure planes occurred because of the shear sliding of the lower and upper parts of the columns after the cores were crushed. Similar observations were reported in previous studies [49, 50, 59]. Compression-controlled failure was observed for all specimens, due to concrete crushing for the FRP RC columns, and due to concrete crushing and yielding under compression for the steel RC column. No bars or ties rupturing or buckling occurred. Despite this, the specimen reinforced with BFRP ties at 120 mm spacing (B-T120-0) exhibited two peak loads before failure. The first peak load occurred at the time of cracking, and the second peak

occurred after some cover spalling had occurred at a load level of 76% of the first peak load, with the second peak being lower than the first peak. This indicates that the BFRP ties were activated in confining the concrete core after cover spalling.

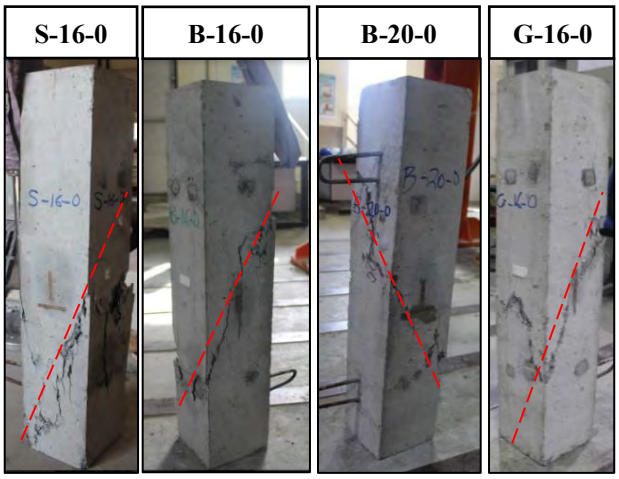


(a)

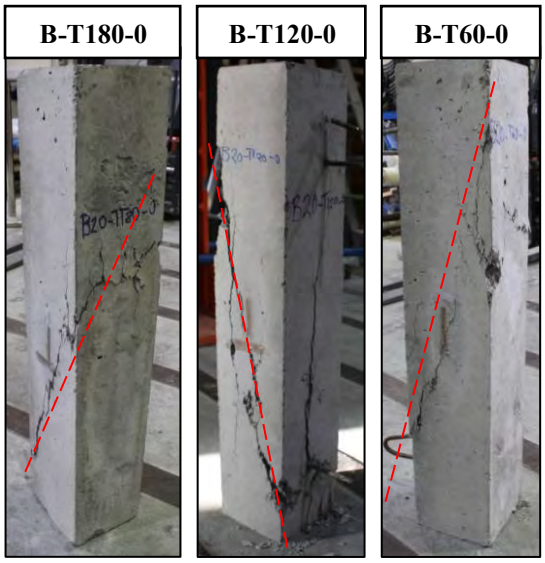


(b)

Figure 4.1: Photos of column specimens tested under concentric loads, after failure, for (a) Group 1 and (b) Group 2

**4.1.2. Eccentrically-loaded columns.** For columns tested under *e/h* ratio of 22.2% (S-16-40, B-16-40, B-20-40, G-16-40, B-T60-40, B-T120-40 and B-T180-40), concrete cracks appeared on the compression sides first followed by cracks on the

tension sides. Vertical and inclined compression cracks appeared at the columns' mid-heights at about 90% to 99% of the peak loads, followed by horizontal cracks on the tension sides. Three to four primary parallel cracks usually appeared at mid-heights on the tension sides of all specimens, and steadily propagated towards the lateral sides. Prior to that, no cracks were visible on the concrete cover. As the load increased, cracks on both tension and compression sides increased and widened, even after reaching peak loads.

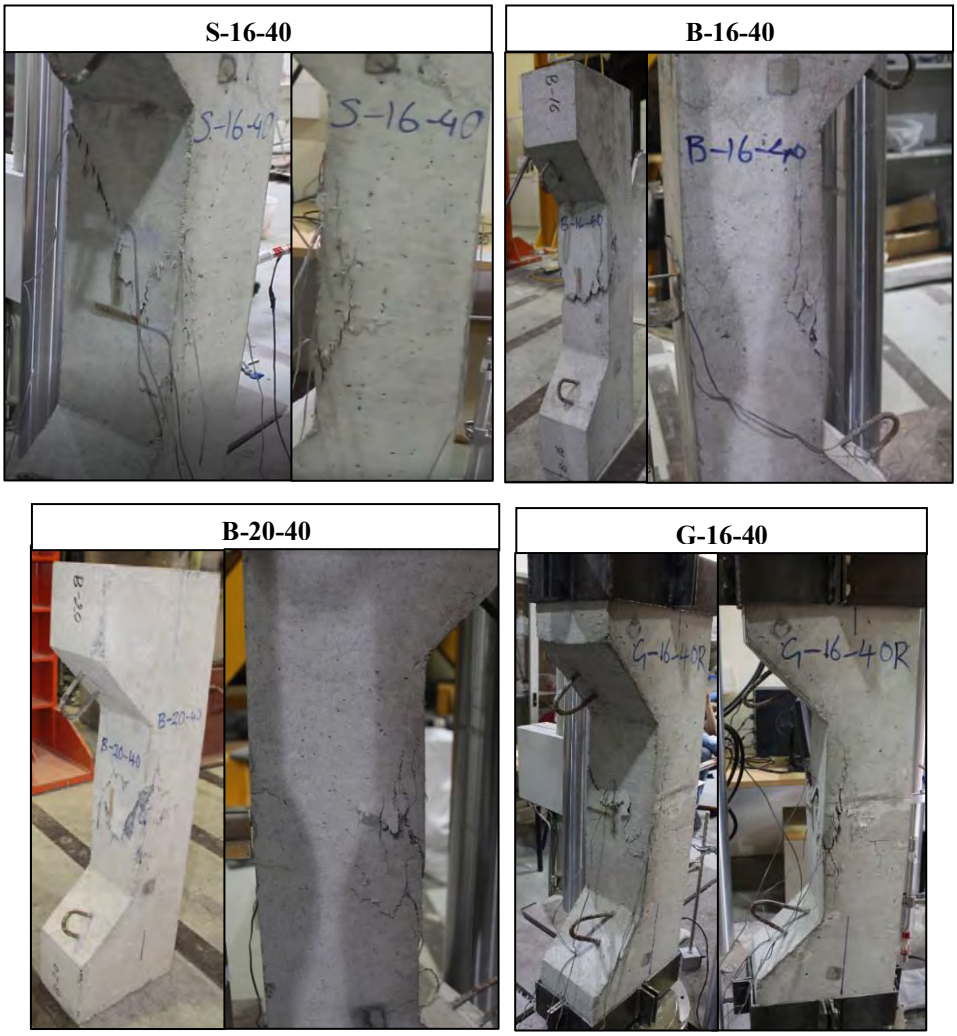


Figure 4.2: Photos of Group 1 column specimens tested under 40 mm eccentricity, after failure

It was observed that for columns of Group 1 (S-16-40, B-16-40, B-20-40 and G-16-40), reinforced transversely with steel ties, the concrete cover remained intact and attached to the concrete core, with little or no cover spalling, as shown in Figure 4.2.

On the other hand, concrete cover spalling was more obvious in columns of Group 2 (B-T60-40, B-T120-40 and B-T180-40), reinforced transversely with BFRP ties, as shown in Figure 4.3. This could be due to the differences in the concrete compressive strength and ties type between columns of Group 1 and those of Group 2. The failure mode for all columns at this level of eccentricity was compression failure, characterized by concrete crushing for the FRP RC columns, and concrete crushing accompanied by yielding of the compression bars for the steel RC column. No rupturing or buckling of the bars or ties occurred.

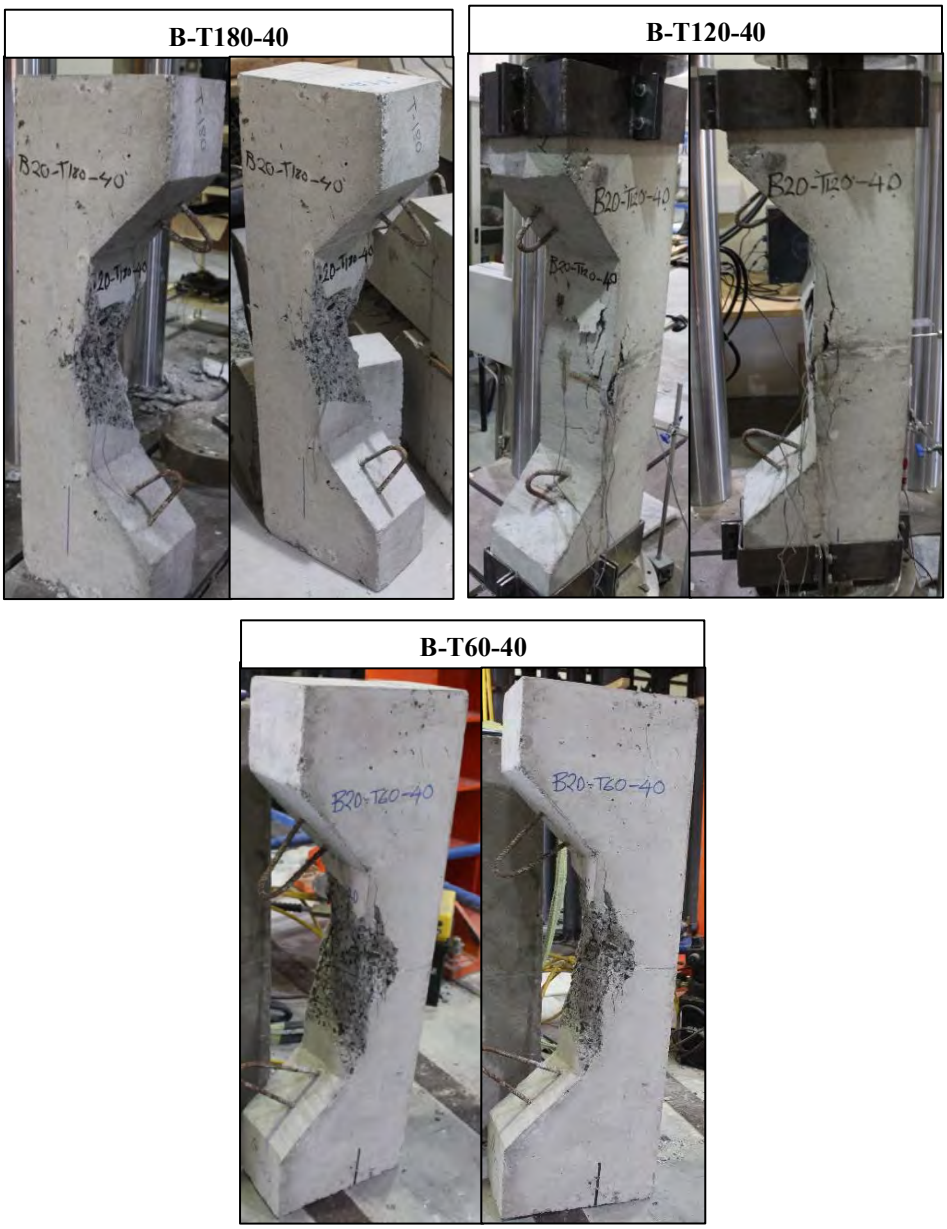


Figure 4.3: Photos of Group 2 column specimens tested under 40 mm eccentricity, after failure

The failure modes of column specimens tested under *e/h* ratio of 44.4% (S-16-80, B-16-80, B-20-80, G-16-80, B-T60-80, B-T120-80 and B-T180-80) were similar to those of columns tested under *e/h* ratio of 22.2%. However, under *e/h* ratio of 44.4%, cracks appeared on the tension sides first, followed by cracks on the compression sides. This occurred as the columns' neutral axes shifted more towards the compression sides with increasing bending stresses at this level of eccentricity, resulting in higher stresses developing at the tension sides.

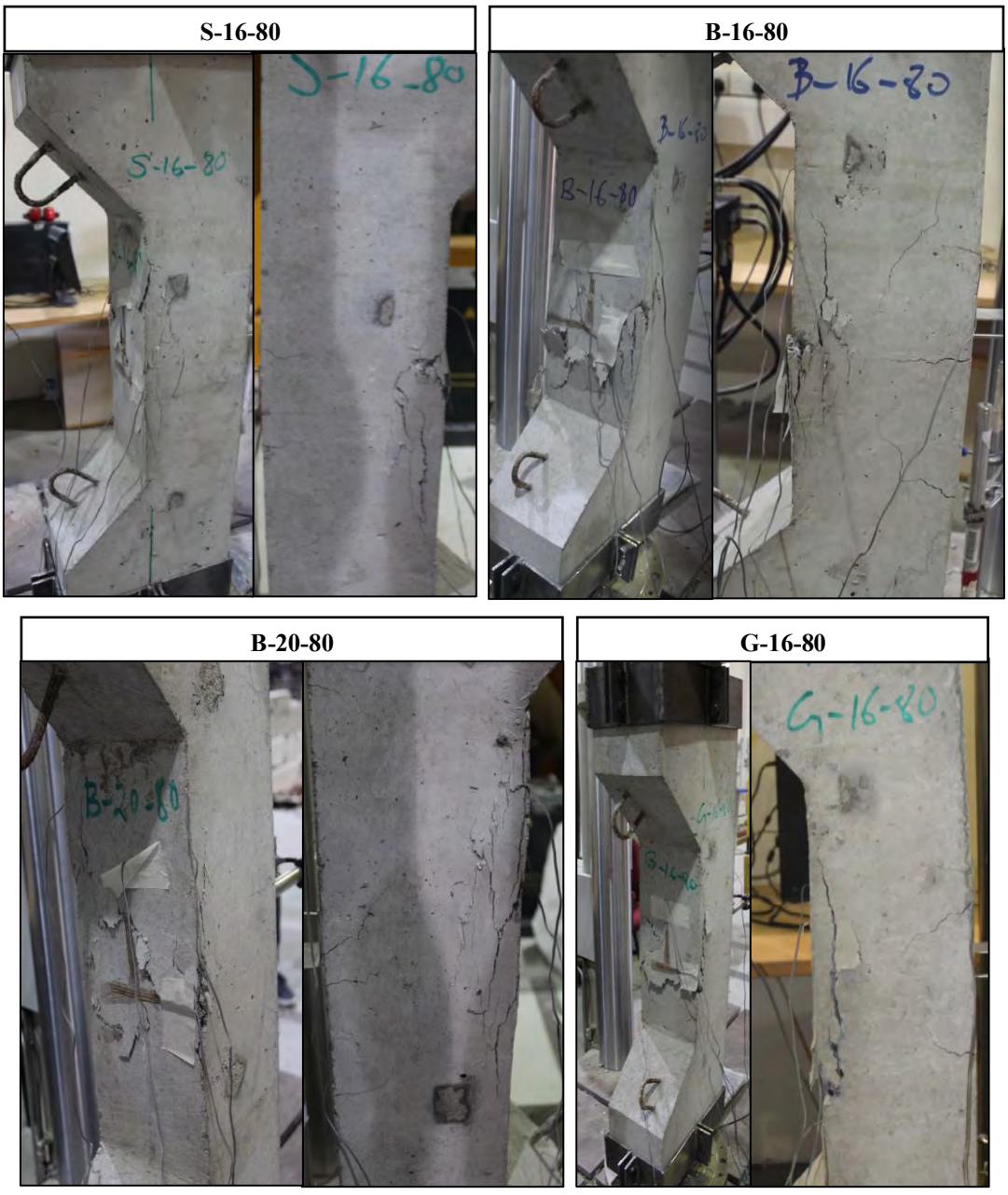


Figure 4.4: Photos of Group 1 column specimens tested under 80 mm eccentricity, after failure

Also, the initiation and propagation of cracks were affected by the longitudinal reinforcement type. For specimen S-16-80, longitudinally reinforced with steel bars, tension cracks first appeared at about 98% of the peak load, followed by compression cracks that appeared after peak load was reached. On the other hand, tension cracks appeared earlier during the tests for the specimens longitudinally reinforced with BFRP bars (B-16-80 and B-20-80), at 87% to 90% of the peak loads, followed by compression cracks appearing almost at peak loads. Tension cracks were even faster to appear with the specimen longitudinally reinforced with GFRP bars, at 54% of the peak load, followed by compression cracks at 95% of the peak load. Specimens B-T180-80, B-T120-80 and B-T60-80, confined with BFRP ties, had tension cracks appearing at about 61%, 46% and 73% of their peak loads, respectively, followed by compression cracks that appeared almost at peak loads.


Figure 4.5: Photos of Group 2 column specimens tested under 80 mm eccentricity, after failure

Similar to the observations made for columns tested under *e/h* ratio of 22.2%, concrete cover cracked but remained intact and attached to the concrete core for the specimens of Group 1 confined with steel ties (S-16-80, B-16-80, G-16-80 and B-20-80), as shown in Figure 4.4. Conversely, cover spalling was more obvious in specimens of Group 2 confined with BFRP ties (B-T60-80, B-T120-80 and B-T180-80), as shown in Figure 4.5. This again could be due to the differences in the concrete compressive strength and ties type for columns of both groups. Cover spalling occurred with separation of large pieces of concrete in specimen B-T60-80, confined with BFRP ties at reduced spacing of 60 mm. This could be attributed to the formation of a separation plane between the concrete cover shell and the concrete core due to the reduced spacing, as was also found in other studies [41, 56, 59, 62, 71]. At this level of eccentricity, failure was also compression-controlled due to concrete crushing for the FRP RC columns, and concrete crushing accompanied by yielding of compression bars for the steel RC columns. It should be noted that the column specimens were opened by an electric drill after the tests ended, to check for the conditions of the bars and ties, and to better understand the failure modes. It was found that the steel and FRP bars and ties remained intact after loading, with no rupturing or buckling detected, confirming the failure modes observed.

Again, the failure modes were influenced by the transverse reinforcement spacing. The specimens confined with BFRP ties at spacing of 60 mm exhibited second peak loads, which occurred after the cracks widened and the concrete cover separated, at load levels of 81% and 74% of first peak loads for specimens B-T60-40 and B-T60-80, respectively. The second peak loads for both specimens were lower than the first peak loads. Also, it was evident that, at high level of eccentricity of $e/h$ = 44.4%, reducing the BFRP ties spacing to 60 mm resulted in larger crack spacing, of 150 to 200 mm, compared to 50 to 100 mm for BFRP ties spacing of 120 mm or 180 mm. This confirms that reducing ties spacing improves the effectiveness of BFRP ties in confining the concrete core.

### 4.2. Strength and Deformation Capacities

A summary of the experimental results, in terms of peak loads ($P_{max}$), and the corresponding concrete strains on compression ($\varepsilon_{c1}$) and tension sides ($\varepsilon_{c2}$), axial strains in longitudinal reinforcement on compression ($\varepsilon_{bar1}$) and tension sides ($\varepsilon_{bar2}$), and mid-height axial displacements ($\delta$) and lateral deflections ($\Delta$), is shown in Table 4.1.

Table 4.1: Summary of Experimental Results

| | Column ID | $P_{max}$ (kN) | $\varepsilon_{c1}$ (με) | $\varepsilon_{c2}$ (με) | $\varepsilon_{bar1}$ (με) | $\varepsilon_{bar2}$ (με) | $\delta$ (mm) | $\Delta$ (mm) | $P_{bar}$ (kN) | $P_{bar}$ / $P_{max}$ (%) |
|---|---|---|---|---|---|---|---|---|---|---|
| **Group 1 ($f'_c$ = 34.4 MPa)** | S-16-0 | 1305 | -1887 | -2423 | -2594 | -2761 | 1.45 | - | 409 | 31.4 |
| | S-16-40 | 744 | -2639 | 1735 | -90[a] | 228[a] | 0.98 | - | - | - |
| | S-16-80 | 514 | -2627 | 3860 | -1825 | 1243 | 1.83 | 3.32 | - | - |
| | B-16-0 | 1077 | -2101 | -2277 | -2550 | -3371 | 1.56 | - | 117 | 10.9 |
| | B-16-40* | 577 | -3044 | 1668 | -3062 | 2958 | 0.91 | 2.56 | - | - |
| | B-16-80 | 347 | -3215 | 8421 | -2240 | 2038 | 0.98 | 3.88 | - | - |
| | B-20-0 | 1080 | -1950 | -2914 | -2926 | -3745 | 1.60 | - | 192 | 17.8 |
| | B-20-40 | 720 | -2771 | 866 | -2494 | -253[b] | 1.36 | 0.71 | - | - |
| | B-20-80 | 412 | -3780 | 3256 | -567[c] | 2224 | 1.01 | 3.64 | - | - |
| | G-16-0 | 1046 | -2852 | -2705 | -3817 | -2279 | 1.60 | - | 110 | 10.5 |
| | G-16-40* | 585 | -2765 | 1487 | -2669 | 130[c] | 1.49 | 2.51 | - | - |
| | G-16-80 | 364 | -2946 | 121 | -2567 | 3114 | 1.15 | 3.82 | - | - |
| **Group 2 ($f'_c$ = 28.4 MPa)** | B-T60-0 | 879 | -1988 | -2062 | -3008 | -2329 | 1.37 | - | 154 | 17.5 |
| | B-T60-40 | 518 | -2513 | 476 | -12** | 1107** | 1.15 | 1.58 | - | - |
| | B-T60-80 | 315 | -2295 | 2164 | -1712 | 140[c] | 0.93 | 2.85 | - | - |
| | B-T120-0 | 792 | -1904 | -974 | -1643 | -2173 | 0.68 | - | 110 | 13.9 |
| | B-T120-40 | 520 | -2463 | 256 | -1512 | -75[b] | 0.90 | 1.28 | - | - |
| | B-T120-80 | 324 | -2817 | 71 | -985 | 2492 | 1.19 | 2.99 | - | - |
| | B-T180-0 | 875 | -2284 | -1973 | -924 | -2647 | 3.30 | - | 103 | 11.8 |
| | B-T180-40 | 568 | -3424 | 550 | -1752 | -567[b] | 1.50 | 1.75 | - | - |
| | B-T180-80 | 334 | -2785 | 4416 | -739 | 2720[c] | 1.12 | 3.60 | - | - |
| | B-T60-80R (replicate) | 302 | -2200 | 7493 | -1521 | 2008 | 0.14 | - | - | - |

* Due to errors in tests, columns were cast and tested again with Group 2 having $f'_c$ = 28.4 MPa.
** Very low or very high strain values due to strain gauge malfunctioning.
[a] Low strain values at peak are due to bar stresses changing from compression to tension, or vice versa, as load increases.
[b] Rebar is on tension side, but subject to compression first followed by tension. At peak load, rebar was under compression.
[c] Strain gauge damaged before peak load.

Group 1 columns were prepared to study the effects of the longitudinal reinforcement type and ratio on the overall behavior of the columns. The maximum axial loads sustained by specimens B-16-0 and B-20-0 were 1077 kN and 1080 kN, respectively, showing that increasing the BFRP longitudinal reinforcement ratio has insignificant effect on strength. At this stage, the measured average axial strains in the BFRP longitudinal bars were 2811 με and 3336 με for specimens B-16-0 and B-20-0, respectively, which are close to 11% and 16.5% of the ultimate tensile strains of the 16 mm diameter BFRP bars (25200 με) and the 20 mm diameter BFRP bars (20200 με),

respectively. The contributions of the bars to the ultimate columns capacities, reported as $P_{bar}/P_{max}$ in Table 4.1, were calculated by multiplying the measured average axial strains in the longitudinal bars ($\varepsilon_{bar}$) with the total cross-sectional area of the bars ($A_f$) and the bars' elastic modulus ($E_f$). Using those measured strain values, the average contribution to the ultimate column capacity of the 16 mm BFRP bars was calculated as 10.9%, and was 17.8% for the 20 mm diameter BFRP bars. The maximum axial load sustained by the column longitudinally reinforced with GFRP bars was 1046 kN, which is only 3% lower than its counterpart column longitudinally reinforced with BFRP bars. The measured average axial strain in the GFRP bars at peak load was 3048 με, which is about 17.4% of their ultimate tensile strain (17500 με), from which the average bars contribution to the ultimate column's capacity was calculated as 10.5%. Testing of plain concrete columns might also provide some insight into the strength contribution of the longitudinal reinforcement to the columns' ultimate capacities. In this study, however, the strength contribution was calculated from the measured axial strain values of the bars, which may provide more accurate results as outlined in the previous statements.

The ultimate capacity of the steel RC column (S-16-0) was 1305 kN, and the corresponding average strain in the bars was 2678 με, which is almost equal to the yield strain of the steel bars, and contributed 31.4% to the ultimate column's capacity. This contribution is equivalent to the strength contribution of steel bars as calculated from the design equation of steel RC columns according to ACI 318-14 [44]. The average concrete strains at peak loads for columns S-16-0, B-16-0, G-16-0 and B-20-0 were 2155 με, 2189 με, 2779 με and 2432 με, respectively, with an average value of 2389 με, which is close to the unconfined concrete strain. At this stage, the confinement of the ties had not yet been activated. Even though it was ensured that the columns are subjected to pure axial loads, cracks formation was non-uniform around the columns resulting in some eccentricity of load. This resulted in the differences in strain values between $\varepsilon_{bar1}$ and $\varepsilon_{bar2}$, measured from the two bars to which strain gauges were attached, for some concentrically-loaded specimens. Similar observations were noted in other studies [50].

As would be expected, the ultimate axial capacities of the columns decreased as the load eccentricity increased, as shown in Table 4.1. Strength reductions of the eccentrically-loaded columns, compared to the concentrically-loaded ones, are calculated from the difference in ultimate strength between the two columns divided by

the ultimate strength of the concentrically-loaded column. Based on this, the steel RC columns tested under *e/h* ratios of 22.2% and 44.4%, exhibited strength reductions of 43% and 61%, respectively. Similarly, the BFRP RC columns tested under eccentric loads, B-16-40 and B-16-80, showed strengths reductions of 35% and 68%, respectively. The BFRP RC columns having a higher longitudinal reinforcement ratio of 3.88%, B-20-40 and B-20-80, had strength reductions of 33% and 62%, respectively Also, GFRP RC columns G-16-40 and G-16-80, showed strength reductions of 32% and 65%, respectively. Overall, the strength reductions due to the eccentric loads were almost the same for all columns irrespective of the longitudinal reinforcement type or ratio.

Columns of Group 2 were prepared to investigate the effects of using BFRP ties as transverse reinforcement compared to steel ties, as well as the effects of reducing BFRP ties spacing, on the overall behavior of RC columns. Peak loads recorded for columns B-T60-0, B-T120-0 and B-T180-0 were close, at 879 kN, 792 kN and 875 kN, respectively, with a maximum percentage difference of 10%. The corresponding measured average axial strains in the BFRP bars were 2669 με, 1908 με and 1786 με, for columns B-T60-0, B-T120-0 and B-T180-0, respectively, which are around 13.2%, 9.4% and 8.8% of the ultimate tensile strain of 20 mm diameter BFRP bars (20200 με), respectively. The calculated contributions of the bars to the axial capacities of the columns were found to be 17.5%, 13.9% and 11.8% for columns B-T60-0, B-T120-0 and B-T180-0, respectively. This confirms that reducing the spacing of BFRP ties to 60 mm provides effective confinement to the BFRP bars, and helps enhance their strength contributions. Similar results were reported for other types of longitudinal and transverse FRP reinforcements [41, 49-51].

The ultimate capacities of the columns decreased as the load eccentricity increased. Using the same definition for strength reduction used earlier, the strength reductions for columns B-T60-40 and B-T60-80, transversely reinforced with BFRP ties at 60 mm spacing, were 41% and 66%, respectively. For columns B-T120-40 and B-T120-80, transversely reinforced with BFRP ties at 120 mm spacing, the strength reductions were 34% and 59%, respectively. In addition, the strength reductions for columns B-T180-40 and B-T180-80, confined with BFRP ties at 180 mm spacing, were 35% and 62%, respectively. It can be observed that reducing the tie spacing does not significantly affect the reductions in strengths from increasing the load eccentricities.

It should be noted that specimen B-T60-80R was cast and tested as a replicate specimen for column B-T60-80, in order to validate the testing procedure and test results. Comparing the results of both specimens, very close values and responses are observed. The maximum difference in the ultimate capacities of both columns is found to be only 4%, as reported in Table 4.1. Also, the responses of both columns in terms of strains, deformation and failure modes were similar. Figure 4.6 shows samples of graphs of load versus concrete strain and load versus longitudinal reinforcement strain, for both columns, which show similar responses. Thus, this validates the tests conducted.

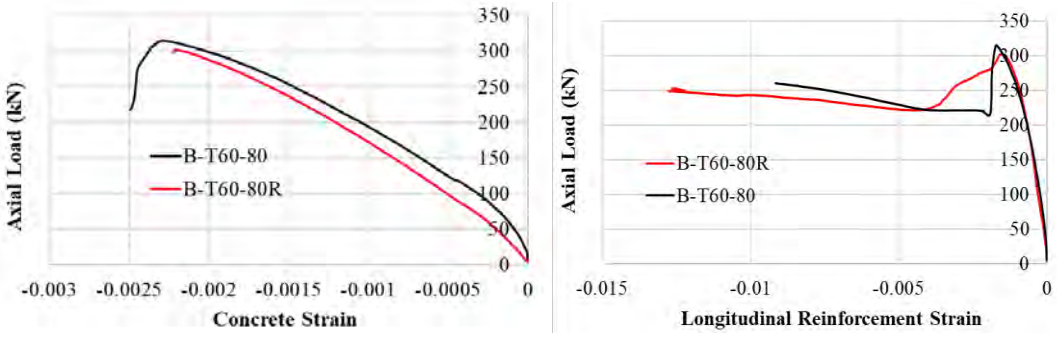


(a) (b)

Figure 4.6: Axial load versus (a) concrete strain and (b) longitudinal reinforcement strain, for columns B-T60-80 and B-T60-80R

### 4.3. Axial Displacement and Lateral Deflection Behavior

During the tests, the axial displacements were recorded by LVDTs mounted in a vertical position at the mid-height of each column. Figure 4.7 shows the graphs of axial load versus axial displacement for columns of Groups 1 and 2. As shown in Figure 4.7, all columns exhibited similar axial load-axial displacement responses, irrespective of the type or ratio of longitudinal reinforcement. The axial load- axial displacement curves of the specimens can be divided into three stages. The first stage constitutes the initial linear ascending branch which continues up to around 70% to 90% of the peak load. The second stage is characterized by a semi-linear and flattening branch up to peak load, which highlights a gradual loss of axial stiffness due to propagation of micro cracks. The third stage is a descending post-peak branch. It is found that, for all columns, the initial axial stiffness decreases with each increase in load eccentricity.

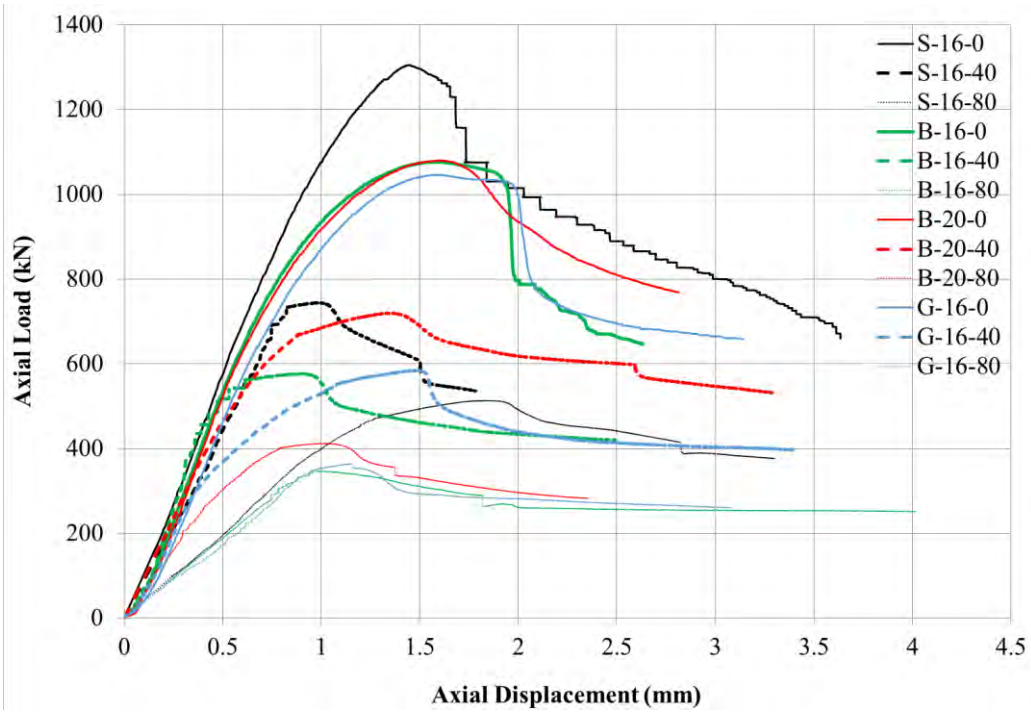


(a)

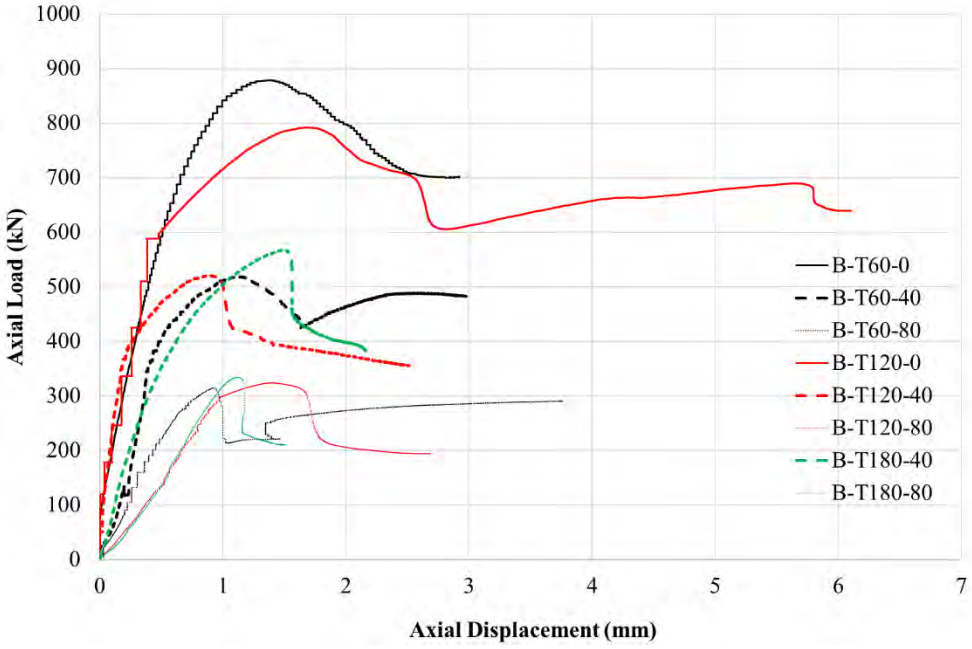


(b)

Figure 4.7: Axial load vs. axial displacement curves for (a) Group 1 and (b) Group 2

For the columns tested under concentric loads, the initial axial stiffness varied from 1025 kN/mm to 1240 kN/mm. The initial axial stiffness values ranged from 775

kN/mm to 930 kN/mm, and from 310 kN/mm to 725 kN/mm for columns tested under *e/h* ratios of 22.2% and 44.4%, respectively. Moreover, as can be seen from Figure 4.7 b, for the columns that were well confined with BFRP ties at 60 mm spacing, a fourth stage to the load-displacement curve is characterized by second peak loads which occurred after cover spalling. However, column B-T60-0, tested under concentric loads, did not show a second peak load. Instead, column B-T120-0, confined with BFRP ties at 120 mm spacing and tested under concentric loads, exhibited a second peak load after cover spalling. No axial load-axial displacement curve is available for column B-T180-0, as the LVDT malfunctioned during testing. For all concentrically-loaded columns, the strength decay after peak is almost the same. However, it is evident from the axial load-axial displacement curves for eccentrically-loaded columns that the post-peak strength decay was more rapid for columns of Group 2 confined with BFRP ties, as compared to columns of Group 1 confined with steel ties. The axial displacement values at peak loads are shown in Table 4.1 for all columns.

The lateral deflections of the columns were also measured by LVDTs mounted at mid-heights of the columns during testing. Figure 4.8 shows the curves of axial loads versus mid-height lateral deflections for the columns tested under eccentric loads of Groups 1 and 2. The axial load-lateral deflection curves are divided into three stages. The first stage is represented by a vertical straight line which demonstrates the stage at which almost no lateral deflection has occurred, since the formation of cracks had not yet started. It should be noted that the unexpectedly prolonged initial vertical straight line of specimen B-20-40 is a result of errors with the LVDT, and is not representative of the column's behavior. Also, no axial load-lateral deflection curve is available for specimen S-16-40 due to errors with the LVDT. It is observed that the first stage of the axial load-lateral deflection curves continued for longer for columns of Group 2 as compared to columns of Group 1. In addition, stage 1 lasted up to 3%, 13% and 21% of the peak loads for specimens B-T180-80, B-T120-80 and B-T60-80, respectively, showing that reducing the BFRP ties spacing improved the lateral stiffness of the columns. Once cracking in the concrete started, the axial load-lateral deflection curves showed semi-linear branches with decreasing slopes up to peak loads, demonstrating the reductions in the lateral stiffness of the columns. The third stage occurs after peak loads, where loads decrease and lateral deflections increase progressively. As with the axial load-axial displacement response, the initial lateral stiffness decreased with each

increase in load eccentricity. However, the lateral deflection values at peak loads increased with each increase in eccentricity. Values of the lateral deflections at peak loads are shown in Table 4.1 for all columns. Further, it is observed that the columns confined with BFRP ties at reduced spacing of 60 mm and 120 mm, continued to deflect laterally after peak loads were reached, as compared to columns confined with BFRP ties at 180 mm, as shown in Figure 4.8.

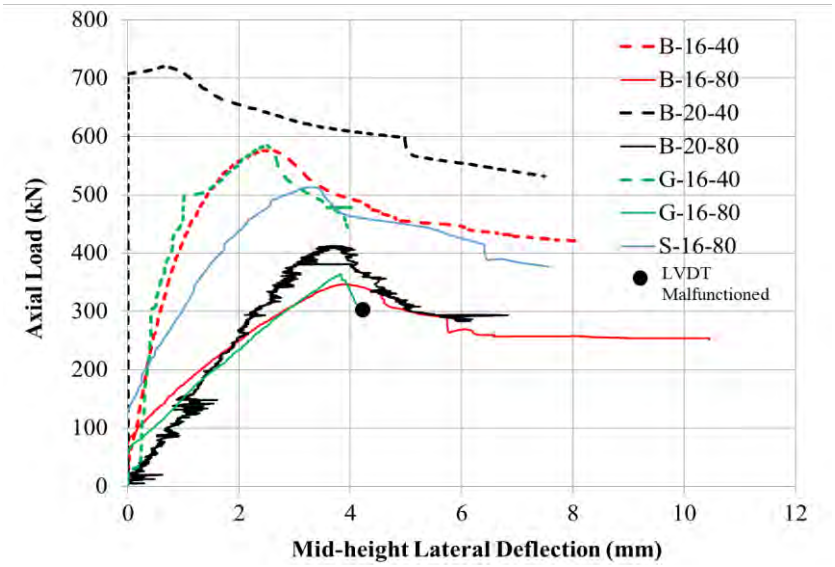


(a)

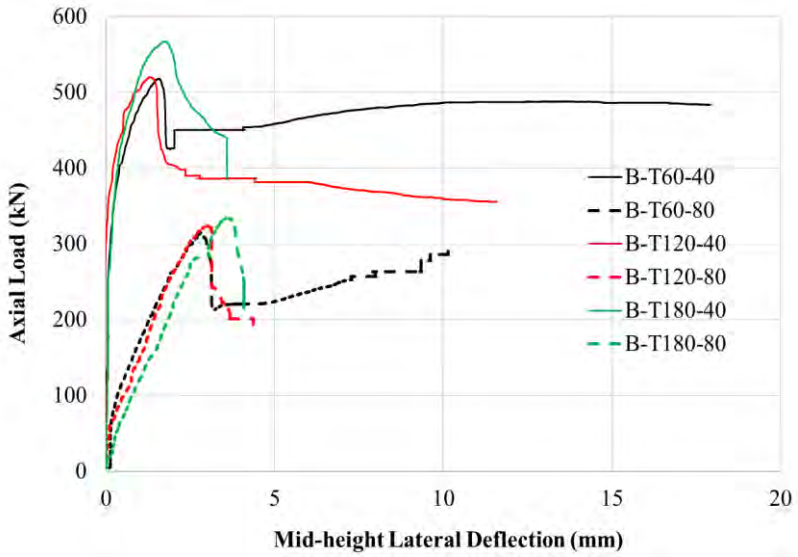


(b)

Figure 4.8: Axial load vs. mid-height lateral deflection curves for (a) Group 1 and (b) Group 2

### 4.4. Longitudinal Reinforcement and Concrete Strain Responses

Axial strains in the longitudinal reinforcement and in the concrete were recorded by strain gauges installed on both the compression and tension sides at mid-heights of the specimens, where maximum stresses are expected. Figure 4.9 shows the axial load versus concrete compressive strain curves for all columns of Groups 1 and 2. The initial slope of the curve is mainly affected by the level of eccentricity, where it decreases as the load eccentricity increases. Nonetheless, for all columns, the concrete response is linearly elastic up until the formation of cracks, after which a non-linear branch develops till peak load. The failure mode for all columns is governed by concrete crushing, and this can be depicted from the axial load vs. strain curves for concrete in which concrete crushing strain is reached at peak loads. The maximum recorded concrete strains varied between 0.0024 to 0.0038 at failure, which are close to the concrete crushing strains specified by ACI 440.1R-15 [2] (-0.003) and by CSA S806-12 [27] (-0.0035). It is noticed that at all levels of load eccentricity, the FRP RC columns developed higher concrete strains at failure than steel RC columns. This can be attributed to the lower modulus of elasticity of FRP bars which results in lower axial stiffness of FRP-RC columns as compared to steel-RC columns, and thus higher strains in concrete.

Figure 4.10 shows the axial loads versus longitudinal reinforcement axial strains curves for columns of Groups 1 and 2. The tensile and compressive axial strain responses of all bars show an initial linear branch increasing gradually up to the point where micro-cracks start forming. This is followed by a semi-linear ascending branch until peak loads, which ends with a descending branch until complete failure. The graphs also show that under eccentric loads, the FRP RC and the steel RC columns exhibited similar strain responses. Conversely, under concentric loads, the steel RC column shows a long flattening curve post peak, demonstrating ductile behavior. This behavior is much less obvious in FRP RC columns under pure axial loads. The maximum reported tensile and compressive strains in the longitudinal reinforcement at peak loads are shown in Table 4.1. Under concentric loads, the FRP longitudinal bars of specimens B-16-0, B-20-0, G-16-0, B-T60-0, B-T120-0 and B-T180-0, developed strains at peak which are close to 11%, 16.5%, 17.4%, 13.2%, 9.4% and 8.8% of their ultimate tensile strains, respectively. The steel longitudinal reinforcement of specimen S-16-0 developed tensile strains at peak that are almost equal to their yield strain.

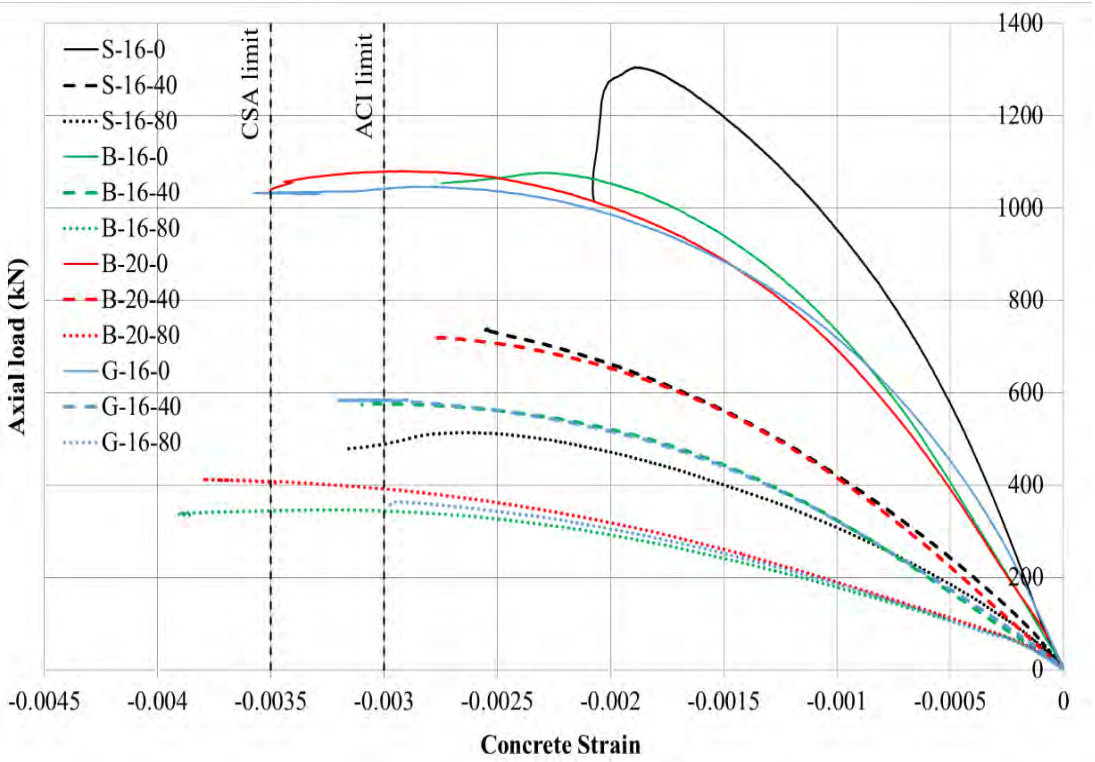


(a)

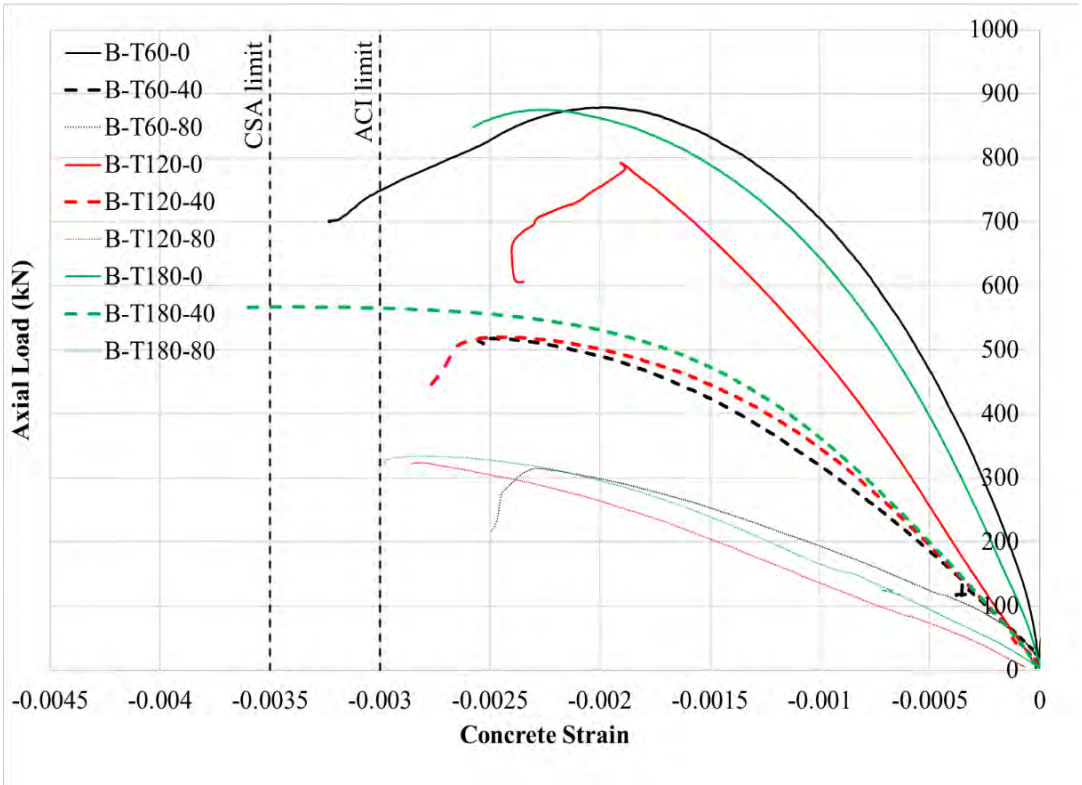


(b)

Figure 4.9: Axial load vs. concrete compressive strain curves for (a) Group 1 and (b) Group 2

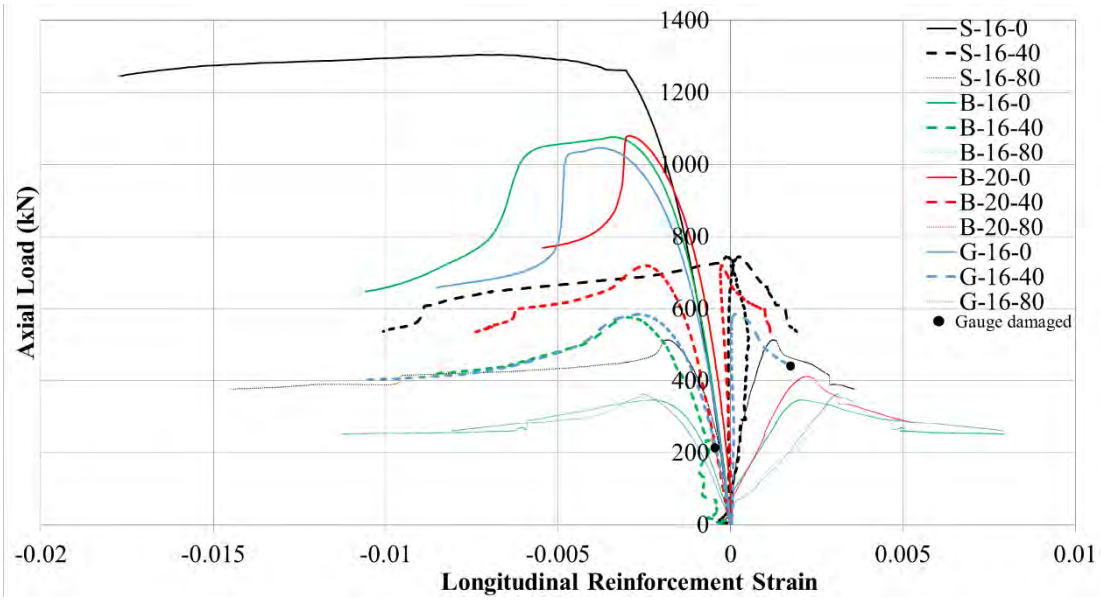


(a)

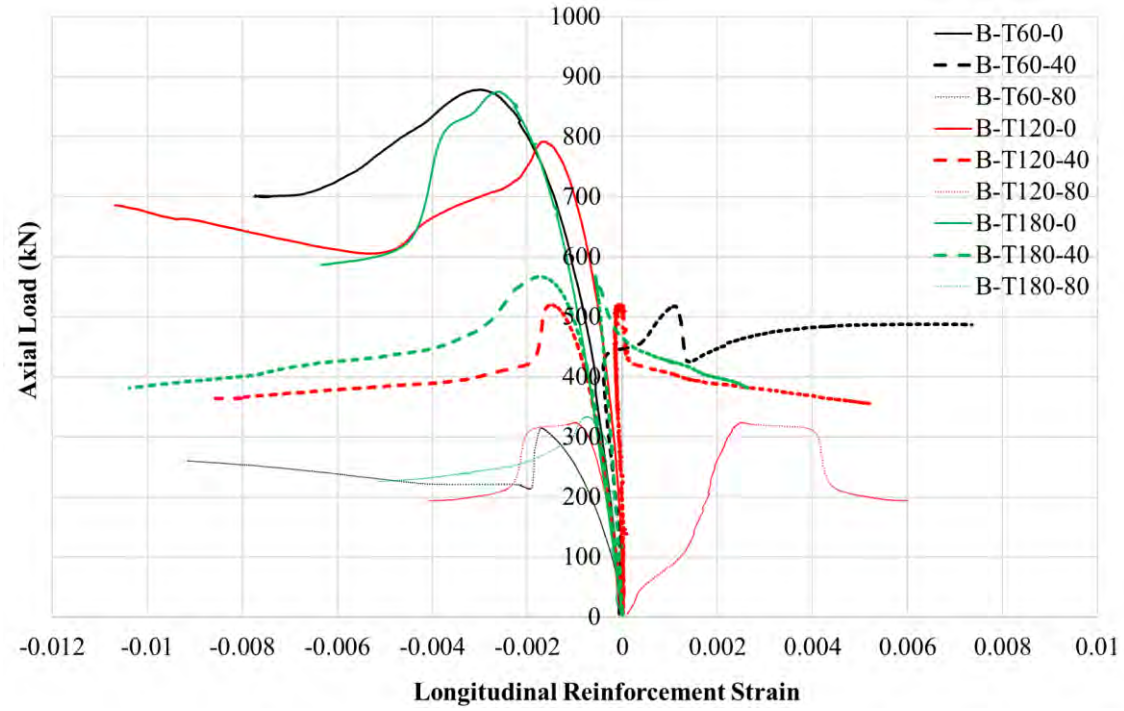


(b)

Figure 4.10: Axial load vs. longitudinal reinforcement strain curves for (a) Group 1 and (b) Group 2

Under a load eccentricity of 40 mm ($e/h$ = 22.2%), the position of the neutral axis was near the tension side of the specimens. Thus, the specimens cross-sections were still under full compressive stresses up to the peak loads, and the longitudinal bars

on the tension sides were either under compression, or developed minimal tensile stresses. For specimens B-16-40, G-16-40, B-20-40, B-T120-40 and B-T180-40, the average strains on the compression sides, at peak, were 12.2%, 15.3%, 12.3%, 7.5% and 8.7% of their ultimate tensile strains, respectively. No data is available for the compressive strains in longitudinal reinforcement of specimen B-T60-40, due to errors with strain gauges. Strains in the reinforcement on the tension sides, at peaks, for specimens B-20-40 and G-16-40, were 1.25% and 0.74%, of the ultimate tensile strains of longitudinal bars, before gauges were damaged. On the other hand, minimal compressive and tensile stresses were recorded in the longitudinal reinforcement for specimen S-16-40 at peak, as the stresses transitioned from compressive to tensile stresses, or vice versa, as shown in Figure 4.10a. Also, very low compressive stresses were recorded at peak loads for the longitudinal reinforcement on the tension sides of specimens B-T120-40 and B-T180-40, before the bars were under tensile stresses.

Under 80 mm eccentricity ($e/h$ = 44.4%), the neutral axis to depth ratio decreased as the load eccentricity increased. Therefore, the longitudinal bars on the tension sides experienced pure tensile stresses from start of test up to complete failure. At this eccentricity level, the reinforcement on the tension and compression sides developed similar strain values at peak loads. In specimens B-16-80, G-16-80 and B-T120-80, the longitudinal reinforcements, at peaks, reached tensile strains of 8.9%, 14.7% and 12.3%, and compressive strains of 8.1%, 17.8% and 4.9% of their ultimate tensile strains, respectively. The longitudinal reinforcement in specimen B-20-80 developed tensile strains of 11% of their ultimate tensile strain, and compressive strain of 2.8% of their ultimate tensile strain, before the gauge was damaged. The tensile and compressive strains in the reinforcement in specimen S-16-80, at peak, were at 73% and 50% of the yield strain of steel, respectively. In specimens B-T60-80 and B-T180-80, the longitudinal reinforcement reached compressive strains of 8.5% and 3.7% of their ultimate tensile strains, respectively. No data is available for tensile strains in longitudinal reinforcement of specimens B-T60-80 and B-T180-80, due to errors with strain gauges.

# Chapter 5. Discussion of Results

In this chapter, detailed discussion and analysis of the results presented in the previous chapter are provided. The effects of each of the test parameters on the overall behavior of the columns are evaluated and discussed. This is followed by explanations of the experimental axial load-bending moment interaction diagrams developed for the columns. Finally, the design equations currently proposed by FRP RC design codes and by other studies from the literature, are evaluated in light of the results obtained from this study.

## 5.1. Effects of Test Parameters on the Overall Behavior of FRP RC Columns

In this study, the parameters investigated include the longitudinal reinforcement type (steel, BFRP and GFRP bars), BFRP longitudinal reinforcement ratio (2.48% and 3.88%), loading eccentricity ($e/h$ = 0, 22.2% and 44.4%), transverse reinforcement type (steel and BFRP ties) and BFRP transverse reinforcement spacing (60, 120 and 180 mm). In order to study the effects of changing each of these parameters on the overall behavior of RC columns, graphs of axial load versus longitudinal reinforcement strains, axial load versus axial displacements, and axial load versus lateral deflections are compared for all columns. Since the column specimens were cast from different concrete batches, normalized load values are plotted in the graphs for comparisons. The axial loads are normalized with respect to the cylinder concrete strength multiplied by the gross sectional area of the columns ($P/0.85f'_cA_g$).

Moreover, the confinement efficiency and ductility indices for the columns are calculated and compared. The efficiency of the ties in improving the confined concrete core strength is indicated by the confinement efficiency. The confinement efficiency is calculated as the ratio of the confined concrete strength ($f'_{cc}$) to the unconfined concrete strength ($f'_{co}$). The confined concrete strength ($f'_{cc}$) is calculated for each column as the peak load divided by the confined concrete area delineated by the centreline of the ties. The $f'_{co}$ value is considered as $0.85f'_c$, where $f'_c$ is the concrete cylinder strength. Values of the confinement efficiency (CE) for concentrically-loaded columns are shown in Table 5.1. Ductility can be defined as a measure of the ability of structural material to undergo significant plastic deformation without fracturing. Ductility is a desired property in structural design as it protects structures against unpredicted overloading and/or load reversals. It is thus essential that RC columns possess adequate ductility.

Table 5.1: Normalized Strengths, Confined Concrete Strength Factors and Ductility Indices of All Columns

| | Column Identification | $P_{max}$ (kN) | CE | DI | $P_{concrete}$ (kN) | $P_{concrete}/P_{max}$ (%) | $P_{norm}$ |
|---|---|---|---|---|---|---|---|
| **Group 1 ($f'_c$ = 34.4 MPa)** | S-16-0 | 1305 | 2.32 | 1.35 | 896 | 68.7 | 82.5 |
| | S-16-40 | 744 | | 1.39 | | | |
| | S-16-80 | 514 | | 1.54 | | | |
| | B-16-0 | 1077 | 2.48 | 2.00 | 959 | 89.1 | 88.3 |
| | B-16-40* | 577 | | 2.45 | | | |
| | B-16-80 | 347 | | 1.64 | | | |
| | B-20-0 | 1080 | 2.30 | 2.08 | 888 | 82.1 | 82.9 |
| | B-20-40 | 720 | | 2.30 | | | |
| | B-20-80 | 412 | | 1.81 | | | |
| | G-16-0 | 1046 | 2.42 | 1.89 | 936 | 89.5 | 86.2 |
| | G-16-40* | 585 | | 2.20 | | | |
| | G-16-80 | 364 | | 1.31 | | | |
| **Group 2 ($f'_c$ = 28.4 MPa)** | B-T60-0 | 879 | 2.27 | 3.11 | 725 | 82.5 | 81.9 |
| | B-T60-40 | 518 | | 2.61 | | | |
| | B-T60-80 | 315 | | 1.43 | | | |
| | B-T120-0 | 792 | 2.14 | 4.47 | 682 | 86.1 | 77.1 |
| | B-T120-40 | 520 | | 4.23 | | | |
| | B-T120-80 | 324 | | 1.56 | | | |
| | B-T180-0 | 875 | 2.42 | 1.43 | 772 | 88.2 | 87.3 |
| | B-T180-40 | 568 | | 2.03 | | | |
| | B-T180-80 | 334 | | 1.12 | | | |
| | B-T60-80R (replicate) | 302 | | 3.56 | | | |

* Due to errors in tests, columns were cast and tested again with Group 2 having $f'_c$ = 28.4 MPa.

Conventionally, ductility is measured by the ultimate displacement to yield displacement ratio. However, there is no unified definition for ultimate displacement. A few methods are used in the literature to calculate the ductility indices of FRP RC columns. One method was developed by Foster and Attard [100] in which the ductility of RC columns is calculated from the area under the axial load-axial displacement curves for the columns. Another method was developed by Pessiki and Peironi [71] in which the column ductility is calculated as the ratio of the ultimate axial displacement ($\delta_u$) to the yield axial displacement ($\delta_y$), given by:

$$DI = \frac{\delta_u}{\delta_y} \qquad (5.1)$$

The latter method was adopted in this study. In this method, the yield displacement is estimated to be the axial displacement corresponding to the yield load or to the limit of elastic behavior. The ultimate displacement is taken as the axial displacement at an axial load level of 85% of the peak load in the post-peak descending portion of the axial load-axial displacement curve. The 85% peak load, which was used for comparison purposes, is a reasonable limit at which it can be considered that a column has maintained its ultimate resistance, as explained in Pessiki and Peironi [71]. This method is illustrated in Figure 5.1 for column specimen B-16-0.

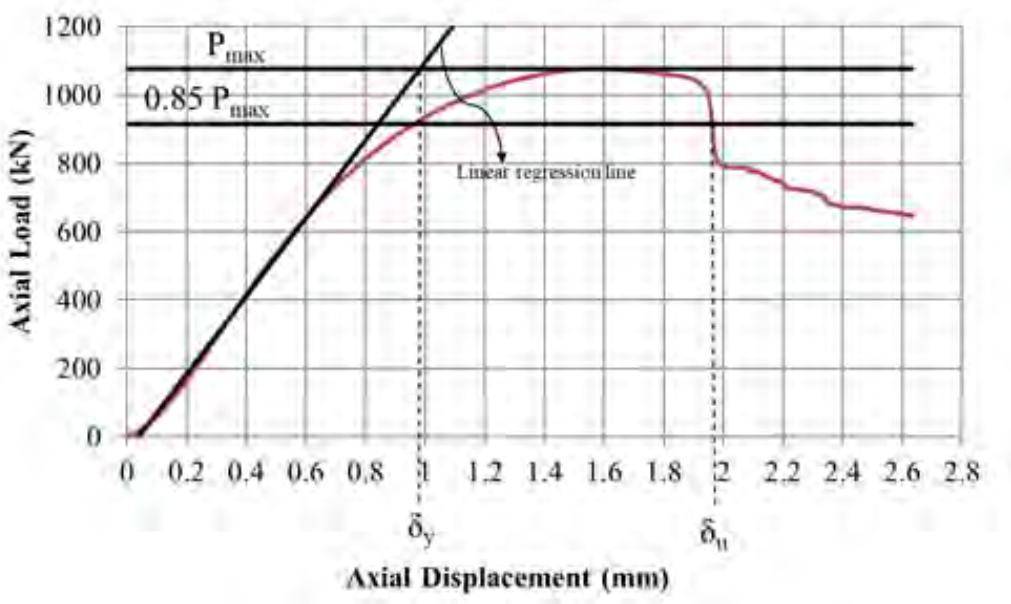


Figure 5.1: Determination of displacements for calculating columns ductility index (graph of specimen B-16-0)

For each column specimen, a best-fit line is plotted to the initial linear portion of the load-displacement curve, as shown in Figure 5.1. The displacement at the intersection of this line with a horizontal line corresponding to the peak load of the column, is labelled as displacement corresponding to the elastic behavior limit ($\delta_y$). The displacement corresponding to the intersection of the descending portion of the load-displacement curve with a horizontal line at 85% of peak load, is labelled as ultimate axial displacement ($\delta_u$). The ductility index for the column is then calculated as the ratio

of the displacements obtained, as shown by Equation 5.1. Values of the ductility indices (DI) for all columns are shown in Table 5.1.

Also, values of the force carried by the concrete ($P_{concrete}$), calculated as the difference between the ultimate load ($P_{max}$) and the load carried by the bars ($P_{bar}$), are shown in Table 5.1 for all columns. Normalized load values ($P_{norm}$) for the load carried by the concrete are shown in Table 5.1, for concentrically-loaded columns. Those values are calculated as the difference between the peak load and the force carried by the longitudinal reinforcement, normalized with respect to the cylinder concrete compressive strength multiplied by the net concrete area ($(P_{max} - P_{bar})/(f'_c A_c)$).

**5.1.1. Effect of longitudinal reinforcement type.** Graphs of normalized axial load versus concrete strain, longitudinal rebar strain, axial displacement and lateral deflection, are shown in Figures 5.2, 5.3, 5.4 and 5.5, respectively, for columns having different longitudinal reinforcement types. The column specimens compared in Figures 5.3 to 5.5, were designed to have the same longitudinal reinforcement ratio, except for specimens reinforced with 20 mm diameter BFRP bars. The results show that at all levels of eccentricity, steel RC columns exhibit higher axial load capacities than FRP RC columns. Under concentric loads, steel RC column shows 19% and 22% higher axial load capacities than BFRP RC and GFRP RC columns, respectively. As the load eccentricity increases to *e/h* of 22.2%, the differences in the ultimate capacities between steel RC and FRP RC columns decrease, where steel RC columns show higher peak loads than BFRP RC and GFRP RC columns by only 6.4% and 5%, respectively. However, it is observed that at *e/h* of 44.4%, the steel RC column shows much higher capacity than the BFRP RC and GFRP RC columns by 39% and 34%, respectively.

Moreover, as reported in Table 4.1, steel bars contributed 31.4% to the ultimate capacity of the column, which is much higher than the calculated bar contributions of BFRP and GFRP bars of 10.9% and 10.5%, respectively. Overall, the steel-, BFRP- and GFRP- RC columns showed similar responses up to peak loads in terms of concrete strains, longitudinal reinforcement strains, axial displacements and lateral deflections. The normalized axial load versus concrete strain graphs illustrated in Figure 5.2, show that, on average, the concrete strains at crushing for BFRP RC and GFRP RC columns are higher than those for steel RC columns at all levels of load eccentricity. As previously explained, this could be due to the lower modulus of elasticity of FRP bars

as compared to steel bars which resulted in lower axial stiffness of the FRP-RC columns, and thus higher strains in concrete. This is also supported by the higher calculated normalized concrete load values for FRP RC columns as compared to steel RC columns, as reported in Table 5.1. In addition, the normalized axial load vs. axial displacements curves in Figure 5.4, and the values reported in Table 4.1, show that the steel RC columns developed axial displacement values at peak loads that are lower than those of BFRP- and GFRP- RC columns, under concentric loads.

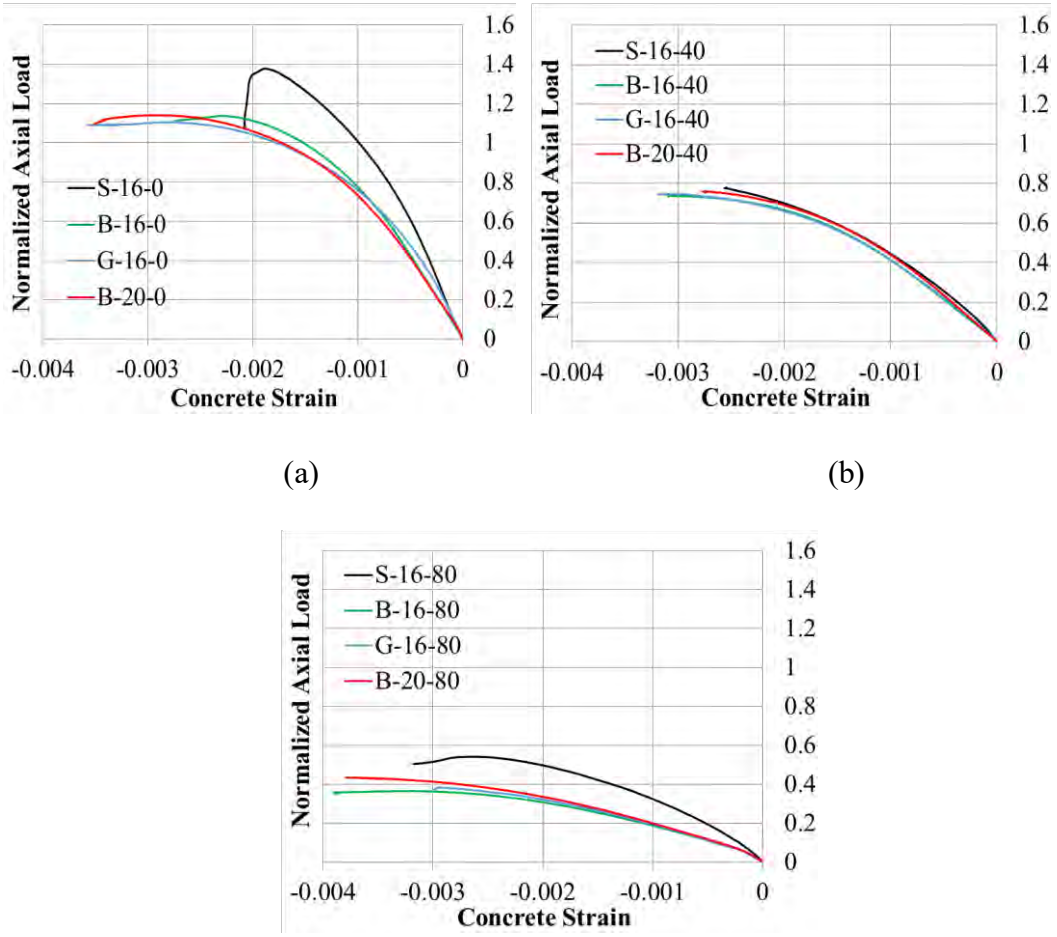


(a) (b)

(c)

Figure 5.2: Normalized axial load vs. concrete strain curves compared for different longitudinal reinforcement types for (a) concentric loads, (b) 40 mm eccentricity and (c) 80 mm eccentricity

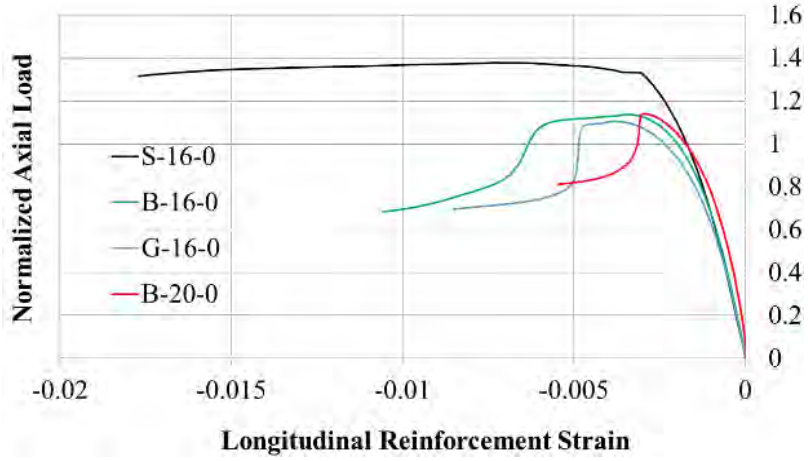


(a)

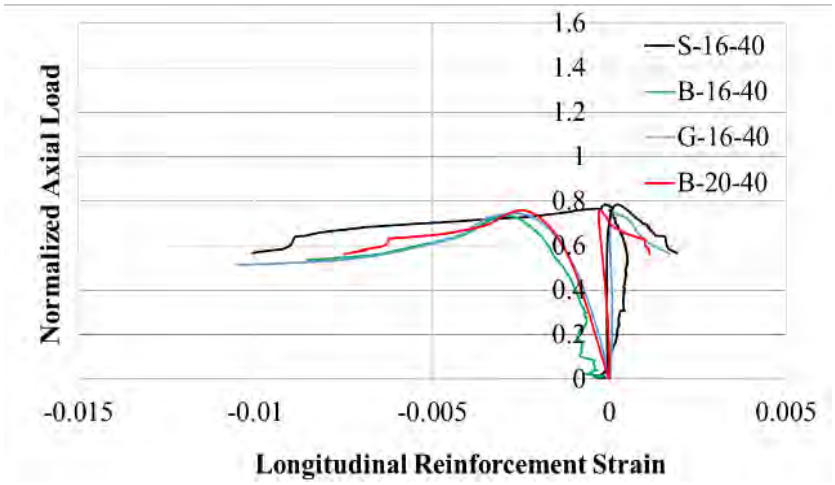


(b)

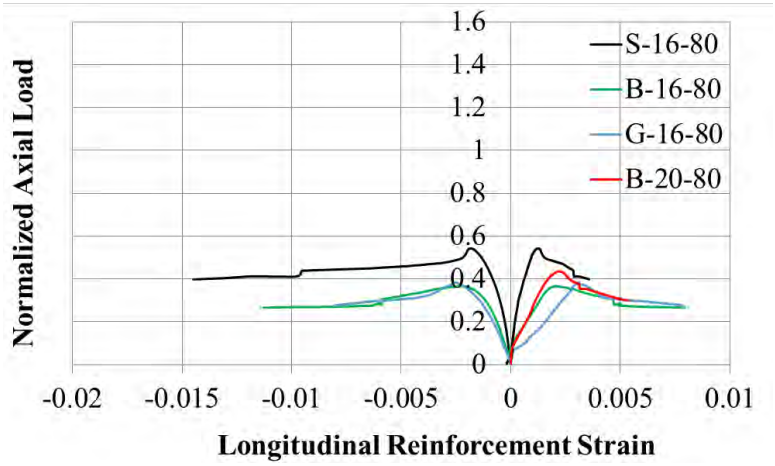


(c)

Figure 5.3: Normalized axial load vs. longitudinal reinforcement strain curves compared for different longitudinal reinforcement types for (a) concentric loads, (b) 40 mm eccentricity and (c) 80 mm eccentricity

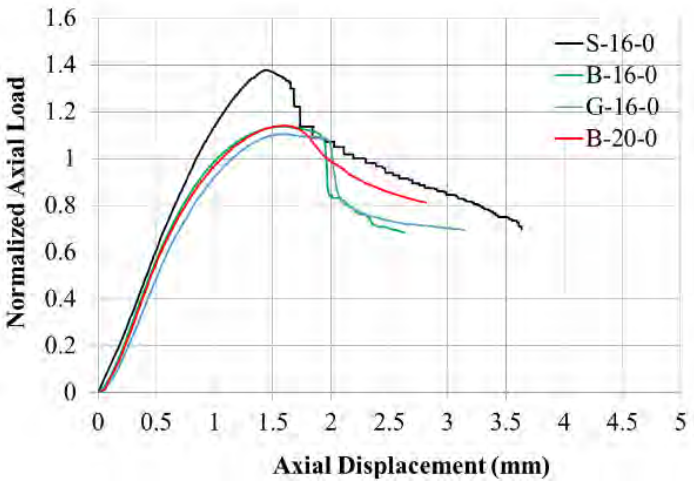


(a)

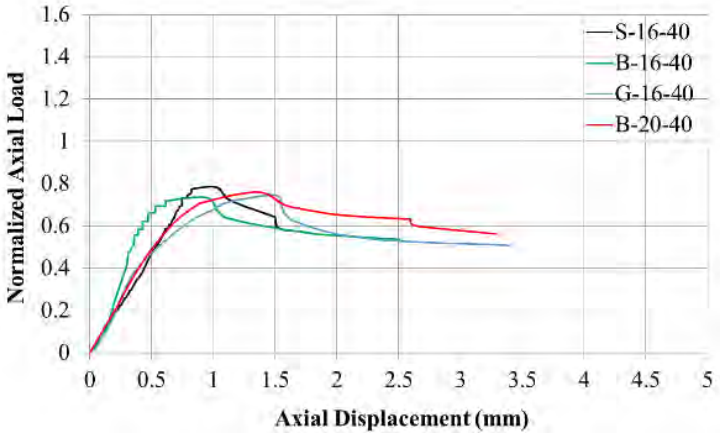


(b)

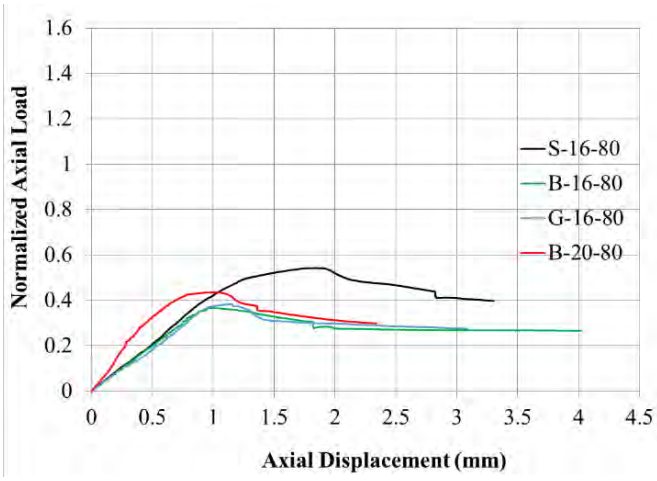


(c)

Figure 5.4: Normalized axial load vs. axial displacement curves compared for different longitudinal reinforcement types for (a) concentric loads, (b) 40 mm eccentricity and (c) 80 mm eccentricity

The axial displacements at ultimate loads were also lower for steel RC columns than for FRP-RC columns under *e/h* ratio of 22.2%, except for specimen B-16-40 which showed lower axial displacement at peak load than its counterpart steel RC specimen. At *e/h* ratios of 44.4%, steel RC columns exhibited higher axial displacements at peak loads than FRP RC columns. BFRP RC and GFRP RC columns show higher ductility than steel RC columns by 6% to 55% and by 16% to 45%, respectively. This is because, at peak loads, the strain values of BFRP and GFRP bars were less than 11% and 17% of their ultimate tensile strains, respectively, whereas steel bars reached their yield strains. Thus, it would be expected the FRP RC columns would sustain more loads and deformations after peak loads. Similar findings were reported in other studies [56]. This is also supported by the axial load-lateral deflection responses shown in Figure 5.5, which show that BFRP and GFRP RC columns develop larger lateral deflections than steel RC columns at every load level. No axial load-lateral deflection data is available for specimens S-16-40 and B-16-40 due to errors with LVDT. Similar results were reported in previous studies [35, 48, 49, 51, 56], whereas other studies showed that FRP RC columns were less ductile than steel RC columns at low eccentricities, and were more ductile at high eccentricities [57, 59].

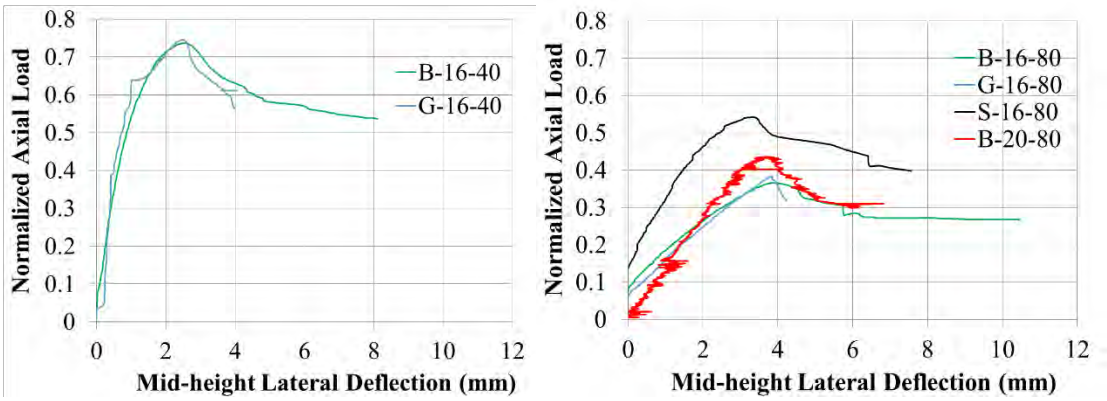


(a) (b)

Figure 5.5: Normalized axial load vs. mid-height lateral deflection curves compared for different longitudinal reinforcement types for (a) concentric loads, (b) 40 mm eccentricity and (c) 80 mm eccentricity

From all the reported results, there were insignificant differences between BFRP RC and GFRP RC columns in terms of overall strain and displacement responses,

peak loads and bars strength contributions. However, BFRP RC columns were found to be more ductile than their counterpart GFRP RC columns, at all levels of eccentricities, as shown by the ductility indices reported in Table 5.1.

As explained in previous chapters, column specimens reinforced with four 20 mm diameter BFRP bars were designed to have an equivalent strength to columns reinforced with 16 mm diameter steel bars ($f_y A_{st} = 0.35\, f_{fu} A_f$). Since the modulus of elasticity of steel is around four times higher than that of BFRP, comparing the overall behavior of those two sets of columns is essential in determining the effects of replacing steel reinforcement with BFRP reinforcement having an equivalent strength, rather than an equal reinforcement ratio. The results show that with the equivalent strength method adopted, steel RC columns still show higher axial capacities than BFRP RC columns by 19%, 3.3% and 22% at concentric loads, *e/h* of 22.2% and *e/h* of 44.4%, respectively. Also, the bars strength contribution of steel RC columns is still higher than for BFRP RC columns, as shown in Table 4.1. In general, it is noticed that the observations regarding overall column behavior, ductility, axial displacements, lateral deflections, concrete strains and longitudinal reinforcement strain responses are very much the same for BFRP RC columns designed with the equivalent strength method as compared to those designed with the same reinforcement ratio method. Even though it was concluded in a previous study that using a 0.35 reduction factor to account for the lower compressive strength of glass FRP bars as compared to their tensile strength provided accurate and conservative predictions of the capacities of GFRP RC columns, this factor might not be adequate for BFRP bars. The present results suggest that in order to obtain ultimate capacities and bars strength contributions equivalent to those of steel RC columns, higher longitudinal reinforcement ratios would be required for BFRP RC columns.

**5.1.2. Effect of longitudinal reinforcement ratio.** Column specimens B-20-0, B-20-40, B-20-80 and specimens B-16-0, B-16-40 and B-16-80, were designed to study the effect of different BFRP longitudinal reinforcement ratios of 2.48% and 3.88%. The results show that the columns having a larger BFRP longitudinal reinforcement ratio (3.88%) attain higher ultimate capacities than their counterparts having lower reinforcement ratio (2.48%), at all eccentricity values. However, the columns have very close ultimate capacity values under concentric loads and eccentric loads of *e/h* of 22.2%, with percentage differences of only 0.3% and 3%, respectively. The differences

in the ultimate capacities between the columns is larger at eccentric load of *e/h* of 44.4%, in which specimens with larger BFRP reinforcement ratios show 17% higher axial capacities than those with smaller BFRP reinforcement ratios.

Additionally, the strength contribution of BFRP bars to the ultimate column capacity was found to be higher for column with larger reinforcement ratio, at 17.8%, as compared to the one with smaller reinforcement ratio, at 10.9%, as shown in Table 4.1. This is a result of the higher ultimate strains reached in the 20 mm diameter BFRP bars and their larger cross-sectional area, as compared to the 16 mm diameter BFRP bars. Moreover, specimens with larger BFRP reinforcement ratios showed larger axial displacements at peak loads than those with smaller BFRP reinforcement ratios, at all load levels.

In addition, higher lateral deflections occurred with eccentrically-loaded specimens having lower BFRP reinforcement ratios than those with higher BFRP reinforcement ratios. Nonetheless, column ductility was higher for larger BFRP reinforcement ratios than for smaller ones, by 4% and 10% at concentric and 80 mm eccentric loads, respectively. However, at 40 mm eccentricity, the ductility of BFRP RC column with lower reinforcement ratio was slightly higher than for the one with larger reinforcement ratio by 6%. Overall, the BFRP RC columns for both longitudinal reinforcement ratios showed similar responses of axial load versus concrete strains, longitudinal reinforcement strains, axial displacements and lateral deflections.

**5.1.3. Effect of eccentricity-to-depth (*e/h*) ratio.** Three different loading conditions were investigated in this study, including concentric loads, and eccentric loads at *e/h* of 22.2% and 44.4%. As explained under section 4.2, the failure modes of the columns were mainly affected by the level of applied eccentricity. Columns tested under concentric loads experienced compression-controlled failure, where diagonal failure planes occurred due to the shear sliding of the lower and upper parts of the columns after the cores were crushed. On the other hand, similar failure modes were observed for columns tested under *e/h* of 22.2% and 44.4%. However, under *e/h* of 22.2%, compression cracks occurred first followed by tension cracks, whereas for *e/h* of 44.4%, tension cracks occurred first followed by compression cracks. Also, reductions in the ultimate capacities of columns due to the eccentric loads were almost the same for all specimens regardless of the longitudinal reinforcement type. However,

the BFRP RC columns having a higher longitudinal reinforcement ratio of 3.88%, showed lower strength reductions than those reinforced with a lower BFRP longitudinal reinforcement ratio of 2.48%. It was also found that the initial axial and lateral stiffness of the columns decreased considerably with each increase in load eccentricity.

**5.1.4. Effect of transverse reinforcement type.** Specimens of Group 2 were prepared to study the effects of using BFRP ties as compared to steel ties, on the overall columns' behavior. Confinement of concrete columns by transverse reinforcement improves strength and ductility by restraining lateral dilation. Also, by restraining concrete dilation, transverse reinforcements are known to delay the damage process [101]. In this study, specimens B-20-0, B-20-40 and B-20-80, transversely reinforced with steel ties at 180 mm spacing, and specimens B-T180-0, B-T180-40 and B-T180-80, transversely reinforced with BFRP ties at 180 mm spacing, are used to study the effect of replacing steel ties with BFRP ties. Normalized axial load versus concrete strains, longitudinal bars strains, axial displacements and lateral deflections, are shown in Figures 5.6 to 5.9, respectively, for the mentioned column specimens. Comparing the normalized axial load values for the columns, the specimens confined with steel ties showed very slightly higher axial capacities than the ones confined with BFRP ties by 1.9%, 4.7% and 2%, at concentric loads, *e/h* of 22.2% and *e/h* of 44.4%, respectively. In addition, there was insignificant difference in the confinement efficiencies of both columns, in which specimen B-T180-0, confined with BFRP ties, showed only 5% higher confinement efficiency than specimen B-20-0, confined with steel ties, as shown in Table 5.1. However, it was found that the BFRP bar strength contribution was higher in the column confined with steel ties than in the column confined with BFRP ties by around 40%, as shown in Table 4.1.

Additionally, for the same tie spacing, columns confined with steel ties showed very similar responses to their counterparts confined with BFRP ties in terms of axial load versus concrete strain at all levels of eccentricity, as shown in Figure 5.6. Likewise, Figures 5.7 to 5.9 show similar responses in terms of axial load versus longitudinal reinforcement strain, axial displacements and lateral deflections, for columns confined with steel ties and those confined with BFRP ties. However, this cannot be generalized for all load eccentricity levels, since some data were not available for some columns due to errors with the strain gauges and the LVDTs. The results, therefore, demonstrate that BFRP ties can have comparable confinement efficiencies to steel ties having the

same ties spacing. This suggests that the provisions of CSA-S806-12 [27] and ACI440.1R-15 [2] for FRP transverse reinforcement, which mandate maximum spacing equal to the least column dimension, 16 times the diameter of the longitudinal bars, or 48 times the diameter of the ties, can ensure adequate confinement of the concrete core of FRP-RC columns. These requirements are similar to those mandated by ACI 318-14 [44] and CSA-A23.3-14 [86] for steel transverse reinforcement. Similar results were reported in previous studies [51, 53, 54, 59].

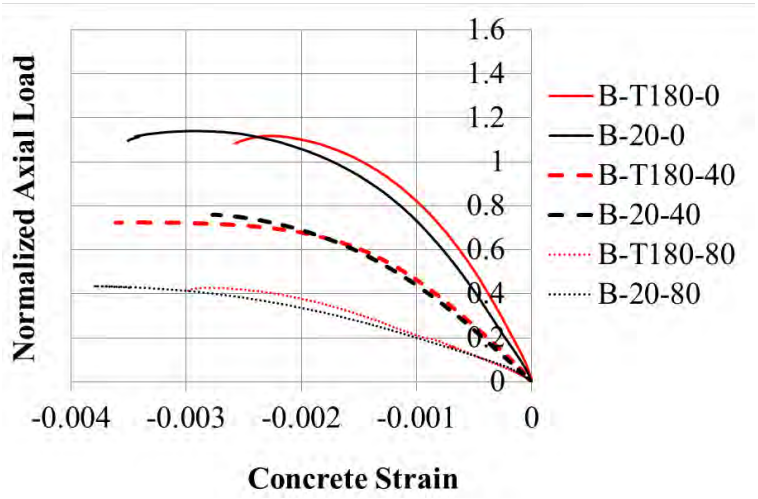


Figure 5.6: Normalized axial load vs. concrete strain curves compared for different transverse reinforcement types

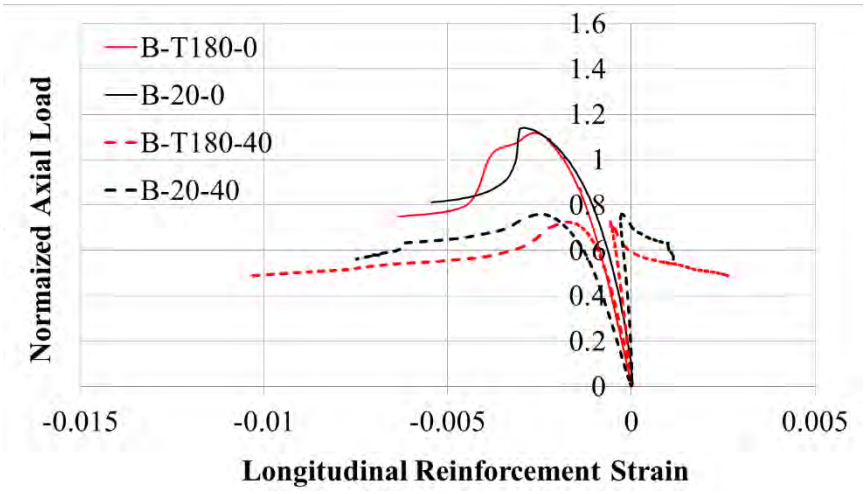


Figure 5.7: Normalized axial load vs. longitudinal reinforcement strain curves compared for different transverse reinforcement types

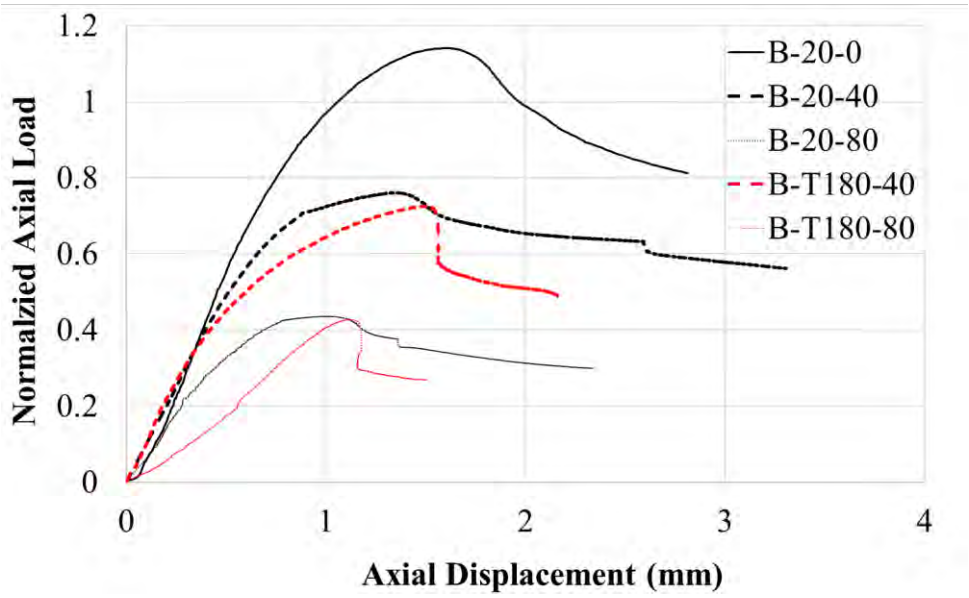


Figure 5.8: Normalized axial load vs. axial displacement curves compared for different transverse reinforcement types

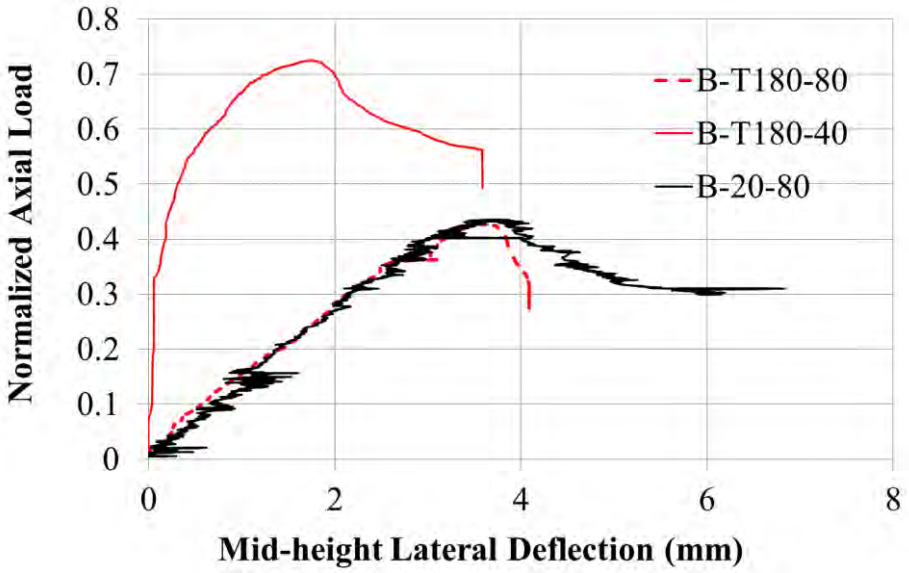


Figure 5.9: Normalized axial load vs. mid-height lateral deflection curves compared for different transverse reinforcement types

In general, transverse reinforcements (ties) in RC columns do not experience high strains/stresses at low levels of axial deformation. As the axial deformation increases and stresses start approaching peak values, microcracks start forming and propagating in the concrete core, which cause the core to dilate and transverse stresses to increase.

This, in turn, imposes stresses in the transverse reinforcement activating their confinement effects. The impact of confinement provided by the ties on the peak and post-peak cracking behavior and deformability of the tested columns is evaluated by analysing the dilation and volumetric strain responses. Figure 5.10 shows graphs of volumetric strain versus axial strain and dilation ratio versus axial strain for columns B-20-0 and B-T180-0, confined with steel ties and BFRP ties, respectively. Volumetric strain is defined as the change in volume per unit volume, in a tri-axial state of stress, and is given by:

$$\varepsilon_v = \varepsilon_a + 2\varepsilon_l \qquad (5.2)$$

where, $\varepsilon_a$ = axial strain and $\varepsilon_l$ = lateral strain.

The assumption is that a positive volumetric strain designates volume reduction, while a negative value designates volume expansion. It should be noted that the volumetric strain described herein is ideal since it is measured at mid-height of the specimens, while the rest of the cross-section does not behave as the mid-height cross section due to restraints at the boundaries. The mid-height cross-section is least affected by the boundary conditions. The dilation ratio is defined as the ratio of lateral strain to axial strain, and its initial value for plain concrete (known as the Poisson's ratio) ranges from 0.15 to 0.22. This ratio approaches 0.5 at the unstable crushing stage when the concrete axial strain reaches around 0.002, beyond which it increases with an almost vertical slope.

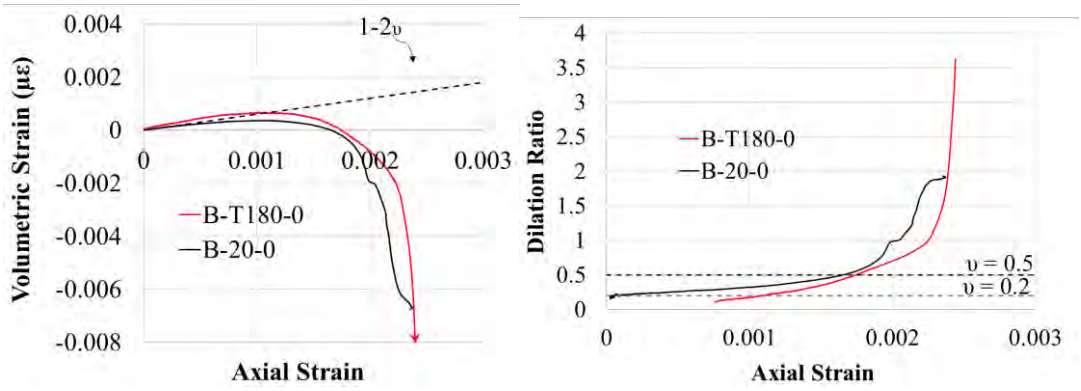


(a) (b)

Figure 5.10: Graphs of (a) volumetric strain versus axial strain and (b) dilation ratio versus axial strain, for specimens B-20-0 and B-T180-0

It can be seen from Figure 5.10a, that the initial slopes of the two curves is close to 1-2υ (where υ is the plain concrete's Poisson's ratio assumed to be 0.2), corresponding to the perfectly elastic condition. The curves then deviate from this line as peak loads are approached, and reach their maximum points. Those points are points of reversal in volumetric strain, and correspond to the start of uncontrolled crack growth leading to failure. The post-peak curves of both specimens develop gradually and in a similar manner, showing stable crack progression and indicating that both the steel and BFRP ties were active in confining the concrete core. Figure 5.10b shows that, the dilation ratio of specimen B-20-0 starts from 0.2 and increases fairly linearly up to 0.5 at an axial strain value of around 0.0016. Past this point, the dilation ratio increases more rapidly and reaches a value of almost 1.0 at an axial strain value of 0.002. In the case of specimen B-T180-0, the dilation ratio starts from a value of 0.13 and increases fairly linearly up to a value of 0.5 at an axial strain of about 0.0017. The dilation ratio then continues to increase at almost the same rate up to a value close to 1.0 at which the axial strain is about 0.0022. Past this point, the dilation ratio increases more rapidly with an almost vertical slope up to failure. These results show that the steel and BFRP ties demonstrated similar confinement efficiencies, and similar control of crack propagation. Consequently, it can be concluded that BFRP ties could provide efficient confinement to the concrete core and increase columns' deformation capacities, as was also reported for other FRP ties in previous studies [35, 46, 50, 52, 53, 58, 60, 78, 85].

**5.1.5. Effect of transverse reinforcement spacing.** Column specimens of Group 2 were prepared to study the effects of reducing BFRP ties spacing on the overall behavior of the columns. Since columns of Group 2 were all cast from the same concrete batch, graphs for normalized loads are not required. The results show that reducing BFRP ties spacing did not have any significant effect on the ultimate capacities of the columns, with the maximum percentage difference in the axial capacities of the columns being less than 10%. However, reducing BFRP ties spacing to 60 mm resulted in a higher strength contribution of the BFRP bars as compared to 120 mm and 180 mm spacing, by 23% and 39%, respectively, as listed in Table 4.1. Reducing tie spacing from 180 mm to 120 mm increased bar strength contribution by 16%. Also, Table 5.1 shows that reducing the tie spacing from 180 mm to 60 mm improved column ductility by 74%, 25% and 24% at concentric loads, *e/h* of 22.2% and *e/h* of 44.4%, respectively. It is also found that the ductility of columns confined with BFRP ties at reduced spacing

of 60 mm and 120 mm, was higher than that of columns confined with steel ties at 180 mm, at all load eccentricities, as shown in Table 5.1, despite the lower concrete compressive strength of columns of Group 2, confined with BFRP ties, as compared to columns of Group 1, confined with steel ties. Contrary to expectations, columns confined with BFRP ties at 120 mm showed higher ductility than those confined with BFRP ties at both 180 mm and 60 mm, for all load levels. No obvious reason is available for this observation. In addition, there were insignificant differences in the confinement efficiency values between the columns having different BFRP ties spacing. At 60 mm ties spacing, the column's confinement efficiency was about 6% higher than at 120 mm ties spacing, and was around 6% lower than at 180 mm ties spacing.

Figures 4.7b, 4.8b, 4.9b and 4.10b, show that the columns had similar axial displacement, lateral deflection, concrete strain and longitudinal reinforcement strain responses at all eccentricity levels. However, column specimens B-T120-0, B-T60-40 and B-T60-80, showed second peak loads after the concrete cover had spalled. This indicates that reducing the BFRP tie spacing can improve confinement of the concrete core. Also, the columns having BFRP ties spacing of 120 mm and 60 mm showed lower rates of strength decay than those with BFRP ties spacing of 180 mm, for all loading conditions, indicating that reduced tie spacing can improve columns ductility. The failure modes for all columns were similar irrespective of the BFRP ties spacing, and were characterized by compression failure due to concrete crushing. Thus, it can be concluded that reducing BFRP ties spacing would have more pronounced effect on confinement efficiency and ductility than on strength capacity of FRP RC columns. Similar conclusions were also reached in previous studies [49, 50].

Figure 5.11 shows graphs of volumetric strain versus axial strain, and dilation ratio versus axial strain for columns B-T60-0, B-T120-0 and B-T180-0. It can be seen from Figure 5.11a, that the initial slopes of the curves for specimens B-T60-0 and B-T180-0 is close to 1-2υ (where υ is the plain concrete's Poisson's ratio assumed to be 0.2), corresponding to the perfectly elastic condition. The curves then deviate from this line as peak loads are approached, and reach their maximum points, which correspond to the start of uncontrolled crack growth leading to failure. Column B-T60-0 reached a higher axial strain value, of 0.0023, at this maximum point, which indicates that a reduced tie spacing of 60 mm allowed for more effective confinement of the concrete

core and delayed crack propagation. The post-peak curves of all specimens then develop gradually up to failure.

Additionally, Figure 5.11b shows that specimen B-T60-0 has an average dilation ratio ranging from 0.2 to 0.25 up to an axial strain value of approximately 0.002, and reaches 0.5 at an axial strain of around 0.003 past which it increases with an almost vertical slope up to failure. On the other hand, specimen B-T120-0 has an average dilation ratio of 0.3 up to an axial strain of about 0.0015, and reaches a value of 0.5 at an axial strain of about 0.0018 past which it increases with an almost vertical slope up to failure. Specimen B-T180-0 showed similar response to specimen B-T120-0, in which the dilation ratio starts from 0.13 and reaches 0.5 at an axial strain of about 0.0017. The dilation ratio then continues to increase at almost the same rate up to a value close to 1.0 at an axial strain of about 0.0022, past which it increases with an almost vertical slope up to failure. Pessiki and Peironi [71] reported that the confinement of spirals becomes ineffective as the spiral pitch becomes close to the diameter of the column's core. This can explain the similarity in the confinement efficiency between specimens B-T180-0 and B-T120-0, despite the reduced ties spacing of specimen B-T120-0, in which the 120 mm spacing is close to the 115 mm core width of columns tested in this study. Overall, the results show that reducing the BFRP ties spacing improves the confinement efficiency of BFRP-RC columns, and allows for more controlled crack propagation.

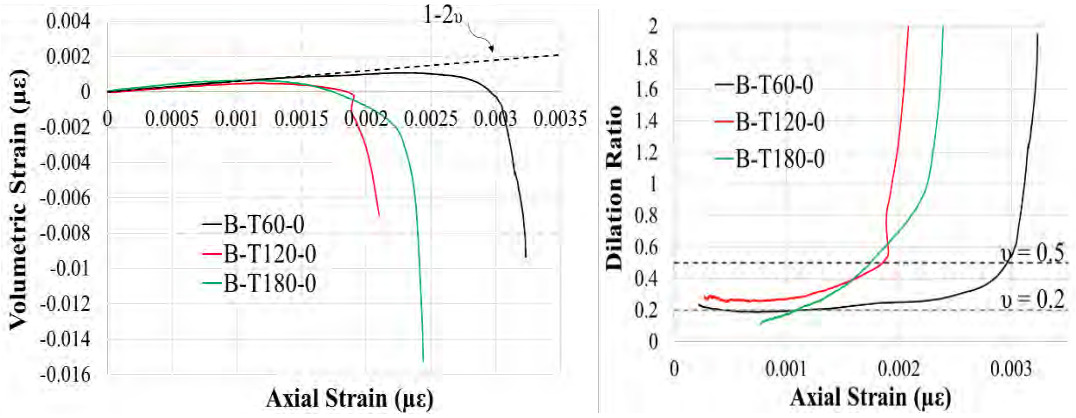


(a) (b)

Figure 5.11: Graphs of (a) volumetric strain versus axial strain and (b) dilation ratio versus axial strain, for specimens B-T60-0, B-T120-0 and B-T180-0

## 5.2. Experimental Axial Load – Bending Moment Interaction Diagrams

In this study, three loading conditions were considered, including concentric loading, and loading under 40 mm eccentricity and 80 mm eccentricity. The experimental results of the study were used to plot normalized axial load-bending moment (*P-M*) interaction diagrams for all columns, in terms of normalized axial force ($K_n$) and normalized bending moment ($R_n$). The $K_n$ and $R_n$ values are calculated as:

$$K_n = \frac{P_n}{f_c' A_g} \tag{5.3}$$

$$R_n = \frac{M_n}{f_c' A_g h} \tag{5.4}$$

where, $P_n$ = ultimate axial load sustained by column,

$M_n$ = bending moment corresponding to the ultimate axial load of each column,

$f'_c$ = concrete compressive strength,

$A_g$ = is the column's gross sectional area, and

$h$ = is the column dimension (equal to 180 mm for all columns),

The moment values used for developing the interaction diagrams consist of two moments, $M_{n1}$ and $M_{n2}$. $M_{n1}$ is calculated based on the initial eccentricity, and $M_{n2}$ is the secondary moment developed due to the lateral mid-height deflections of the columns, considering the *P-δ* effects. $M_{n1}$ and $M_{n2}$ moments are given by:

$$M_n = M_{n1} + M_{n2} = P_n (e + \Delta)$$

where, $e$ = initial applied eccentricity value, and

$\Delta$ = mid-height lateral deflection in column at peak load (values of which are shown in Table 4.1.)

Figure 5.12 shows the normalized axial load-bending moment interaction diagrams for columns of Groups 1 and 2. Three points were used to develop the *P-M* curves for each set of specimens. The first point represents the column specimens tested under concentric loads, and the second and third points represent the column specimens tested under 40 mm and 80 mm eccentricities, respectively. In order to allow for a complete representation of the *P-M* interaction diagram for the steel RC columns, a fourth point was added to the *P-M* curve which represents the theoretical capacity of a steel RC

column under pure flexural loads, having the same dimensions and reinforcement details as the columns tested in this study. The fourth point on the *P-M* curve was determined from the flexural capacity equations for steel RC beams based on ACI 318-14 code [44].

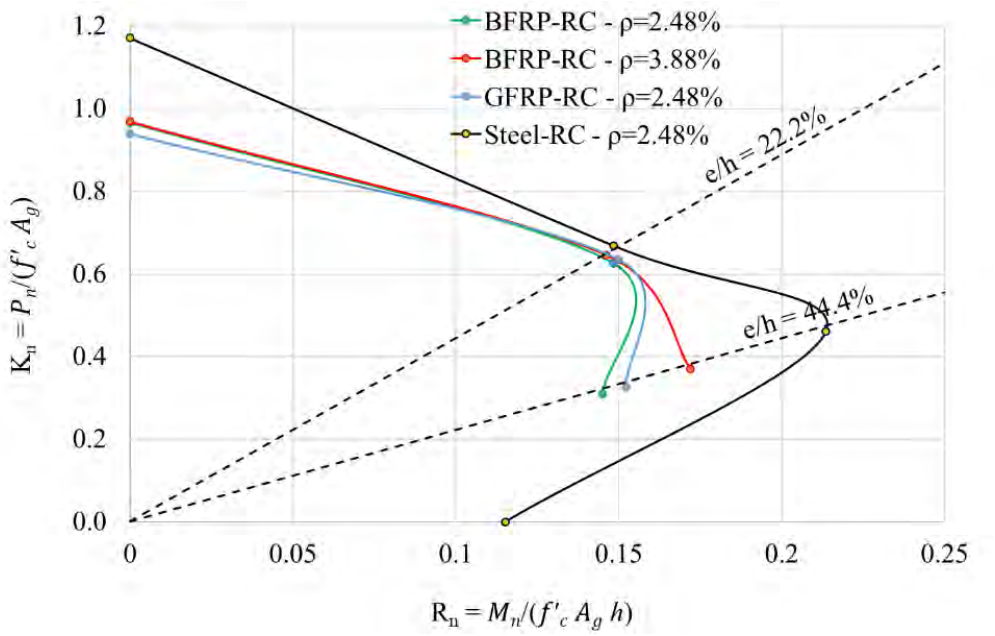


(a)

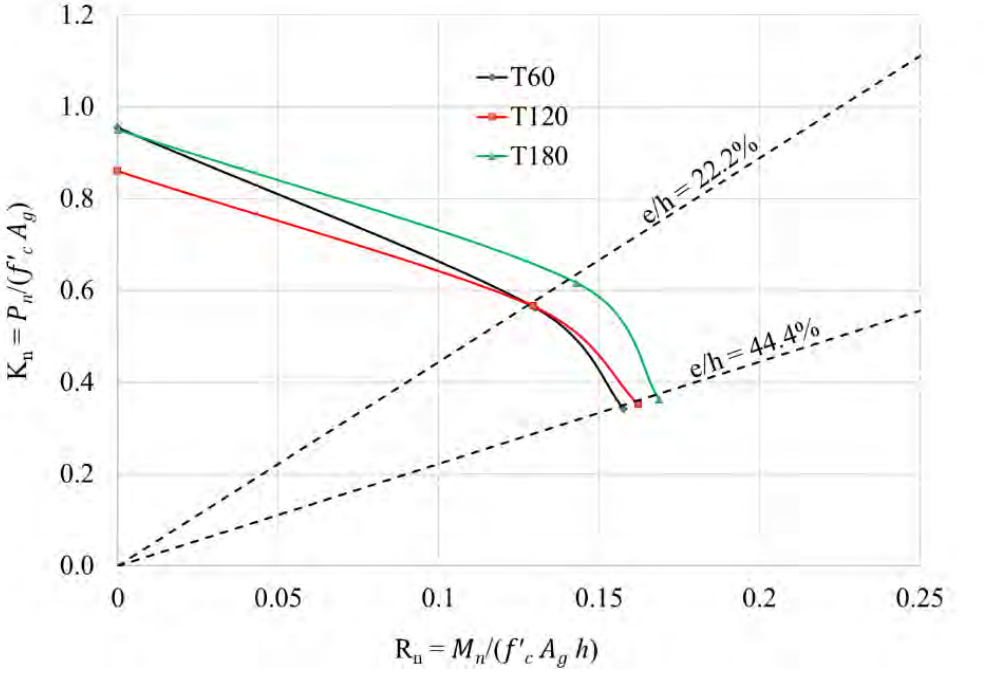


(b)

Figure 5.12: Normalized experimental axial load-bending moment interaction diagrams for columns of (a) Group 1 and (b) Group 2

The *P-M* interaction diagrams are shown separately for each set of columns in Figures 5.13 to 5.19, where the strain gradients at the first three points of the *P-M* curves are also shown. The *P-M* curves of Figure 5.12a show that the capacities of the steel RC columns are higher than those of the BFRP RC or GFRP RC columns reinforced with the same longitudinal reinforcement ratio (2.48%), at every eccentricity level. Also, the results show that capacities of the steel RC columns are higher than those of the BFRP RC columns designed to have equivalent strength to the steel RC ones, which is represented by the red *P-M* curve in Figure 5.12a. This is owing to the lower elastic modulus of FRP bars as compared to steel bars. Additionally, there were insignificant differences in the capacities of the columns reinforced with GFRP and BFRP bars at the same longitudinal reinforcement ratio of 2.48%, at all levels of eccentricity. Moreover, the *P-M* curves of Figure 5.12a, show that the columns reinforced with a higher BFRP longitudinal reinforcement ratio of 3.88%, showed very close capacities to those of BFRP RC or GFRP RC columns, reinforced with the same longitudinal reinforcement ratio of 2.48%, at low levels of eccentricity. Nevertheless, as the eccentricity increases, the BFRP RC columns with higher longitudinal reinforcement ratio exhibit higher capacities as compared to columns having lower FRP longitudinal reinforcement ratios. This can be due to the higher stiffness of BFRP RC columns at higher longitudinal reinforcement ratios, which allows them to develop higher tensile stresses as bending stresses increase.

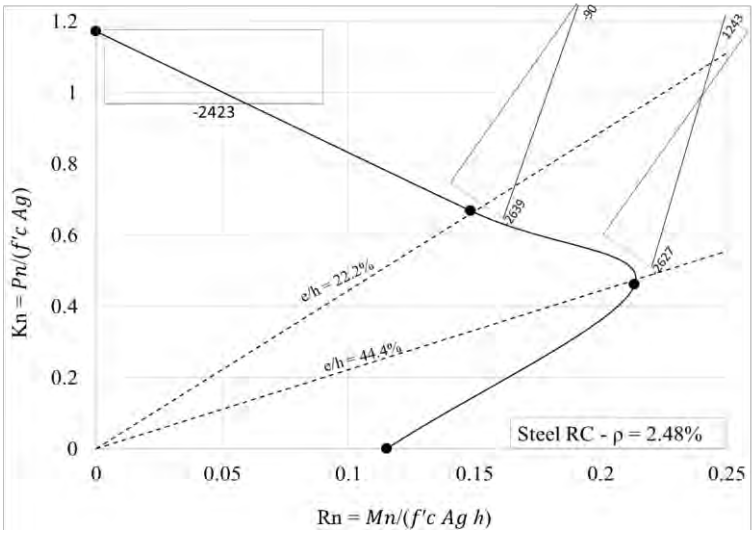


Figure 5.13: Normalized experimental axial load-bending moment interaction diagrams with strain gradients for steel RC columns

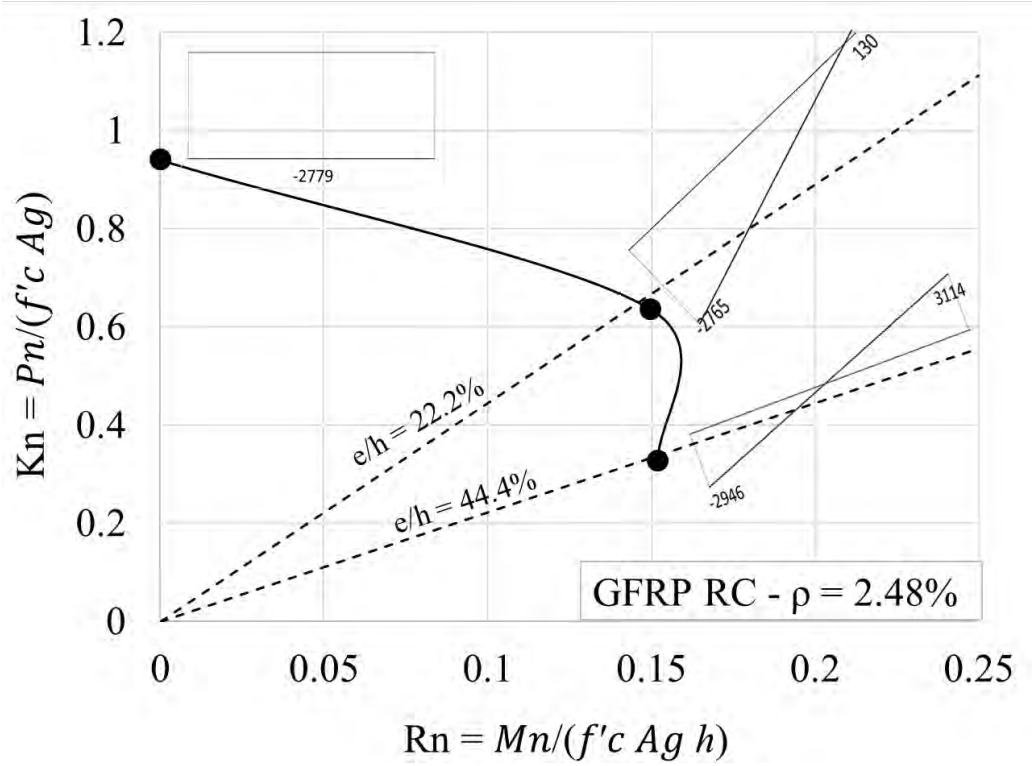


Figure 5.14: Normalized experimental axial load-bending moment interaction diagrams with strain gradients for GFRP RC columns

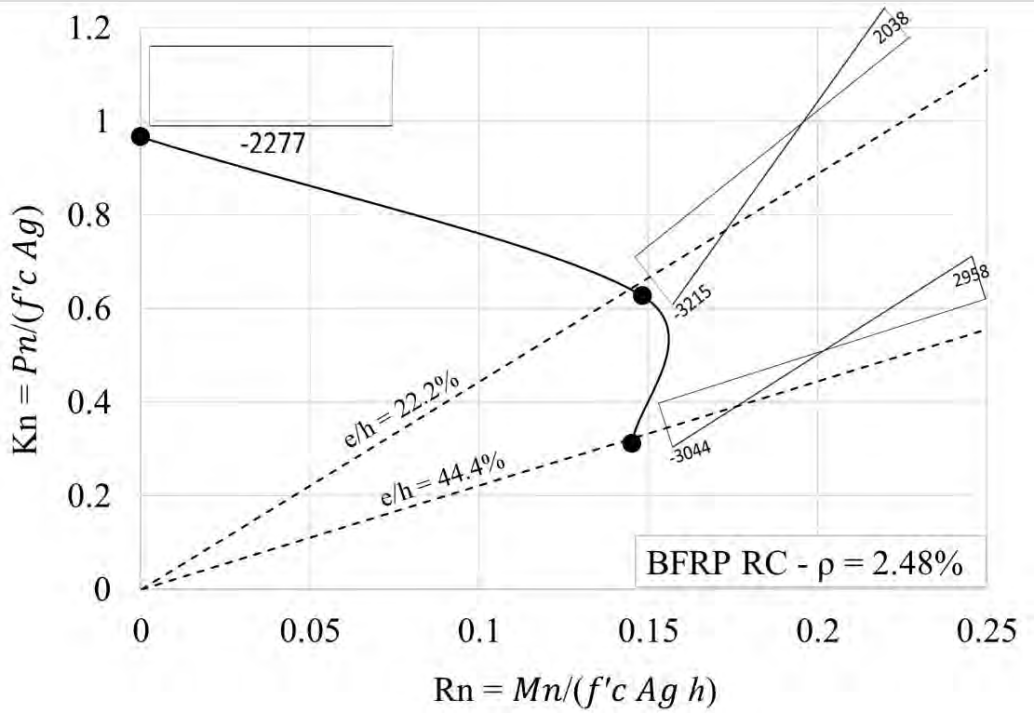


Figure 5.15: Normalized experimental axial load-bending moment interaction diagrams with strain gradients for BFRP RC columns at longitudinal reinforcement ratio of 2.48%

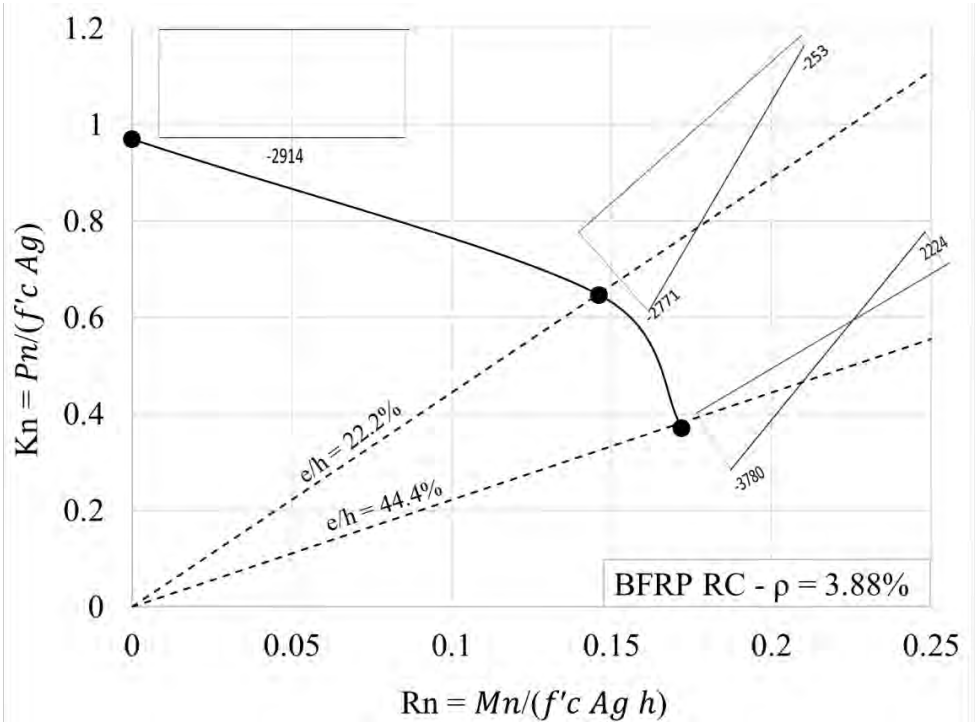


Figure 5.16: Normalized experimental axial load-bending moment interaction diagrams with strain gradients for BFRP RC columns at longitudinal reinforcement ratio of 3.88%

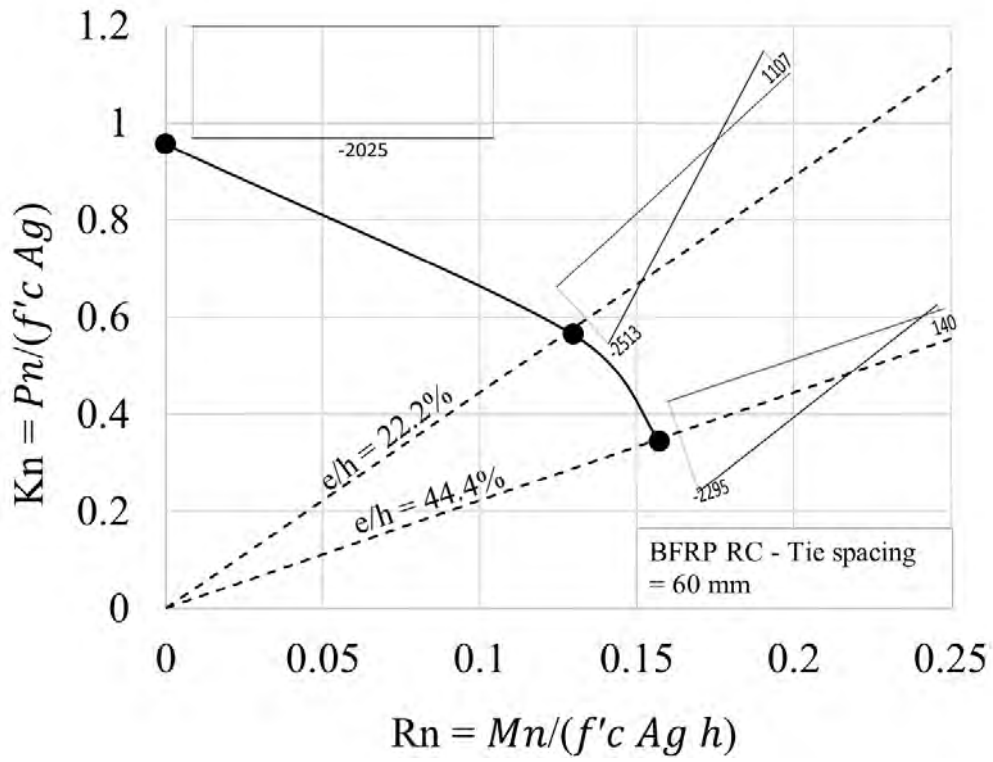


Figure 5.17: Normalized experimental axial load-bending moment interaction diagrams with strain gradients for BFRP RC columns at BFRP ties spacing of 60 mm

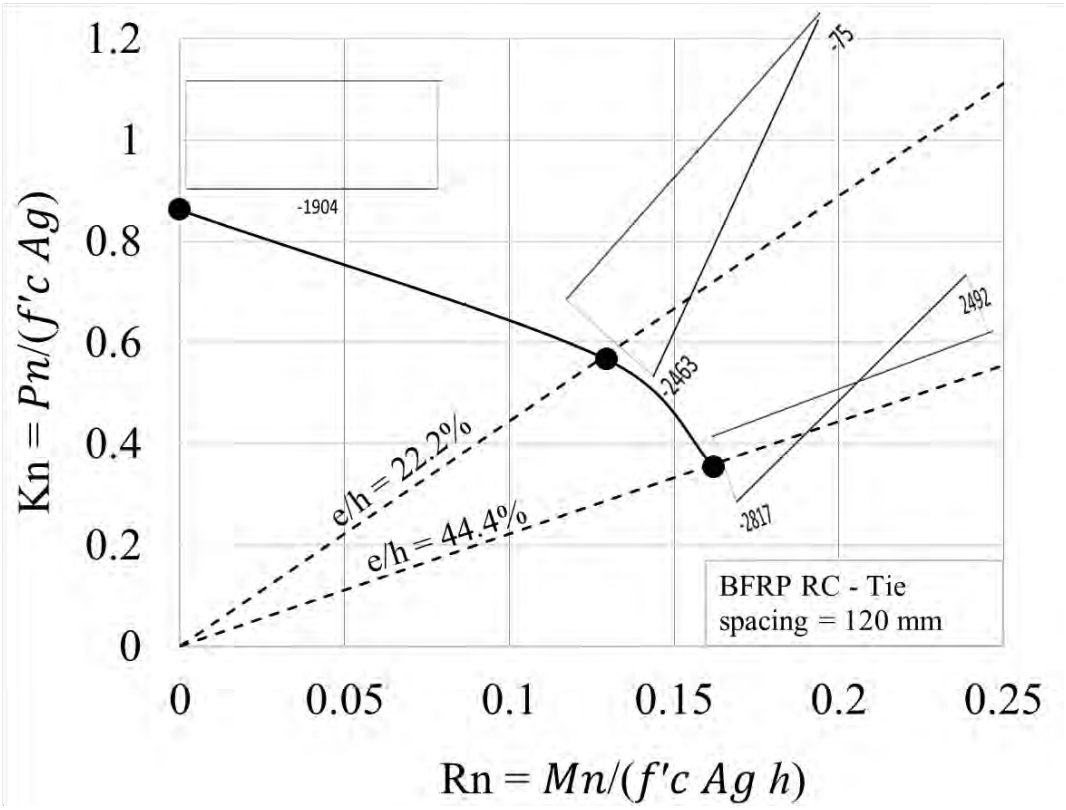


Figure 5.18: Normalized experimental axial load-bending moment interaction diagrams with strain gradients for BFRP RC columns at BFRP ties spacing of 120 mm

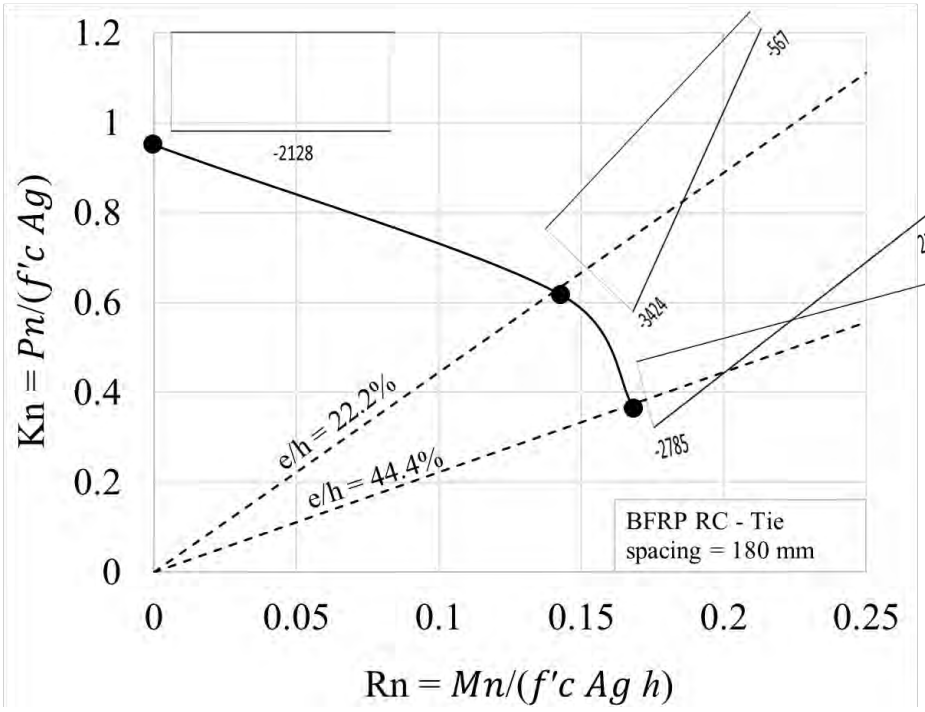


Figure 5.19: Normalized experimental axial load-bending moment interaction diagrams with strain gradients for BFRP RC columns at BFRP ties spacing of 180 mm

### 5.3. Evaluation of Proposed Design Equations for FRP RC Columns

A number of design equations have been proposed in the literature for determining the ultimate axial capacities of short FRP RC columns, as shown in Table 2.3. The equations were analysed in the introduction section, and the concept behind each one was explained. Average ratios of the predicted axial capacities of the columns tested in this study, as calculated by each of the proposed equations, to their experimental axial capacities ($P_{pred}/P_{exp}$), are illustrated by bar charts shown in Figures 5.20 and 5.21, for BFRP-RC and GFRP-RC columns, respectively. Analysis of the predicted-to-experimental capacity ratios of columns tested in previous studies, which was presented in the introduction section, showed that Equation 2.3, which assumes compressive contribution of FRP bars of 25% of their ultimate tensile capacities, gives the most accurate predictions of the ultimate capacities of FRP-RC columns. The reduction factor 0.25 was proposed in a previous study for columns reinforced with CFRP bars, and was found to yield accurate predictions of the columns' ultimate capacities [50]. Nevertheless, the 0.25 reduction factor proposed for CFRP bars was found to be inadequate for BFRP bars, as given by using Equation 2.3, which resulted in overestimation of the axial capacities of BFRP-RC columns by 18%. On the other hand, using the 0.25 reduction factor in Equation 2.3 results in only 3% overestimation of the capacities of GFRP-RC columns, as shown in Figure 5.21.

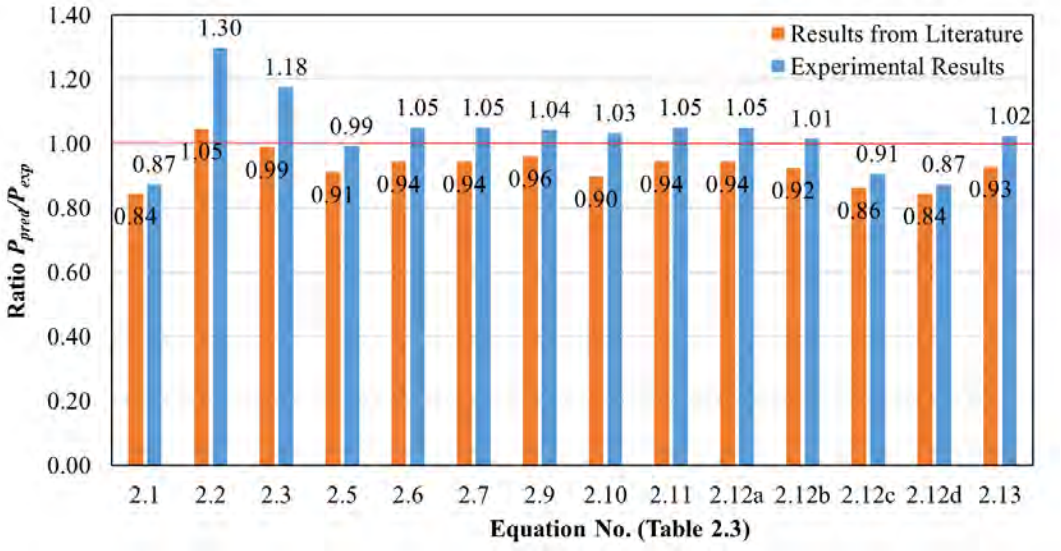


Figure 5.20: Predicted-to-experimental capacity ratios from proposed design equations for BFRP-RC columns

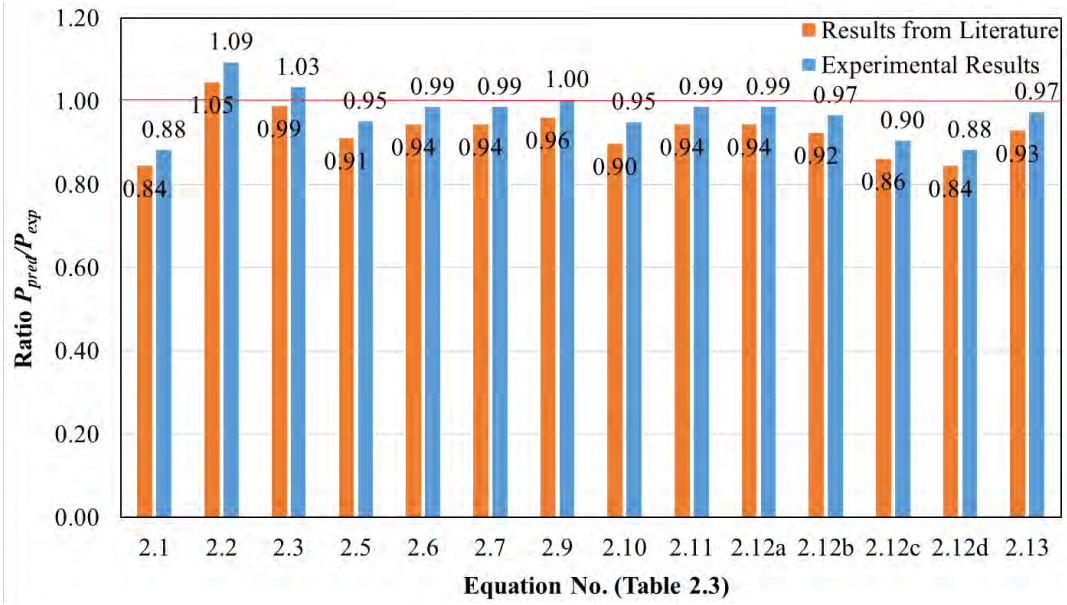


Figure 5.21: Predicted-to-experimental capacity ratios from proposed design equations for GFRP-RC columns

Equation 2.5, which is proposed by Mohamed et al. [51] and assumes the compressive strain in FRP bars to be equal to 0.002, which is concrete strain at the onset of micro-cracking in the plastic stage, was found to provide the most accurate predictions of the axial capacities of BFRP-RC columns ($P_{pred}/P_{exp}$ = 0.99). Equation 2.5 provided fairly good predictions of GFRP-RC columns capacities ($P_{pred}/P_{exp}$ = 0.95). Moreover, evaluating the recommendations of the current FRP design codes, CSA S806-12 [27] and ACI440.1R-15 [2], to ignore the contribution of FRP bars in compression, several of the previous studies [42, 56, 58, 60, 67, 68] concluded that the contribution of FRP bars is significant and should not be ignored. In this study, ignoring the contribution of FRP bars to the capacity of columns in Equations 2.1, 2.12c and 2.12d, resulted in predicted-to-experimental axial capacity ratios for the columns from 0.87 to 0.91. This confirms conclusions from previous studies that the recommendations of the FRP design codes are conservative, and that the contribution of FRP bars to the ultimate capacities of the columns should not be neglected.

In this study, specimens reinforced with four 20 mm diameter BFRP bars were designed based on the equivalent strength of four 16 mm diameter steel bars using a reduction factor of 0.35 to account for the lower compressive strength of BFRP bars as compared to their tensile strength ($f_y A_{st} = 0.35\, f_{fu} A_f$), as was done in previous

studies [47, 49]. Some previous studies reported that the 0.35 reduction factor was found to provide accurate predictions of the ultimate capacities of RC columns reinforced with GFRP bars [47, 49]. However, based on the experimental results of this study, it was concluded that the reduction factor of 0.35 would not be adequate for BFRP bars. This conclusion is further confirmed by analysis of the proposed design equations, in which Equation 2.2, which assumes compressive strength of FRP bars of 35% of their ultimate tensile strength, was found to overestimate the columns' capacities by 30%. Also, Equation 2.2 resulted in overestimation of the capacities of GFRP-RC columns tested in this study by 9%.

As shown in Figure 5.20, equations 2.6, 2.7, 2.9, 2.10, 2.11, 2.12a and 2.12b, which assume maximum strain in the FRP bars of 0.0024 to 0.003, equivalent to crushing strain in concrete, were found to overestimate the ultimate capacities of BFRP-RC columns by only 1 to 4%. However, the same equations resulted in accurate predictions of the capacities of GFRP-RC columns, where ratios of $P_{pred}/P_{exp}$ ranged from 0.95 to 1.0. It should be noted that Equations 2.13 and 2.5 are similar, but with the difference that Equation 2.13 considers the area of the bars in the gross area of the column, whereas the bar area is deducted from the gross area in Equation 2.5.

Consequently, it can be concluded that the axial capacities of BFRP RC columns might not be accurately predicted by the same equations used for other types of FRP RC columns. Also, as previously concluded from the analysis of the literature, considering the contribution-to-capacity of FRP bars based on the ultimate concrete strain in the design equations, provide the most accurate predictions of the FRP-RC columns' capacities. Assuming strain in FRP bars equal to strain in concrete at the onset of cracking, of 0.002, in design equations, can yield the most accurate predictions of BFRP-RC columns' capacities.

# Chapter 6. Conclusion and Future Work

In this thesis, a critical review of the literature on fiber-reinforced polymer - reinforced concrete (FRP-RC) columns is presented, and an experimental investigation is conducted on the overall behavior of FRP-RC columns under different test parameters. A total of 22 RC columns were cast and tested, including 3 GFRP-RC columns and 16 BFRP-RC columns, as well as 3 steel-RC columns serving as control specimens. The loading conditions investigated included concentric and eccentric loads. Of the 16 BFRP-RC columns, 9 columns were transversely reinforced with steel ties, and 7 columns were transversely reinforced with BFRP ties, to study the effects of BFRP ties on the columns' overall behavior. The test parameters included the longitudinal reinforcement type (steel, GFRP and BFRP), the BFRP longitudinal reinforcement ratio (2.48% and 3.88%), the transverse reinforcement type (steel and BFRP ties), the BFRP transverse reinforcement spacing (60, 120 and 180 mm), and the loading eccentricity ($e/h$ = 0, 22.2% and 44.4%). The effects of the test parameters on the behavior of the columns were studied in terms of the columns' ultimate capacities, deformation capacities and ductility, and strength contribution of longitudinal reinforcement. It should be emphasized that all discussions and conclusions are for columns tested under static loading conditions; the columns' behavior could be different under cyclic and creep loadings. The following conclusions are made from the results of this research:

- The failure modes of the tested columns were mainly affected by the level of eccentricity, and by the transverse reinforcement type and spacing. Failure modes were observed to be similar for columns subjected to the same loading conditions, irrespective of the longitudinal reinforcement type or ratio, with all columns experiencing a compression-controlled failure mode due to concrete crushing for FRP RC columns, and concrete crushing and yielding of steel reinforcement for steel RC columns. However, under high eccentric loads, failure modes of columns were also affected by the type of longitudinal reinforcement.
- At all levels of load eccentricities, steel RC columns exhibited higher axial load capacities than FRP RC columns. The capacities of steel RC columns were higher than those of FRP RC columns by around 19 to 22%, under pure axial

loads. However, as the load eccentricity increased, the differences in the ultimate capacities between steel RC and FRP RC columns decreased. This could be attributed to the high strains developed in FRP bars at ultimate resulting in high contribution-to-capacity of FRP bars in tension.

- The contribution of steel bars to the ultimate capacities of the columns was found to be 31.4%, whereas the strength contributions of BFRP and GFRP bars were lower, at 10.9% and 10.5%, respectively.
- The ductility of columns reinforced with BFRP or GFRP bars was higher than the ductility of columns reinforced with steel bars, at all load eccentricities, by up to 55% and 45%, respectively.
- There were insignificant differences between BFRP RC and GFRP RC columns in terms of overall strain and displacement responses, peak loads and bars strength contributions. However, BFRP RC columns were found to be more ductile than their counterpart GFRP RC columns, at all levels of eccentricity, as calculated by their ductility indices.
- Increasing the longitudinal reinforcement ratio for BFRP RC columns does not significantly affect the ultimate capacities of the columns under pure axial loads, but results in higher columns' ultimate capacities under eccentric loads. The differences in the ultimate capacities between the columns increase as load eccentricities increase. Increasing BFRP longitudinal reinforcement ratio from 2.48% to 3.88% increases the columns' axial capacities by 3%, and 17% at *e/h* of 22.2% and 44.4%, respectively.
- Increasing BFRP longitudinal reinforcement ratio from 2.48% to 3.88%, increased the contribution of BFRP bars to the ultimate capacity of the columns from 10.9% to 17.8%. However, increasing the BFRP longitudinal reinforcement ratio did not significantly affect the strain and deformation responses of the columns.
- BFRP ties have proven to provide efficient confinement to the concrete core and to increase columns' deformation capacities.
- BFRP ties were found to have comparable confinement efficiencies to steel ties having the same ties spacing. This suggests that the provisions for FRP transverse reinforcement of the current FRP-RC design codes, CSA-S806-12 [27] and ACI440.1R-15 [2], can ensure adequate confinement of the concrete core of FRP-RC columns.

- Reducing BFRP ties spacing did not have any significant effect on the ultimate capacities of the columns, with the maximum percentage difference in the axial capacities of the columns being 10%. However, reducing BFRP ties spacing to 60 mm resulted in a higher strength contribution of the BFRP bars as compared to 120 mm and 180 mm spacing, by 23% and 39%, respectively. Also, reducing the tie spacing from 180 mm to 60 mm improved column ductility by 74%, 25% and 24% at concentric loads, *e/h* of 22.2% and *e/h* of 44.4%, respectively.
- BFRP RC columns confined with BFRP ties at different spacing showed similar axial displacement, lateral deflection, concrete strain and longitudinal reinforcement strain responses at all eccentricity levels.
- Overall, reducing BFRP ties spacing would have more pronounced effect on confinement efficiency and ductility than on strength capacity of FRP RC columns.
- Evaluation and analysis of the proposed design equations for FRP-RC columns in the literature show that considering the contribution-to-capacity of FRP bars based on the ultimate concrete strain in the design equations, provides the most accurate predictions of the columns' capacities. Assuming strain in FRP bars equal to strain in concrete at the onset of cracking, of 0.002, in design equations, can yield the most accurate predictions of BFRP-RC columns' capacities.
- It is concluded that the axial capacities of BFRP RC columns might not be accurately predicted by the same equations applicable to other types of FRP RC columns.

The critical literature review, and analysis of the experimental results have shed light on the structural performance of FRP-RC columns; however, further investigations are deemed necessary for a better understanding of such performance, which can be summarized as follows:

- The uncertainty encountered in evaluating the compression properties of FRP bars has led to contradicting results on their contribution to the load-carrying capacities of the tested columns. Therefore, there is a need to standardize the tests used to evaluate such properties, similar to other standard tests related to FRP bars.
- Very few studies have focused on the structural performance of eccentrically-

loaded and slender FRP-RC columns. More tests are deemed necessary to quantify the contribution of the FRP bars in tension and whether it is necessary to limit the contribution of FRP bars in compression.

- Very few tests have reported on the seismic performance of FRP-RC columns and therefore, no definite conclusion can be made on their performance. Columns constitute the main resisting structural element in seismic areas, which requires more experimental and analytical investigations on the topic.
- Various approaches are used in the literature to determine the ductility of FRP-reinforced columns. It is recommended that a standardized method of determining the ductility of FRP-reinforced columns be developed in order to have a better understanding of the ductility performance of such columns especially under seismic loadings.
- The use of HSC, FRC, IPC in FRP-reinforced columns has received little attention despite the promising results obtained from the few studies reported in the literature. Concrete mixes that can provide adequate deformation and high ductility are recommended for FRP-reinforced columns to overcome the brittleness of the bars and to efficiently utilize their high tensile properties. Further studies are definitely needed to fill the gap in this area.
- Further experimental and analytical studies are encouraged to investigate the feasibility of using hybrid reinforcement (FRP and steel bars) in columns as an alternative to all-FRP-reinforced columns. Moreover, the use of hybrid reinforcement with HSC or FRC mixes may also provide a promising approach to overcome the lack of ductility associated with FRP bars.
- Very limited information is available on the use of BFRP bars as reinforcement for concrete columns, which can be associated to the recent introduction of basalt fibers to the construction industry. Further experimental investigations are definitely required.
- More research is required into the effects of confining RC columns with FRP transverse reinforcement, and on the effects of FRP transverse reinforcement ratios. In particular, more studies are needed to quantify the effects of BFRP transverse reinforcements on the behavior of FRP-RC columns.
- The long-term behavior and durability of FRP-RC columns when exposed to harsh environmental conditions has received little attention. Likewise, the

performance of FRP-reinforced columns under extreme loading conditions and fatigue should be further investigated.

- The design equations proposed in the literature can accurately predict the load-carrying capacities of short columns. More analytical studies are needed to investigate the performance of the slender ones.

Finally, the use of FRP bars to reinforce concrete elements in compression has reached a milestone. The available design equations are deemed satisfactory in predicting the load-carrying capacities of short FRP-reinforced columns. Therefore, it seems that it is time for code authorities to recognize the use of FRP in compression members. Simultaneously, research investigations must continue to fill the gap in our understanding on the unresolved topics.

## References


[1] L. Hollaway, "The evolution of and the way forward for advanced polymer composites in the civil infrastructure," *Construction and Building Materials,* vol. 17, no. 6, pp. 365-378, Sep. 2003.

[2] American Concrete Institute, "Guide for the design and construction of structural concrete reinforced with fiber-reinforced polymer (FRP) bars," ACI 440.1R-15, ACI Committee 440, Farmington Hills, MI, USA, 2015.

[3] P. K. Mallick, *Fiber-reinforced composites: materials, manufacturing, and design*, 3rd ed. CRC press, 2007.

[4] G. H. Koch, M. P. Brongers, N. G. Thompson, Y. P. Virmani, and J. H. Payer, "Corrosion cost and preventive strategies in the United States," US DOT, Washington, DC, USA, FHWA-RD-01-156, 2002.

[5] M. Leeming, "UK experience of plate bonding with advanced composite materials," in *Recent Advances in Bridge Engineering. Proceedings of the US-Europe Workshop on Bridge Engineering. Technical University of Catalonia, Spain and Iowa State University*, Barcelona, Spain, 1996, pp. 544-555.

[6] H. C. Boyle and V. M. Karbhari, "Investigation of bond behavior between glass fiber composite reinforcements and concrete," *Polymer-Plastics Technology and Engineering,* vol. 33, no. 6, pp. 733-753, 1994.

[7] V. Brown and C. Bartholomew, "Long-term deflections of GFRP-reinforced concrete beams," in *First International Conference on Composites in Infrastructure*, Tucson, Arizona, USA, 1996, pp. 389-400.

[8] T. Uomoto, H. Mutsuyoshi, F. Katsuki, and S. Misra, "Use of fiber reinforced polymer composites as reinforcing material for concrete," *Journal of Materials in Civil Engineering,* vol. 14, no. 3, pp. 191-209, 2002.

[9] C. Bedard, "Composite reinforcing bars: assessing their use in construction," *Concrete International,* vol. 14, no. 1, pp. 55-59, 1992.

[10] M. Pearson, T. Donchev, and M. Limbachiya, "An investigation into the sustainability of FRP reinforcing bars," in *Proc. Fourth International Conference on Durability & Sustainability of Fiber Reinforced Polymer (FRP) Composites for Construction and Rehabilitation*, Quebec City, Canada, 2011, pp. 20-22.

[11] U. Meier, "Carbon fiber-reinforced polymers: modern materials in bridge engineering," *Structural Engineering International,* vol. 2, no.1, pp. 7-12, 1992.

[12] L. Taerwe, "FRP activities in Europe: survey of research and applications," in *Proc. Third International Symposium on Non-Metallic (FRP) Reinforcement for Concrete Structures (FRPRCS-3)*, Sapporo, Japan, 1997, pp. 59-74.

[13] L. Ye *et al.*, "FRP in civil engineering in China: research and applications," in *Fibre-Reinforced Polymer Reinforcement for Concrete Structures: (In 2 Volumes)*: World Scientific, 2003, pp. 1401-1412.

[14] B. Drouin, G. Latour, and H. Mohamed, "More than 10 years successful field applications of FRP bars in Canada," in *CDCC 2011, The 4th Int. Conf. on Durability and Sustainability of Fiber Reinforced Polymer (FRP) Composites for Construction and Rehabilitation*, Quebec City, Canada, 2011, vol. 20.

[15] S. H. Rizkalla, "A new generation of civil engineering structures and bridges," in *Proc. Third International Symposium on Non-metallic (FRPRC) Reinforcement for Concrete Structures, Sapporo, Japan*, 1997, vol.1, pp.113-128.

[16] F. Abed and A. R. Alhafiz, "Effect of basalt fibers on the flexural behavior of concrete beams reinforced with BFRP bars," *Composite Structures,* vol. 215, pp. 23-34, 2019.
[17] F. Abed and N. ElMesalami, "Effect of Harsh Environmental Conditions on the Bond-Dependent Coefficient of GFRP Bars in Concrete Beams," in *2019 Advances in Science and Engineering Technology International Conferences (ASET)*, 2019: IEEE, pp. 1-5.
[18] F. Abed, H. El-Chabib, and M. AlHamaydeh, "Shear characteristics of GFRP-reinforced concrete deep beams without web reinforcement," *Journal of Reinforced Plastics and Composites,* vol. 31, no. 16, pp. 1063-1073, 2012.
[19] M. A. Adam, M. Said, A. A. Mahmoud, and A. S. Shanour, "Analytical and experimental flexural behavior of concrete beams reinforced with glass fiber reinforced polymers bars," *Construction and Building Materials,* vol. 84, pp. 354-366, 2015.
[20] Y. A. Al-Salloum and T. H. Almusallam, "Creep effect on the behavior of concrete beams reinforced with GFRP bars subjected to different environments," *Construction and Building Materials,* vol. 21, no. 7, pp. 1510-1519, 2007.
[21] A. F. Ashour, "Flexural and shear capacities of concrete beams reinforced with GFRP bars," *Construction and Building Materials,* vol. 20, no. 10, pp. 1005-1015, 2006.
[22] A. El Refai and F. Abed, "Concrete contribution to shear strength of beams reinforced with basalt fiber-reinforced bars," *Journal of Composites for Construction,* vol. 20, no. 4, 04015082, 2015.
[23] F. Elgabbas, E. A. Ahmed, and B. Benmokrane, "Physical and mechanical characteristics of new basalt-FRP bars for reinforcing concrete structures," *Construction and Building Materials,* vol. 95, pp. 623-635, 2015.
[24] American Concrete Institute, "Guide for the Design and Construction of Structural Concrete Reinforced with FRP Bars," ACI 440.1R-06, ACI Committee 440, Farmington Hills, MI, USA, 2006.
[25] American Concrete Institute, "Prestressing Concrete Structures with FRP Tendons," ACI 440.4R-04, ACI Committee 440, Farmington Hills, MI, USA, 2004.
[26] Canadian Standard Association, "Design and construction of building structures with fibre-reinforced polymers," CSA-S806-02, Mississauga, Ontario, Canada, 2002.
[27] Canadian Standard Association, "Design and construction of building structures with fibre-reinforced polymers," CSA-S806-12, Mississauga, Ontario, Canada, 2012.
[28] International Federation for Structural Concrete in Europe, "FRP reinforcement in RC structures," fib Bulletin 40, 2007.
[29] Intelligent Sensing for Innovative Structures, "Reinforcing Concrete Structures with Fibre Reinforced Polymers (FRPs)," Design Manual No. 3, ISIS Canada, Manitoba, Canada, 2012.
[30] Japan Society of Civil Engineers, "Recommendation for Design and Construction of Concrete Structures using Continuous Fiber Reinforcing Materials," JSCE, Tokyo, Japan, 1997.
[31] S. Raj, V. R. Kumar, B. B. Kumar, and N. R. Iyer, "Basalt: structural insight as a construction material," *Sādhanā,* vol. 42, no. 1, pp. 75-84, 2017.

[32] A. El Refai, F. Abed, and A. Altalmas, "Bond durability of basalt fiber–reinforced polymer bars embedded in concrete under direct pullout conditions," *Journal of Composites for Construction,* vol. 19, no. 5, 04014078, 2014.

[33] A. Altalmas, A. El Refai, and F. Abed, "Bond degradation of basalt fiber-reinforced polymer (BFRP) bars exposed to accelerated aging conditions," *Construction and Building Materials,* vol. 81, pp. 162-171, 2015.

[34] Canadian Standard Association, "Canadian Highway Bridge Design Code," CSA-S6-14, Mississauga, Ontario, Canada, 2014.

[35] M. Elchalakani and G. Ma, "Tests of glass fibre reinforced polymer rectangular concrete columns subjected to concentric and eccentric axial loading," *Engineering Structures,* vol. 151, pp. 93-104, 2017.

[36] W. Wu, "Thermomechanical properties of Fiber Reinforced Plastic (FRP) bars," Ph.D. dissertation, West Virginia University, Morgantown, WVa, USA, 1992.

[37] O. Chaallal and B. Benmokrane, "Physical and mechanical performance of an innovative glass-fiber-reinforced plastic rod for concrete and grouted anchorages," *Canadian Journal of Civil Engineering,* vol. 20, no. 2, pp. 254-268, 1993.

[38] K. Kobayashi and T. Fujisaki, "Compressive behavior of FRP reinforcement in non-prestressed concrete members." in *Non-Metallic (FRP) Reinforcement for Concrete Structures: Proceedings of the Second International RILEM Symposium*, 1995, vol. 29: CRC Press, pp. 267-274.

[39] D. Deitz, I. Harik, and H. Gesund, "Physical properties of glass fiber reinforced polymer rebars in compression," *Journal of Composites for Construction,* vol. 7, no. 4, pp. 363-366, 2003.

[40] A. Tavassoli, J. Liu, and S. Sheikh, "Glass fiber-reinforced polymer-reinforced circular columns under simulated seismic loads," *ACI Structural Journal,* vol. 112, no. 1, pp. 103-114, 2015.

[41] G. Maranan, A. Manalo, B. Benmokrane, W. Karunasena, and P. Mendis, "Behavior of concentrically loaded geopolymer-concrete circular columns reinforced longitudinally and transversely with GFRP bars," *Engineering Structures,* vol. 117, pp. 422-436, 2016.

[42] L. Sun, M. Wei, and N. Zhang, "Experimental study on the behavior of GFRP reinforced concrete columns under eccentric axial load," *Construction and Building Materials,* vol. 152, pp. 214-225, 2017.

[43] W. Xue, F. Peng, and Z. Fang, "Behavior and Design of Slender Rectangular Concrete Columns Longitudinally Reinforced with Fiber-Reinforced Polymer Bars," *Structural Journal,* vol. 115, no. 2, pp. 311-322, 2018.

[44] American Concrete Institute, "Building code requirements for structural concrete and commentary," ACI 318-14, Farmington Hills, MI, USA, 2014.

[45] K. Khorramian and P. Sadeghian, "Experimental and analytical behavior of short concrete columns reinforced with GFRP bars under eccentric loading," *Engineering Structures,* vol. 151, pp. 761-773, 2017.

[46] A. De Luca, F. Matta, and A. Nanni, "Behavior of full-scale glass fiber-reinforced polymer reinforced concrete columns under axial load," *ACI Structural Journal,* vol. 107, no. 5, pp. 589-596, 2010.

[47] H. Tobbi, A. S. Farghaly, and B. Benmokrane, "Concrete columns reinforced longitudinally and transversally with glass fiber-reinforced polymer bars," *ACI Structural Journal,* vol. 109, no. 4, pp. 551-558, 2012.

[48] C. P. Pantelides, M. E. Gibbons, and L. D. Reaveley, "Axial load behavior of concrete columns confined with GFRP spirals," *Journal of Composites for Construction,* vol. 17, no. 3, pp. 305-313, 2013.
[49] M. Z. Afifi, H. M. Mohamed, and B. Benmokrane, "Axial capacity of circular concrete columns reinforced with GFRP bars and spirals," *Journal of Composites for Construction,* vol. 18, no. 1, 04013017, 2013.
[50] M. Z. Afifi, H. M. Mohamed, and B. Benmokrane, "Strength and Axial Behavior of Circular Concrete Columns Reinforced with CFRP Bars and Spirals," *Journal of Composites for Construction,* vol. 18, no. 2, 04013035, 2014.
[51] H. M. Mohamed, M. Z. Afifi, and B. Benmokrane, "Performance evaluation of concrete columns reinforced longitudinally with FRP bars and confined with FRP hoops and spirals under axial load," *Journal of Bridge Engineering,* vol. 19, no. 7, 04014020, 2014.
[52] H. Tobbi, A. S. Farghaly, and B. Benmokrane, "Behavior of concentrically loaded fiber-reinforced polymer reinforced concrete columns with varying reinforcement types and ratios," *ACI Structural Journal,* vol. 111, no. 2, pp. 375-386, 2014.
[53] M. Z. Afifi, H. M. Mohamed, O. Chaallal, and B. Benmokrane, "Confinement model for concrete columns internally confined with carbon FRP spirals and hoops," *Journal of Structural Engineering,* vol. 141, no. 9, 04014219, 2014.
[54] A. Hadhood, H. M. Mohamed, and B. Benmokrane, "Experimental study of circular high-strength concrete columns reinforced with GFRP bars and spirals under concentric and eccentric loading," *Journal of Composites for Construction,* vol. 21, no. 2, 04016078, 2016.
[55] T. A. Hales, C. P. Pantelides, and L. D. Reaveley, "Experimental evaluation of slender high-strength concrete columns with GFRP and hybrid reinforcement," *Journal of Composites for Construction,* vol. 20, no. 6, 04016050, 2016.
[56] M. N. Hadi, H. Karim, and M. N. Sheikh, "Experimental investigations on circular concrete columns reinforced with GFRP bars and helices under different loading conditions," *Journal of Composites for Construction,* vol. 20, no. 4, 04016009, 2016.
[57] M. N. Hadi and J. Youssef, "Experimental investigation of GFRP-reinforced and GFRP-encased square concrete specimens under axial and eccentric load, and four-point bending test," *Journal of Composites for Construction,* vol. 20, no. 5, 04016020, 2016.
[58] A. Hadhood, H. M. Mohamed, and B. Benmokrane, "Axial Load–Moment Interaction Diagram of Circular Concrete Columns Reinforced with CFRP Bars and Spirals: Experimental and Theoretical Investigations," *Journal of Composites for Construction,* vol. 21, no. 2, 04016092, 2016.
[59] M. N. Hadi, H. A. Hasan, and M. N. Sheikh, "Experimental Investigation of Circular High-Strength Concrete Columns Reinforced with Glass Fiber-Reinforced Polymer Bars and Helices under Different Loading Conditions," *Journal of Composites for Construction,* vol. 21, no. 4, 04017005, 2017.
[60] A. Hadhood, H. M. Mohamed, F. Ghrib, and B. Benmokrane, "Efficiency of glass-fiber reinforced-polymer (GFRP) discrete hoops and bars in concrete columns under combined axial and flexural loads," *Composites Part B: Engineering,* vol. 114, pp. 223-236, 2017.
[61] A. Hadhood, H. M. Mohamed, and B. Benmokrane, "Strength of circular HSC columns reinforced internally with carbon-fiber-reinforced polymer bars under

axial and eccentric loads," *Construction and Building Materials,* vol. 141, pp. 366-378, 2017.

[62] H. A. Hasan, M. N. Sheikh, and M. N. Hadi, "Performance evaluation of high strength concrete and steel fibre high strength concrete columns reinforced with GFRP bars and helices," *Construction and Building Materials,* vol. 134, pp. 297-310, 2017.

[63] X. Zhang and Z. Deng, "Experimental study and theoretical analysis on axial compressive behavior of concrete columns reinforced with GFRP bars and PVA fibers," *Construction and Building Materials,* vol. 172, pp. 519-532, 2018.

[64] M. Elchalakani, A. Karrech, M. Dong, M. M. Ali, and B. Yang, "Experiments and finite element analysis of GFRP reinforced geopolymer concrete rectangular columns subjected to concentric and eccentric axial loading," *Structures*, vol. 14, pp. 273-289, 2018.

[65] A. Tabatabaei, A. Eslami, H. M. Mohamed, and B. Benmokrane, "Strength of compression lap-spliced GFRP bars in concrete columns with different splice lengths," *Construction and Building Materials,* vol. 182, pp. 657-669, 2018.

[66] X. Fan and M. Zhang, "Behaviour of inorganic polymer concrete columns reinforced with basalt FRP bars under eccentric compression: An experimental study," *Composites Part B: Engineering,* vol. 104, pp. 44-56, 2016.

[67] M. Guérin, H. Mohamed, B. Benmokrane, C. Shield, and A. Nanni, "Effect of Glass Fiber-Reinforced Polymer Reinforcement Ratio on Axial-Flexural Strength of Reinforced Concrete Columns," *ACI Structural Journal,* vol. 115, no. 4, pp. 1049-1061, 2018.

[68] M. Guérin, H. M. Mohamed, B. Benmokrane, A. Nanni, and C. K. Shield, "Eccentric Behavior of Full-Scale Reinforced Concrete Columns with Glass Fiber-Reinforced Polymer Bars and Ties," *ACI Structural Journal,* vol. 115, no. 2, pp. 489-499, 2018.

[69] J. Youssef and M. N. Hadi, "Axial load-bending moment diagrams of GFRP reinforced columns and GFRP encased square columns," *Construction and Building Materials,* vol. 135, pp. 550-564, 2017.

[70] H. Karim, M. N. Sheikh, and M. N. Hadi, "Axial load-axial deformation behaviour of circular concrete columns reinforced with GFRP bars and helices," *Construction and Building Materials,* vol. 112, pp. 1147-1157, 2016.

[71] S. Pessiki and A. Pieroni, "Axial Load Behavior of Large Scale Spirally Reinforced High Strength Concrete Columns," *Structural Journal,* vol. 94, no. 3, pp. 304-314, 1997.

[72] A. Mirmiran, W. Yuan, and X. Chen, "Design for slenderness in concrete columns internally reinforced with fiber-reinforced polymer bars," *Structural Journal,* vol. 98, no. 1, pp. 116-125, 2001.

[73] F. Shaikh, "Deflection hardening behaviour of short fibre reinforced fly ash based geopolymer composites," *Materials & Design,* vol. 50, pp. 674-682, 2013.

[74] B. Nematollahi, J. Sanjayan, and F. U. A. Shaikh, "Comparative deflection hardening behavior of short fiber reinforced geopolymer composites," *Construction and Building Materials,* vol. 70, pp. 54-64, 2014.

[75] B. Nematollahi, J. Sanjayan, and F. U. Ahmed Shaikh, "Tensile strain hardening behavior of PVA fiber-reinforced engineered geopolymer composite," *Journal of Materials in Civil Engineering,* vol. 27, no. 10, 04015001, 2015.

[76] J. Wongpa, K. Kiattikomol, C. Jaturapitakkul, and P. Chindaprasirt, "Compressive strength, modulus of elasticity, and water permeability of

inorganic polymer concrete," *Materials & Design,* vol. 31, no. 10, pp. 4748-4754, 2010.

[77] A. Tavassoli and S. A. Sheikh, "Seismic Resistance of Circular Columns Reinforced with Steel and GFRP," *Journal of Composites for Construction,* vol. 21, no. 4, 04017002, 2017.

[78] M. A. Ali and E. El-Salakawy, "Seismic performance of GFRP-reinforced concrete rectangular columns," *Journal of Composites for Construction,* vol. 20, no. 3, 04015074, 2015.

[79] S. Naqvi, K. Mahmoud, and E. El-Salakawy, "Effect of Axial Load and Steel Fibers on the Seismic Behavior of Lap-Spliced Glass Fiber Reinforced Polymer-Reinforced Concrete Rectangular Columns," *Engineering Structures,* vol. 134, pp. 376-389, 2017.

[80] M. G. Elshamandy, A. S. Farghaly, and B. Benmokrane, "Experimental Behavior of Glass Fiber-Reinforced Polymer-Reinforced Concrete Columns under Lateral Cyclic Load," *Structural Journal,* vol. 115, no. 2, pp. 337-349, 2018.

[81] National Research Council of Canada, "National Building Code of Canada," NBCC, Canadian Commission on Building and Fire Codes, Ottawa, Canada, 2005.

[82] A. El Refai, F. Abed, and A. Al-Rahmani, "Structural performance and serviceability of concrete beams reinforced with hybrid (GFRP and steel) bars," *Construction and Building Materials,* vol. 96, pp. 518-529, 2015.

[83] T. El-Maaddawy and A. S. El-Dieb, "Near-surface-mounted composite system for repair and strengthening of reinforced concrete columns subjected to axial load and biaxial bending," *Journal of Composites for Construction,* vol. 15, no. 4, pp. 602-614, 2010.

[84] A. M. Ibrahim, Z. Wu, M. F. Fahmy, and D. Kamal, "Experimental study on cyclic response of concrete bridge columns reinforced by steel and basalt FRP reinforcements," *Journal of Composites for Construction,* vol. 20, no.3, 04015062, 2015.

[85] H. Tobbi, A. S. Farghaly, and B. Benmokrane, "Strength model for concrete columns reinforced with fiber-reinforced polymer bars and ties," *ACI Structural Journal,* vol. 111, no. 4, pp. 789-798, 2014.

[86] Canadian Standard Association, "Design of concrete structures," CSA A23.3, Mississauga, Ontario, Canada, 2014.

[87] H. J. Zadeh and A. Nanni, "Design of RC columns using glass FRP reinforcement," *Journal of Composites for Construction,* vol. 17, no. 3, pp. 294-304, 2012.

[88] American Concrete Institute, "Guide for the Design and Construction of Externally Bonded FRP Systems for Strengthening Concrete Structures," ACI 440.2R-08, ACI Committee 440, Farmington Hills, MI, USA, 2008.

[89] H. Karim, M. Neaz Sheikh, and M. N. Hadi, "Load and moment interaction diagram for circular concrete columns reinforced with GFRP bars and GFRP helices," *Journal of Composites for Construction,* vol. 21, no. 1, 04016076, 2016.

[90] C. C. Choo, "Investigation of rectangular concrete columns reinforced or prestressed with fiber reinforced polymer (FRP) bars or tendons," Ph.D. dissertation, University of Kentucky, Lexington, KY, USA, 2005.

[91] C. C. Choo, I. E. Harik, and H. Gesund, "Minimum reinforcement ratio for fiber-reinforced polymer reinforced concrete rectangular columns," *ACI Materials Journal,* vol. 103, no. 3, pp. 460-466, 2006.

[92] H. Karim, B. Noel-Gough, M. N. Sheikh, and M. N. Hadi, "Strength and ductility behavior of circular concrete columns reinforced with GFRP bars and helices," In *Proc. Joint Conference of the 12th International Symposium on Fiber Reinforced Polymers for Reinforced Concrete Structures (FRPRCS-12) & the 5th Asia-Pacific Conference on Fiber Reinforced Polymers in Structures (APFIS-2015)*, Nanjing, China, 2015, pp. 1-6.

[93] Canadian Standard Association, "Canadian Highway Bridge Design Code," CSA-S6-14, Mississauga, Ontario, Canada, 2014.

[94] American Concrete Institute, "Building code requirements for structural concrete and commentary," ACI 318-11, Farmington Hills, MI, USA, 2011.

[95] ASTM International, "Standard Test Method for Compressive Strength of Cylindrical Concrete Specimens," ASTM C39/C39M-17, West Conshohocken, PA, USA, 2017.

[96] British Standard Institution, "Testing concrete. Method for determination of compressive strength of concrete cubes," BS 1881-116:1983, London, England, 1983.

[97] ASTM International, "Standard Test Method for Splitting Tensile Strength of Cylindrical Concrete Specimens," ASTM C496/C496M-17, West Conshohocken, PA, USA, 2017.

[98] ASTM International, "Standard Specification for Deformed and Plain Carbon-Steel Bars for Concrete Reinforcement," ASTM A615/A615M-18e1, West Conshohocken, PA, USA, 2018.

[99] ASTM International, "Standard Test Method for Tensile Properties of Fiber Reinforced Polymer Matrix Composite Bars," ASTM D7205/D7205M-06, West Conshohocken, PA, USA, 2016.

[100] S. J. Foster and M. M. Attard, "Experimental tests on eccentrically loaded high strength concrete columns," *Structural Journal,* vol.94, no.3, pp.295-303, 1997.

[101] A. Mirmiran and M. Shahawy, "Dilation characteristics of confined concrete," *Mechanics of Cohesive-frictional Materials: An International Journal on Experiments, Modelling and Computation of Materials and Structures,* vol.2, no.3, pp.237-249, 1997.

## Vita

Nouran ElMesalami was born in 1994, in Al Ain, United Arab Emirates. She completed Cambridge International Advanced Level examinations during her secondary education, achieving straight A*s in all subjects. She joined the American University of Sharjah in February, 2013, and graduated Summa Cum Laude with a Bachelor's of Science degree in Civil Engineering in December, 2016. After which, she pursued masters studies in Civil Engineering at AUS, in January, 2017. During her undergraduate and graduate studies, she has co-authored a total of 10 conference and journal papers, and has presented in a number of international conferences. She received the *Graduate Student Research, Scholarly, and Creative Work Excellence Award* from AUS for the academic year 2018-2019. Her research interests are in structural engineering and materials, with particular interest in sustainable civil engineering practices and materials. After completing one year of her graduate studies, she started working as a Bridge Engineer at AECOM Middle East Limited, in Dubai, UAE. During her professional work as a structural engineer, she has worked on a number of large projects, inside and outside the UAE, and has gained valuable experience in structural engineering.